NASA CR 112236

ADHESIVE-BONDED SINGLE-LAP JOINTS

TECHNICAL REPORT

by

L. J. HART-SMITH

Prepared under Contract NAS1-11234
Douglas Aircraft Company
McDonnell Douglas Corporation
3855 Lakewood Blvd
Long Beach, California 90846

JANUARY 1973

for

Langley Research Center
Hampton, Virginia 23366

NATIONAL AERONAUTICS AND SPACE ADMINISTRATION

ABSTRACT

Explicit analytical solutions are derived for the static load-carrying capacity of single-lap adhesive-bonded joints. A purely-elastic analysis represents a considerable improvement over the classical solution by Goland and Reissner. Also, the quantitative influence of adhesive plasticity in shear is established. This beneficial influence is shown to be capable of explaining the premature failure predictions by elastic analyses. Yielding of metal adherends at the ends of the joint as the result of the eccentric load path is shown usually to be the factor initiating failure for all but very short overlaps. In the case of filamentary composite adherends, fracture of those 0° filaments closest to the bond usually initiates an interlaminar shear failure within the laminates. For thicker adherends, the dominant failure mode is shown to be that of peel stresses in the adhesive and the associated interlaminar tension stresses in filamentary composite adherends. The quantitative effects of adherend stiffness imbalance are accounted for in this investigation.

KEYWORD DESCRIPTORS

Bonded Joints
Adhesive Stresses and Strains
Adherend Thermal Mismatch
Adherend Stiffness Imbalance
Adhesive Peel Stresses
Eccentric Load Path
Single-Lap Joints
Static Strength
Elastic-Plastic Formulation
Adhesive Shear Stresses
Advanced Composite Joints
Low Structural Efficiency

FOREWORD

This report was prepared by the Douglas Aircraft Company, McDonnell Douglas Corporation, Long Beach, California under the terms of Contract NAS1-11234. One summary report (NASA CR 2218) and four technical reports (NASA CR 112235, -6, -7, and -8) cover the work, which was performed between November 1971 and January 1973. The program was sponsored by the National Aeronautics and Space Administration's Langley Research Center, Hampton, Virginia. Dr. M. F. Card and Mr. H. G. Bush were the Contracting Agency's Technical Monitors.

The basic concept of bonded joint shear analysis by classical mechanics of continuous structures in terms of the elastic-plastic adhesive model was developed initially under Douglas Irad funding between 1968 and 1970. This contract has permitted the work to be expanded greatly in both scope and detail. All of the peel-stress studies were performed under this contract.

CONTENTS

ILLUSTRATIONS

SYMBOLS

A,B,C,F	=	Integration constants
c	=	Half length of overlap (in.)
D	=	Flexural rigidity of adherends (lb in.^{2})
d	=	Length of elastic zone in adhesive bond (in.)
E	=	Young's modulus (longitudinal) for adherend (psi)
E_c, E_c'	=	Adhesive peel (transverse tension) moduli (psi)
e	=	Eccentricity (in.)
G	=	Adhesive shear modulus (psi)
K	=	Coefficient [see Equation (71)]
k	=	Eccentricity factor [see Equation (39)]
k_b	=	$D / [Et^3 / 12(1 - \nu^2)]$ = bending stiffness parameter for filamentary composite adherends
ℓ	=	Overlap (length of bond) (in.)
ℓ_1, ℓ_4	=	Length of adherends outside the joint (in.)
M	=	Bending moment in adherend (lb in. / in.)
M_o	=	Bending moment in adherend at end of overlap (lb in. / in.)
P	=	Applied load on joint (lb)
s	=	Co-ordinate aligned along load path (different origin from x)
T	=	Direct stress resultants in adherend(s) (lb / in.)
t	=	Thickness of adherend (in.)
u	=	Axial displacement in adherend adjacent to bond (in.)
V	=	Transverse shear force on adherend (lb / in.)
w	=	Transverse displacement of adherend under eccentric load (in.)
x	=	Axial (longitudinal) co-ordinate aligned along load path

γ = Adhesive shear strain

γ_e = Elastic adhesive shear strain

γ_p = Plastic adhesive shear strain

ζ = Axial co-ordinate (different origin from x)

η = Thickness of adhesive layer (in.)

λ, λ' = Exponents of elastic shear stress distribution ($in.^{-1}$)

ν = Poisson's ratio for adherends

ξ = Exponent of bending stress distribution in adherend ($in.^{-1}$)

σ_{av} = (P/t) = Average adherend stress (psi)

σ_{max} = Maximum adherend stress (resultant of direct and bending loads) (psi)

σ_p, σ_c = Peel stresses in adhesive (psi)

σ_y = Yield stress of adherend (psi)

τ, τ_a = Adhesive shear stress (psi)

τ_{av} = Average adhesive shear stress (psi)

τ_p = Plastic adhesive shear stress (psi)

χ = Peel stress distribution exponent ($in.^{-1}$)

SUBSCRIPTS

a,c = Adhesive (cement)

n = Property normal to plane of adherends (e.g. E_n = transverse modulus of adherend)

1,2,3 / 4,5 = Different regions of the adherends in single-lap joint

SUMMARY

This report presents analyses of the influence of a variety of factors on the strength of adhesive-bonded single-lap joints. The classical approach of Goland and Reissner is improved and extended. A deficiency in their determination of the critical bending moment in the adherends at the ends of the overlap is overcome. Additional factors included in the analyses are adhesive plasticity (in terms of the Douglas elastic-plastic approach), stiffness imbalance between the adherends, and the influence of laminated filamentary composite adherends (as distinct from isotropic metal adherends).

Three distinct and characteristic failure modes are predicted. The first is that of failure of the adherend just outside the joint due to the in-plane stresses resulting from the combination of direct load stresses and bending stresses resulting from the eccentricity in the load path. While necessarily less than 100 percent efficient, this first mode is the strongest of the three. The second mode is the failure of the adhesive layer in shear. While prior elastic studies have concentrated on this failure mode and much of the single-lap joint design practice is so oriented, the inclusion of adhesive plasticity in the analysis has demonstrated that this potential failure mode is extremely rare in structural practice. The third failure mode may be manifest in either of two forms and is associated with the adhesive peel stresses. With metal adherends which are too thick to yield in bending under the eccentric load path, the observed failure in the third mode is that of the adhesive peel stress. With filamentary composite adherends, on the other hand, the interlaminar tension strength is so much less than the peel strength of good structural adhesives that the failure occurs within the continuous laminate at the end(s) of the joint.

Adherend thermal mismatch is discussed only qualitatively but the effects of adherend stiffness imbalance on the joint strength are characterized quantitatively. Any adherend imbalance is shown to effect significant strength reductions down to a weaker joint than could be formed with two adherends each identical with the weaker adherend of the unbalanced joint.

Several digital computer programs have been prepared for the iterative solution of the mathematical equations derived. The need for iteration arises because account is taken of the significant bending moment relief associated with structural (elastic) deformations under load.

The standard half-inch lap shear test is discussed. The failure observed is only infrequently associated with failure of the adhesive in shear. Therefore a case is presented for restricting this test to quality control work, for which it is ideally suited, and for not using the values so generated for design purposes.

Because of the eccentricity in the load path, the structural efficiency must inevitably be less than unity. The analyses show the desirability of employing far larger ℓ/t ratios than are needed for load transfer alone in order to improve the efficiency of the entire structure while suffering only a small weight penalty locally at the joints.

1. INTRODUCTION

Numerous theoretical analyses of the mechanics of single-lap adhesive-bonded joints have been made since the original paper by Goland and Reissner (Reference 1) in 1944 accounting for the eccentricity in the load path. Hahn (References 2, 3 and 4) has extended their analysis to dissimilar adherends. Kuenzi and Stevens (Reference 5) used the analysis of Goland and Reissner to illustrate the different behavior of "stiff" and "soft" adhesives in joints while Kutscha and Hofer (Reference 6) have programmed the Goland and Reissner analysis for a digital computer and depicted extensive parametric studies on purely elastic joints. A comprehensive survey and review has been prepared by Kutscha (Reference 7) in 1964.

Some qualitative understanding of the problem has been achieved in the works reported above but an unappreciated deficiency in the determination by Goland and Reissner of the bending moment in the adherend at the end of the joint has been perpetuated ever since. The quantitative significance of these analyses is therefore in doubt, particularly since no allowance has been made for adhesive plasticity either.

Two recent major research investigations into adhesive-bonded joints have included the single-lap joint amongst the geometries analyzed. Both the work of Grimes, Wah, et al (Reference 8) and Dickson, Hsu, and McKinney (Reference 9) have concentrated on filamentary composite adherends. Each team included variation of stresses through the thickness of the adherends in their formulations and, thereby, accounted for effects not considered here. On the other hand, the inclusion of so many other factors prevented such a simple comprehensive accounting of the effects of adhesive plasticity as is derived herein. Furthermore, each omitted to account for the significant stress concentration relief afforded by transverse deflections under load (geometric non-linearities). Both attempted to utilize a continuous Ramberg-Osgood representation of the adhesive properties (which would be more precise than that used here) and neither attained that goal. A piecewise linear solution was obtained in Reference 8, by iteration, through breaking up the length of the joint into a number of segments. In reference 9, the empirical "plastic-zone" approach

attributed to Goodwin (Reference 10) was used to extend the closed-form elastic analysis procedure to include joints with inelastic adhesive stress-strain behavior in shear. Both investigations confirmed the importance of including adhesive plasticity in the analysis. Reference 9 established, on the basis of specific cases analyzed, that interlaminar shear deformation in filamentary composites does not have a major effect on the predicted joint strength but that the interlaminar tension does affect the adhesive shear stress distribution. The authors of Reference 9 expressed surprise at the important role of variation of transverse tension through the thickness of the joint but this is a necessary consequence of allowing the adhesive shear stress to decrease to zero at the ends of the joint, as can be appreciated by examination of the normal and shear stresses on a differential element of the adhesive layer.

In comparing investigations such as References 8 and 9 with the present report it is important to recognize that the basic objectives were different. The objective of the present investigation is a simple rational design technique including only the major joint parameters in the analysis. Here, all effects known (or believed) to be minor have been excluded in order to restrict the amount of data necessary to define a joint. This has led to the generation herein of joint efficiency charts in terms of adherend thickness for a range of overlap-to-thickness ratios for given material combinations. The three major failure modes of bending of the adherend just outside the joint, shearing of the adhesive, and peeling of the adhesive (or laminate by interlaminar tension) have all been accounted for. Perhaps some of the simplifying assumptions here may prove to be excessive and empirical correction factors may need to be developed. Even in this event, however, a sound reference framework has been established for the first time, by identifying the dominant mode of failure for a given material/geometry combination. Certainly, reference to the average shear stress is shown to be unsatisfactory as a basis for design. References 8 and 9 were more specific and detailed in their analyses and significant effort was devoted to reconciling finite-element and analytical solutions. In addition, more emphasis was placed upon precise theory-experiment correlation in those works whereas, here, the approaches of simple upper and lower bounds as well as asymptotic solutions have been employed in the correlation. The different approaches should be regarded as complementary since that adopted here relies on more precise analysis to justify the exclusion of minor effects.

Conversely, the far more extensive parametric studies performed in this investigation serve as a reference to guide more detailed analyses of some particular aspect of bonded joint behavior.

The design of single-lap joints has proceeded essentially independently of the theoretical analyses because of inadequate correlation between theory and experiment and because the analyses have been considered too complicated hitherto. The analytically simpler case of the structurally-superior double-lap joint has been analyzed by the author elsewhere (References 11 and 12), yielding explicit asymptotic solutions simple enough to use for design purposes and it is the intent here to provide comparable information about single-lap joints. It was found in Reference 11 that the single factor most responsible for the adequate agreement achieved between theory and experiment was the consideration of adhesive plasticity. Also, the locked-in pre-strains arising from thermal incompatibility of dissimilar materials in the adherends were found to have a significant effect. Likewise, adherend stiffness imbalance accentuates the adhesive stress and strain concentrations at one end of the joint, leading to reduced efficiencies in comparison with balanced adherends. In the case of single-lap joints, analyzed here, the eccentricity in the load path and the consequent transverse deflections under load dominate the behavior of such joints. The adhesive shear properties prove to have very little to do with the strength of single-lap joints, the failure of which is governed largely by adherend properties and peel stresses. In contrast with the minimal effect of lap length on the strength of practical double-lap joints, lap length is a powerful influence on the adherend strength of single-lap joints. Unfortunately, the lap lengths needed to develop peak efficiency are so great as to impose a significant weight penalty for single-lap joints.

Whereas, in a scarf joint between identical adherends, the adhesive shear stress is very nearly uniform along the length of the joint, in a single-lap joint there is a pronounced trough in the shear stress distribution. Most of the load is transferred through the effective end zones, of limited extent, while the bond in the middle is relatively lightly loaded. The elastic-plastic analysis reported herein predicts that the elastic trough is significantly more effective for long-overlap single-lap joints than is the case for double-lap bonded joints (analyzed in Reference 12). The tearing (transverse tension)

stresses also peak at the ends of the joint and usually prove to be more severe than the shear stresses. There are three distinct failure modes possible, each with an associated criterion. For thin adherends, failure is usually caused by exceeding the maximum "fiber" stress, adjacent to the bond at the end of the overlap, under combined direct and bending stresses. The latter arise from the eccentricity in the load path. For short overlaps, it is possible to initiate failure as the result of exceeding the ultimate shear strain in the adhesive at the end of the joint. For relatively thick adherends, failure results from excessive peel stresses induced by the eccentricity in the load path. In such cases, metal adherends are associated with peel failure of the adhesive at the end of the joint while composite adherends usually fail in interlaminar tension because they are weaker than the adjacent adhesive. These phenomena are illustrated in Figure 1.

Single-lap joints are inherently so inefficient that they should not be used without a support to react the eccentricity in the load path. When so supported, their strength is improved dramatically and approaches one half of that of a double-lap joint of twice the thickness in the central adherend. (The factor one half is the direct result of bonding on both sides of the central adherend in a double-lap joint, which gives twice the bond area of the corresponding single-lap joint.)

2. BALANCED SINGLE-LAP JOINTS (ELASTIC ANALYSIS)

The analysis of double-lap joints (Reference 12) involves only extensional deformations of the adherends. Single-lap joints, on the other hand, are subject to transverse deflections of sufficient magnitude to necessitate consideration because of the eccentric load path. The present analysis (and the author's earlier analysis in Reference 13 likewise) is therefore performed in a series of stages, with the final solution obtained by combination.

Figure 2 depicts the geometry and nomenclature for the analysis of a precisely anti-symmetric single-lap joint of identical adherends. In order to include filamentary composite materials in the analysis, the extensional stiffnesses Et are uncoupled from the bending stiffnesses D through the use of the coefficient

$$k_b = D \; / \; [Et^3 \; / \; 12(1 - \nu^2)] \quad . \tag{1}$$

For purposes of analysis, the joint is divided into the four sections shown.

Throughout the adherend 1, the longitudinal stress resultant (force per unit lateral width) is uniform, at the value P of the load applied. The stress couple M_1 (inch pound per unit width) is then given by the equilibrium equation

$$M_1 = P \left| \left(\frac{t + \eta}{\ell + c} \right) \frac{x}{2} - w_1 \right| \qquad \text{for } 0 \leq x \leq \ell \quad . \tag{2}$$

According to the classical theory for the infinitesimal bending of thin cylindrically deformed plates,

$$\frac{d^2 w_1}{dx^2} = - \frac{M_1}{D} = - \frac{P}{D} \left| \left(\frac{t + \eta}{\ell + c} \right) \frac{x}{2} - w_1 \right| \quad , \tag{3}$$

the solution of which is

$$w_1 = A_1 \cosh(\xi x) + B_1 \sinh(\xi x) + \left(\frac{t + \eta}{\ell + c} \right) \frac{x}{2} \quad , \tag{4}$$

where

$$\xi^2 = P \; / \; D \tag{5}$$

and in which the condition $M_1 = 0$ at $x = 0$ requires that

$$A_1 = 0 \quad . \tag{6}$$

Turning attention now to regions 2 and 3 (see Figure 2), moment equilibrium requires that

$$\left.\begin{aligned} \frac{dM_2}{ds} - V_2 + \tau\left(\frac{t + \eta}{2}\right) &= 0 \\ \frac{dM_3}{ds} - V_3 + \tau\left(\frac{t + \eta}{2}\right) &= 0 \end{aligned}\right\}, \tag{7}$$

while longitudinal force equilibrium requires that

$$\left.\begin{aligned} \frac{dT_2}{ds} + \tau &= 0 \\ \frac{dT_3}{ds} - \tau &= 0 \end{aligned}\right\}, \tag{8}$$

and transverse force equilibrium requires that

$$\left.\begin{aligned} \frac{dV_2}{ds} + \sigma_c &= 0 \\ \frac{dV_3}{ds} - \sigma_c &= 0 \end{aligned}\right\}. \tag{9}$$

From plate theory, with the sign convention depicted in Figure 2,

$$\left.\begin{aligned} \frac{d^2w_2}{ds^2} &= -\frac{M_2}{D} \\ \frac{d^2w_3}{ds^2} &= -\frac{M_3}{D} \end{aligned}\right\}, \tag{10}$$

where

$$D = k_b \frac{Et^3}{12(1 - \nu^2)} \tag{11}$$

defines the flexural rigidity of each adherend.

Defining by u_2 and u_3 the longitudinal displacements of the adherends immediately adjacent to the adhesive, the stress-strain relations for plane strain of elastic adherends give

$$\left.\begin{aligned} \frac{du_2}{ds} &= \frac{1}{Et}\left[T_2 + \frac{6(1-\nu^2)M_2}{k_b t}\right] \\ \frac{du_3}{ds} &= \frac{1}{Et}\left[T_3 - \frac{6(1-\nu^2)M_3}{k_b t}\right] \end{aligned}\right\} . \tag{12}$$

To obtain the relations for a plane stress condition, the Poisson's ratios are dropped from the above equations and those derived from them hereafter.

The adhesive properties are defined to be linearly elastic in transverse tension and perfectly elastic-plastic in shear between the adherends. Therefore

$$\frac{\sigma_c}{E_c} = \frac{(w_3 - w_2)}{\eta} \qquad * \tag{13}$$

and

$$\left.\begin{aligned} \gamma = \frac{\tau}{G} &= \frac{(u_3 - u_2)}{\eta} \qquad \text{for } \gamma \le \gamma_e \\ \tau &= \tau_p \qquad\qquad\quad \text{for } \gamma \ge \gamma_e \end{aligned}\right\} . \tag{14}$$

Prior to determining the adhesive shear stress distribution it is shown by the analysis of Goland and Reissner (Reference 1) to be necessary to evaluate M_1 at $x = \ell$, which must equal M_2 at $s = -c$. Therefore, a differential equation governing w_2 is required. Now,

$$w_2 = [(w_2 + w_3) + (w_2 - w_3)] / 2 \quad , \tag{15}$$

and

---

* Strictly, the transverse stiffness E_c of the adhesive should be replaced by the effective modulus E_c' reflecting the softening due to the limited transverse stiffness of advanced composite adherends and the thinness of the adhesive layer. This procedure is fully explained in Reference 12 and discussed further in Section 11 here.

$$\frac{d^2w_2}{ds^2} + \frac{d^2w_3}{ds^2} = -\frac{1}{D}(M_2 + M_3) \quad , \tag{16}$$

$$\frac{d^3(w_2 + w_3)}{ds^3} = -\frac{1}{D}[V_2 + V_3 - \tau(t + \eta)] \quad , \tag{17}$$

$$\frac{d^4(w_2 + w_3)}{ds^4} = \frac{(t + \eta)}{D}\left(\frac{d\tau}{ds}\right) \quad , \tag{18}$$

while

$$\frac{d^4(w_2 - w_3)}{ds^4} = 2\frac{\sigma_c}{D} = -\frac{2E_c}{\eta D}(w_2 - w_3) \quad . \tag{19}$$

From equation (14) $(w_3 - w_2)$ is equal to the extremely small differential transverse displacement across the very thin adhesive layer and, therefore, $(w_2 - w_3)$ can justifiably be neglected in comparison with $(w_2 + w_3)$ throughout the joint. There is some uncertainty about the first derivative $d(w_2 - w_3)/ds$ but none about the higher derivatives because, at the ends of the joint $(s = \pm c)$,

$$\frac{d^2w_3}{ds^2} = \frac{d^3w_3}{ds^3} = 0 \quad \text{at } s = -c \quad \text{and} \quad \frac{d^2w_2}{ds^2} = \frac{d^3w_2}{ds^3} = 0 \quad \text{at } s = +c \tag{20}$$

and, therefore, for these higher derivatives it is necessary to set

$$w_2 = [(w_2 + w_3) + (w_2 - w_3)] / 2 \tag{21}$$

while, for w_2 and the first derivative, the approximations

$$w_2 \simeq (w_2 + w_3) / 2 \quad , \quad \frac{dw_2}{ds} \simeq \frac{1}{2}\frac{d(w_2 + w_3)}{ds} \tag{22}$$

are adopted.

The continued solution of this problem requires the specification of the adhesive elasto-mechanical properties and, for simplicity, a purely elastic adhesive is considered first. (In the next section, it is shown that the assumption of a perfectly plastic adhesive leads to precisely the same result. The validity of the result is then inferred for all intermediate adhesive characteristics.) Starting from equations (12) and (14),

$$\frac{d\tau}{ds} = \frac{G}{\eta}\left[\frac{du_3}{ds} - \frac{du_2}{ds}\right] = \frac{G}{Et\eta}\left[T_3 - T_2 - \frac{6(1-\nu^2)(M_3 + M_2)}{k_b t}\right] , \qquad (23)$$

$$\frac{d^2\tau}{ds^2} = \frac{G}{Et\eta}\left[2\tau + \frac{6(1-\nu^2)}{k_b}\tau - \frac{6(1-\nu^2)}{k_b}(V_2 + V_3)\right] , \qquad (24)$$

whence

$$\frac{d^3\tau}{ds^3} = \left(2 + \frac{6(1-\nu^2)}{k_b}\right)\left(\frac{G}{Et\eta}\right)\frac{d\tau}{ds} = \left(1 + \frac{3(1-\nu^2)}{k_b}\right)\lambda^2\frac{d\tau}{ds} , \qquad (25)$$

in which

$$\lambda^2 = 2G / Et\eta . \qquad (26)$$

The notation

$$(\lambda')^2 = \left[\frac{1 + 3(1-\nu^2)/k_b}{4}\right]\lambda^2 \qquad (27)$$

is conveniently introduced to account for the uncoupling of the extensional and bending stiffnesses of filamentary composite adherends. The parameter λ plays a powerful role in characterizing the adhesive shear stress distributions for double-lap joints and its retention for the single-lap joint analysis provides a meaningful basis for comparison.

The solution of equation (25) is

$$\tau = A_2 \cosh(2\lambda' s) + B_2 \sinh(2\lambda' s) + C_2 \qquad (28)$$

in which the constant B_2 can evidently be set equal to zero because of the precise anti-symmetry of the joint. Gross horizontal equilibrium of the joint requires that

$$P = \int_{-c}^{+c} \tau\, ds = 2\tau_{av}c = 2\frac{A_2}{2\lambda'}\sinh(2\lambda' c) + 2C_2 c . \qquad (29)$$

Now, combining equations (18) and (28),

$$\frac{d^4(w_2 + w_3)}{ds^4} = \frac{(t + \eta)}{D} A_2(2\lambda')\sinh(2\lambda' s) , \qquad (30)$$

whence

$$\frac{1}{2}(w_2 + w_3) = \frac{(t+\eta)}{2D}\left|\frac{A_2}{8(\lambda')^3}\right|\sinh(2\lambda' s) + A_3 s^3 + B_3 s^2 + C_3 s + F_3 \ . \qquad (31)$$

Again, precise anti-symmetry requires that $B_3 = F_3 \equiv 0$. At the location $x = \ell$, $s = -c$, it is necessary that w_2 and its first two derivatives (with respect to the longitudinal co-ordinate) be continuous. Therefore,

$$w_1 = B_1 \sinh(\xi\ell) + \left(\frac{t+\eta}{\ell + c}\right)\frac{\ell}{2} = w_2 \simeq \frac{1}{2}(w_2 + w_3)$$

$$= -\frac{(t+\eta)}{2D}\left|\frac{A_2}{8(\lambda')^3}\right|\sinh(2\lambda' c) - A_3 c^3 - C_3 c \ , \qquad (32)$$

$$\frac{dw_1}{dx} = B_1\xi\cosh(\xi\ell) + \left(\frac{t+\eta}{\ell + c}\right)\frac{1}{2} = \frac{dw_2}{ds} \simeq \frac{1}{2}\left|\frac{d(w_2 + w_3)}{ds}\right|$$

$$= \frac{(t+\eta)}{2D}\left|\frac{A_2}{4(\lambda')^2}\right|\cosh(2\lambda' c) + 3A_3 c^2 + C_3 \ , \qquad (33)$$

$$\frac{d^2 w_1}{dx^2} = B_1\xi^2 \sinh(\xi\ell) = \frac{d^2 w_2}{ds^2} = \frac{1}{2}\left|\frac{d^2(w_2 + w_3)}{ds^2} + \frac{d^2(w_2 - w_3)}{ds^2}\right|$$

$$= -\frac{(t+\eta)}{2D}\left|\frac{A_2}{2\lambda'}\right|\sinh(2\lambda' c) - 6A_3 c - \frac{M_o}{2D} = -\frac{M_o}{D} \ . \qquad (34)$$

For adherends of typical length,

$$\sinh(\xi\ell) \simeq \cosh(\xi\ell) \simeq \frac{1}{2}e^{\xi\ell} \qquad (35)$$

whence

$$B_1\xi^2\frac{1}{2}e^{\xi\ell} = -M_o/D \ , \qquad (36)$$

where M_o is the bending moment per unit width in the continuous adherend at the end of the joint.

The continuity of the third derivatives of w need not be assured and the fourth condition necessary to determine the integration constants derives from equation (23) in the form

$$A_2 2\lambda' \sinh(2\lambda' c) = \frac{G}{Et\eta}\left[P + \frac{6(1-\nu^2)M_o}{k_b t}\right]. \tag{37}$$

The result required from the equations above is that

$$M_o = P\left(\frac{t+\eta}{2}\right)\frac{\left[1 + \frac{\xi^2\lambda^2}{32(\lambda')^4}\left(1 + \frac{(2\lambda' c)}{3} - \frac{2\lambda' c}{\tanh(2\lambda' c)}\right)\right]}{\left\{1 + \xi c + \frac{\xi^2 c^2}{6} - \frac{(t+\eta)}{2t}\left[\frac{3\lambda^2\xi^2}{32k_b(\lambda')^4}\right]\left[1 + \frac{(2\lambda' c)^2}{3} - \frac{2\lambda' c}{\tanh(2\lambda' c)}\right]\right\}} \tag{38}$$

and, on assessing the quantitative contribution of the respective terms, it is found that

$$M_o \simeq P\left(\frac{t+\eta}{2}\right)\frac{1}{1 + \xi c + \frac{\xi^2 c^2}{6}} \simeq kP\frac{t}{2}\left(1 + \frac{\eta}{t}\right). \tag{39}$$

(This differs fundamentally from the result obtained by Goland and Reissner, which is discussed later.)

Returning now to equations (23), (28), and (29) it is found that

$$\frac{\tau_{av}}{\tau_{max}} = \frac{1}{1 + \left[1 + \frac{3k(1-\nu^2)}{k_b}\left(1 + \frac{\eta}{t}\right)\right]\left[\frac{\lambda^2}{4(\lambda')^2}\right]\left[\frac{2\lambda' c}{\tanh(2\lambda' c)} - 1\right]} \tag{40}$$

which, for isotropic adherends, reduces to the result predicted by Goland and Reissner in the concluding portion of their paper. For a sufficiently long overlap, this elastic analysis of single-lap bonded joints predicts that

$$\frac{\tau_{av}}{\tau_{max}} \to \frac{2}{\lambda' c}. \tag{41}$$

In view of the analysis of double-lap joints (Reference 12) it appears, at first sight, that, for elastic adhesives, single-lap joints are far more efficient than double-lap joints, for which $(\tau_{av}/\tau_{max}) \to 1/\lambda_c$. The reason for this apparent anomaly is the constant term C_2 in equation (28), which is zero for double-lap joints. Here, for long single overlaps,

$$C_2 \to \frac{3}{4}\tau_{av} \tag{42}$$

for the case of isotropic adherends, thereby reducing the influence of the stress concentrations. (For non-isotropic adherends,

$$C_2 \rightarrow \left\{1 - \frac{1}{[1 + 3(1-\nu^2)/k_b]}\right\} \tau_{av} \quad .) \tag{43}$$

On the other hand, a quantitative assessment of equation (40) reveals that the average adhesive stresses developed in single-lap joints do not exceed those developed in the corresponding double-lap joints for either realistic material properties or overlaps not so excessively long as to add undue weight to the structure. In addition to this, the apparent superiority above of single-lap joints refers exclusively to the adhesive shear stress distribution. Unsupported single-lap joints (as analyzed here) are inevitably subjected to a severe bending stress concentration in the adherends at the ends of the joint. Consequent yielding in a metal adherend can cause relative displacements across the adhesive layer which are beyond the capability of the adhesive, causing an otherwise premature adhesive failure. In the case of filamentary composite adherends, failure under inter-laminar tension due to the peel stresses induced at the ends of the overlap prevents the attainment of the potential high shear strength indicated above.

The prime objective of Section 2 is the derivation of the bending moment M_o at the end of the joint. This quantity defines the peak shear and peel stresses in the adhesive (which is why it is important to correct the deficiency, in this regard, of the analysis by Goland and Reissner). The influence of this bending stress on the strength of the adherends is elucidated in Section 3. The analysis of the adhesive shear stress distribution is presented in Section 4 using the more realistic elastic-plastic adhesive formulation. The problem of peel stresses is discussed in Section 5.

Discussion of Goland and Reissner Analysis

The elastic analysis by Goland and Reissner (Reference 1) in 1944 has formed the foundation of most later investigations of single-lap bonded joints. As mentioned above, their determination of the stress couple M_o at the end of the joint is subject to severe restrictions on its applicability, being strictly valid only for light loads and short overlaps. Since their paper is so widely recognized as a leader in the field, it is appropriate to explain fully the limitations implicit in their solution. The sign convention and terminology which they employed differ somewhat from those used here, but there is no difficulty in comparing the two analyses. To complement the equations (2) through (5) here they considered that there was negligible adhesive deformation in the overlap region of the joint and analyzed that portion (2 and 3 in Figure 2) as part of a single cylindrically-bent plate of twice the thickness of each individual adherend. They derived for this region 5 the governing differential equation

$$\frac{d^4 w_5}{ds^4} = -\frac{M_5}{D_5} = -\frac{P}{8D}\left[\left(\frac{t+\eta}{\ell+c}\right)(\ell+s) - w_5 - \frac{(t+\eta)}{2}\right], \qquad (44)$$

of which the solution is

$$w_5 = A_5 \cosh\left(\frac{\xi s}{2\sqrt{2}}\right) + B_5 \sinh\left(\frac{\xi s}{2\sqrt{2}}\right) + \left(\frac{t+\eta}{\ell+c}\right)(\ell+s) - \frac{(t+\eta)}{2}. \qquad (45)$$

Using the boundary conditions

$$\left.\begin{aligned} w_1 &= 0 && \text{at } x = 0, \\ w_1 &= w_5 && \text{at } x = \ell,\ s = -c, \\ dw_1/dx &= dw_5/ds && \text{at } x = \ell,\ s = -c, \\ w_5 &= 0 && \text{at } s = 0, \end{aligned}\right\} \qquad (46)$$

they eventually deduced that, for isotropic adherends,

$$M_o = k\frac{Pt}{2}\left(1 + \frac{\eta}{t}\right) \qquad (47)$$

where their equation (16) is precisely equivalent to

$$k = \frac{1}{\left| 1 + 2\sqrt{2} \tanh\left(\frac{\xi c}{2\sqrt{2}}\right) \right|} \quad . \tag{48}$$

Their solution (44) approaches the asymptote

$$k \to \frac{1}{1 + 2\sqrt{2}} = 0.261 \tag{49}$$

for indefinitely large values of overlap (characterized by ξc), whereas the present solution (40) has, for its asymptote,

$$k = 0 \quad . \tag{50}$$

Figure 3 presents a comparison between the respective solutions. Intuitively one expects that $M_o \to 0$, rather than some definite non-zero value, for joints with very long overlaps. The effect of this discrepancy is that, instead of the result (42) that

$$\frac{\tau_{av}}{\tau_{max}} \to \frac{2}{\lambda c} \tag{51}$$

they predicted that

$$\frac{\tau_{av}}{\tau_{max}} \to \frac{1.12}{\lambda c} \tag{52}$$

for sufficiently long overlaps. Their simplification consequently leads to overly conservative solutions out by a factor of nearly two except for short overlaps or light loads. The fallacy in their reasoning is explained in Figure 4 — they used the equation

$$\frac{M}{D} = - \frac{d^2 w_5}{ds^2} \quad , \tag{53}$$

which implies linear bending stress distributions, to represent a stress distribution which, at the region of interest, was in reality precisely zero over one half of the cross section and anything but anti-symmetric about the middle of the adhesive layer. (They used the correct boundary conditions in the third phase of their analysis, for the adhesive stress distributions, so their equation (49) for the shear stress distribution is sound except for the erroneous evaluation of the bending parameter k.) This is not to suggest that Goland and Reissner believed that the stress distribution shown in Figure 4

approximated the actual situation. Rather, they chose to accept the analytical simplifications ensuing from the assumption that the influence of this approximation was minor. It is now apparent that the assumption that the overlap portion of the joint may be treated as a plate of twice the adherend thickness is both mathematically unnecessary and physically unrealistic. Both the adhesive and adherend maximum stress concentrations are critically dependent on the value calculated for the bending moment M_o at the end of the overlap. The most serious discrepancy associated with their analysis is not that identified by equations (51) and (52). Rather it is that they have under-estimated the limit (yield) strength of the adherends outside the joint by the same factor 1.12 : 2 which follows from the limit for the maximum tension plus bending stress:

$$\frac{\sigma_{max}}{\sigma_{av}} = 1 + 3k\left(1 + \frac{n}{t}\right) \simeq (1 + 3k) \quad . \tag{54}$$

The quantitative effect of this deficiency is illustrated in Figure 3. Because Goland and Reissner effectively over-estimated k in equation (54), an assessment of the efficiency $\eta = \sigma_{av}/\sigma_{max}$ of the adherends just outside the joint would predict even lower efficiencies than those predicted in Section 3 by the present analysis. It clearly affects the adherend efficiency under the eccentric load path and serves as boundary condition for the adhesive shear and peel stresses analyzed below. Consequently, any unnecessary simplifying assumptions in the derivation of M_c must have an adverse effect on the entire joint analysis. Figure 3 shows how the transverse deflections of the joint under load relieve this critical bending moment for long overlaps ($k \to 1$), thereby increasing the joint efficiency ($\eta = \sigma_{av}/\sigma_{max}$) dramatically. This potential benefit appears to have been overlooked in References 8 and 9. In Report No. 1, Figure 21, p. 90 of Reference 8, the influence of this non-linearity (geometric change under load) in the analysis should have appeared as a factor in the range zero to unity on the transverse shear forces $p(t+ t_1)/a$. In Reference 9, only coarse approximation was made in accounting for this effect. With reference to Figure 2 here, a constant radius of curvature was adopted for zone in their analysis, as stated on p. 42 of Volume 1 immediately prior to their equation (85).

3. ADHEREND STRESS DISTRIBUTION DUE TO ECCENTRICITY IN LOAD PATH

As explained above, the eccentricity in the load path of an unsupported single-lap joint induces high bending moments in the adherend(s) at the ends of the overlap. The bending moment is related to the applied load by equation (39) so that the maximum "fiber" stress, adjacent to the bond line at the end of the overlap is given by

$$\sigma_{max} = \frac{P}{t} + \frac{Mc}{I} = \sigma_{av}\left|1 + 3k\left(1 + \frac{n}{t}\right)\right| \tag{55}$$

where

$$k = \frac{1}{1 + \xi c + \frac{\xi^2 c^2}{6}} \qquad \text{and} \qquad k_b = \frac{D}{Et^3/[12(1-\nu^2)]} \; . \tag{56}$$

Here

$$\xi^2 = \frac{P}{D} = \frac{\sigma_{av}}{\sigma_{max}}\left[\frac{12(1-\nu^2)\sigma_{max}}{k_b E t^2}\right] \tag{57}$$

so that, for a given allowable stress σ_{max}, the associated average stress must be determined through iteration. Digital computer programs are used to obtain these solutions. For isotropic adherends, the results are shown in Figure 5. It is immediately evident that very long overlaps are necessary to obtain reasonable structural efficiencies and that large weight penalties in the joint must consequently be accepted in order to avoid low structural efficiencies throughout the entire panels outside a joint. For example, for 7075-T6 aluminum alloy, with an ℓ/t of 10, the average adherend stress is only 25 ksi while plastic hinges develop at a local stress of 70 ksi. The ℓ/t ratio has to exceed 100 for aluminum if the average stress is to attain 95 percent of its yield capacity.

The effects of uncoupling the bending and extensional stiffnesses (by changing the layup sequence for filamentary composite adherends) are revealed in Figure 6. It is apparent that concentrating the 0° filaments near the middle of each laminated adherend (low values of k_b) effectively increases the eccentricity in the overlap, thereby aggravating the inefficiency of such joints. The reason

why high values of k_b are associated with lesser inefficiencies is that, by concentrating the stiff filaments in the outside of the laminate(s), the bending curvatures induced are less than for a uniform interspersion of the cross-plied layers throughout the thickness. The family of curves in Figure 5 represent, in dimensionalized form, the single non-dimensionalized curve in Figure 6 for isotropic (metal) adherends ($k_b = 1$).

The most important conclusion to be drawn from Figures 5 and 6 is that unsupported single-lap joints are inevitably inefficient because of the eccentricity in the load path. In order to approach an acceptable efficiency for the adherend(s) outside the joint, it is necessary to accept the weight penalty of far greater overlaps than are current design practice. To not do so is tantamount to imposing a weight penalty of a factor typically of from two to three on the entire adherends outside the joint in order to save a very much smaller weight in the joint itself.

Before proceeding to the analysis of the adhesive shear stresses, it is appropriate to emphasize that the initiation of joint failure for metal adherends is usually the formation of the plastic hinge(s) at the end(s) of the overlap. This is particularly evident in the standard single-lap half-inch overlap shear test, as illustrated in Figure 1. The failure of the adhesive is usually secondary and in no way represents the shear capacity of the adhesive for double-lap, stepped-lap or scarf joints, or even of single-lap joints having different dimensions.

4. ADHESIVE SHEAR STRESS DISTRIBUTIONS FOR BALANCED ADHERENDS (ELASTIC-PLASTIC ANALYSIS)

Consideration of adhesive plasticity is shown, in Reference 11, to be of paramount importance in reconciling theory and experiment for bonded double-lap joints. The principal need for the elastic analysis of single-lap joints in Section 2 is to simplify the determination of the bending moment M_o at the ends of the joint. It is shown in equation (38) that this moment is essentially independent of the elastic adhesive shear stress distribution within the joint. In the case of an assumed perfectly plastic adhesive ($\tau = \tau_p = \text{const.}$), the approximate result (39) follows precisely from equations (32) through (35) on setting $A_2 = 0$. (Equation (37) does not apply in the case of a perfectly plastic adhesive since it was derived from the first of equations (14) and, instead of the stress derivative $d\tau/dx$, the plastic analysis employs the strain derivative $d\gamma/dx$. Since the result (39) is valid for the extremes of perfectly elastic and perfectly plastic adhesive behavior, it proves convenient (and adequately realistic) henceforth to separate the determination of the elastic-plastic shear stress distribution from that of the governing boundary condition M_o. It is assumed, therefore, that

$$M_o \simeq P\left(\frac{t+\eta}{2}\right)\left(\frac{1}{1+\xi c+\frac{1}{6}\xi^2 c^2}\right) = kP\frac{t}{2}\left(1+\frac{\eta}{t}\right) \qquad (58)$$

for lap joints between adherends of equal stiffness. (The case of adherends of different stiffnesses, in which the bending moments are not the same at each end of the joint, is analyzed in Section 7.)

Figure 7 depicts the geometry and nomenclature for the analysis of a balanced single-lap joint. Both isotropic and filamentary composite adherends are included in the analysis. The equations governing deformations under load are presented in Section 2. Thus, within the elastic region, [from equations (25) to (27)]

$$\frac{d^3\tau}{ds^3} = 4(\lambda')^2\frac{d\tau}{ds}, \qquad \left[(\lambda')^2 = \frac{[1+3(1-\nu^2)/k_b]}{4}\left(\frac{2G}{Et\eta}\right)\right] \qquad (59)$$

(in which the term k_b accounts for the difference between isotropic and filamentary composite materials). In the plastic regions of the joint, [from equations (7) through (14)],

$$\frac{d\gamma}{ds} = \frac{1}{\eta}\left(\frac{du_3}{ds} - \frac{du_2}{ds}\right) = \frac{1}{Et\eta}\left[T_3 - T_2 - \frac{6(1-\nu^2)}{k_b}(M_2 + M_3)\right] , \quad (60)$$

and

$$\frac{d^3\gamma}{ds^3} = \left[1 + \frac{3(1-\nu^2)}{k_b}\right]\left[\frac{2}{Et\eta}\right]\frac{d\tau}{ds} = 0 . \quad (61)$$

Equation (56) has the solution

$$\tau = A_2 \cosh(2\lambda' s) + B_2 \sinh(2\lambda' s) + C_2 \quad (62)$$

in which the constant B_2 can evidently be set equal to zero because of the precise anti-symmetry of the joint. Equation (61) has the solution

$$\gamma = A_3\zeta^2 + B_3\zeta + C_3 \quad (63)$$

in which $ds = d\zeta$, the origin for ζ being at $s = + d/2$.

The constants A_2, C_2, A_3, B_3, C_3 and the unknown ratio d/ℓ are found by satisfying the boundary conditions

$$\gamma = \gamma_e \qquad \text{at } s = d/2,\ \zeta = 0, \quad (64)$$

$$\gamma = \gamma_e + \gamma_p \qquad \text{at } \zeta = (\ell - d)/2, \quad (65)$$

$$d\gamma/ds = d\gamma/d\zeta \qquad \text{at } s = d/2,\ \zeta = 0, \quad (66)$$

$$d^2\gamma/ds^2 = d^2\gamma/d\zeta^2 \qquad \text{at } s = d/2,\ \zeta = 0, \quad (67)$$

$$\frac{d\gamma}{d\zeta} = \frac{P}{Et\eta}\left[1 + \frac{3k(1-\nu^2)}{k_b}\left(1 + \frac{\eta}{t}\right)\right] \qquad \text{at } \zeta = \frac{\ell - d}{2} , \quad (68)$$

and

$$\int_0^{d/2} \tau\, dx + \tau_p\left(\frac{\ell - d}{2}\right) = \tau_{av}\left(\frac{\ell}{2}\right) = \frac{P}{2} \quad (69)$$

Equation (69) is derived by consideration of gross horizontal equilibrium of the joint. Equation (64) permits of the rewriting of equation (62) in the form

$$\tau = G\gamma = A_2 \cosh(2\lambda' s) + \tau_p - A_2 \cosh(\lambda' d) \quad . \tag{70}$$

It proves to be convenient to introduce the notation

$$A_2 \cosh(\lambda' d) = K\tau_p \quad , \tag{71}$$

so that

$$\tau = G\gamma = A_2 \cosh(2\lambda' s) + \tau_p(1 - K) \quad . \tag{72}$$

Equations (64) and (65) enable the constants B_3 and C_3 in equation (63) to be evaluated. Hence

$$\gamma = A_3\zeta^2 - A_3\left(\frac{\ell - d}{2}\right)\zeta + \frac{\gamma_p \zeta}{\left(\frac{\ell - d}{2}\right)} + \gamma_e \quad . \tag{73}$$

Equations (66) and (67) provide for the re-expression of equation (73) in terms of A_2, and thence K, since

$$-A_3\left(\frac{\ell - d}{2}\right) + \frac{\gamma_p}{\left(\frac{\ell - d}{2}\right)} = \frac{A_2}{G}(2\lambda')\sinh(\lambda' d) = \frac{2\lambda'}{G} K\tau_p \tanh(\lambda' d) \tag{74}$$

and

$$2A_3 = \frac{A_2}{G} 4(\lambda')^2 \cosh(\lambda' d) = \frac{4(\lambda')^2}{G} K\tau_p \quad . \tag{75}$$

Therefore

$$\gamma = \gamma_e \left\{ 1 + 2K[(\lambda'\zeta)^2 + \lambda'\zeta \tanh(\lambda' d)] \right\} \quad , \tag{76}$$

so that, when $\zeta = (\ell - d)/2$ where $\gamma = \gamma_e + \gamma_p$,

$$2\left(\frac{\gamma_p}{\gamma_e}\right) = K\left\{ \left[2\lambda'\left(\frac{\ell - d}{2}\right) + \tanh(\lambda' d) \right]^2 - \tanh^2(\lambda' d) \right\} \quad . \tag{77}$$

Equation (68) leads to the expression

$$\frac{\left[1 + [3k(1 - \nu^2)/k_b]\left(1 + \frac{\eta}{t}\right) \right]}{Et\eta} \frac{2G}{2G} \tau_{av}\ell = \frac{\gamma_p}{\left(\frac{\ell - d}{2}\right)} \frac{1}{\gamma_e} \frac{\tau_p}{G} + 2(\lambda')^2\left(\frac{\ell - d}{2}\right) K \frac{\tau_p}{G}, \tag{78}$$

$$\left[1 + \frac{3k(1 - \nu^2)}{k_b}\left(1 + \frac{\eta}{t}\right) \right] \frac{\tau_{av}}{\tau_p}(\lambda\ell)\lambda\left(\frac{\ell - d}{2}\right) = 2\left(\frac{\gamma_p}{\gamma_e}\right) + K\left[2\lambda'\left(\frac{\ell - d}{2}\right) \right]^2 \tag{79}$$

$$= 4\left(\frac{\gamma_p}{\gamma_e}\right) - 4K(\lambda')\left(\frac{\ell - d}{2}\right)\tanh(\lambda' d) \quad . \tag{80}$$

Equation (69) yields the solution

$$\frac{\tau_{av}}{\tau_p}(\lambda'\ell) = 2\lambda'\left(\frac{\ell - d}{2}\right) + (1 - K)(\lambda' d) + K\tanh(\lambda' d) \tag{81}$$

$$= 2\lambda'\left(\frac{\ell - d}{2}\right) + \tanh(\lambda' d) + (1 - K)[\lambda' d - \tanh(\lambda' d)] \quad . \tag{82}$$

The precise solution of equations (77) to (82) to eliminate K and d requires numerical solution, and a digital computer program to accomplish this for isotropic adherends has been developed.

Two salient features of the solution, however, do prove amenable to analytic investigation. These are the important criteria of the maximum load a joint could potentially carry as the overlap is increased indefinitely, and the maximum extent of overlap throughout which fully-plastic adhesive deformation can be maintained. For very long overlaps, equation (58) indicates that $k \to 0$. From equations (77) and (79), then, with $\tanh(\lambda' d) \to 1$,

$$\frac{\tau_{av}}{\tau_p}(\lambda\ell)\lambda\left(\frac{\ell - d}{2}\right) = 8K\left[\lambda'\left(\frac{\ell - d}{2}\right)\right]^2 + 4K\lambda'\left(\frac{\ell - d}{2}\right) \quad . \tag{83}$$

Therefore, eliminating τ_{av}/τ_p by means of equation (79),

$$\left[4K - \left(\frac{\lambda}{\lambda'}\right)^2\right]\left[2\lambda'\left(\frac{\ell - d}{2}\right) + 1\right] = (1 - K)\left(\frac{\lambda}{\lambda'}\right)^2(\lambda' d - 1) \quad . \tag{84}$$

From physical reasoning and equation (71) it is evident that $K \to 1$ as $\lambda'\ell \to \infty$ since, otherwise, the uniform shear stress component C_2 in the elastic region would cause the joint strength to increase indefinitely with increasing overlap. The left-hand side of equation (83) is therefore finite, since the adhesive strain capability limits $\lambda'(\ell - d)/2$, so that the otherwise indeterminate right-hand side can be evaluated. Returning now to equation (82),

$$\frac{\tau_{av}}{\tau_p}(\lambda'\ell) \to \left[5 - \left(\frac{\lambda}{\lambda'}\right)^2\right]\left[2\lambda'\left(\frac{\ell - d}{2}\right) + 1\right] \to 4\sqrt{1 + 2\left(\frac{\gamma_p}{\gamma_e}\right)} \quad , \text{ as } \lambda'\ell \to \infty \; . \tag{85}$$

This is twice as strong as for the corresponding double-lap joint between isotropic adherends (Reference 12), the reason being that 3/4 of the load is carries in the elastic region for the very long single-lap joint while practically none is carried in the elastic trough for long double-lap joints. The extent of plastic deformation in the adhesive at each end of the balanced single-lap joint follows from equation (77),

$$2\lambda'\left(\frac{\ell - d}{2}\right) \rightarrow \sqrt{1 + 2\frac{\gamma_p}{\gamma_e}} - 1 \quad . \tag{86}$$

This is only half as long as for the equivalent double-lap joint for isotropic adherends which is why, in practice, single-lap bonded joints do not develop higher average shear stresses than do double-lap joints.

For the fully-plastic joint, $d \equiv 0$ and, from equations (63), (64), (65) and (68), with $\tau_{av} = \tau_p$,

$$\lambda\ell \leq \sqrt{\frac{4\left(2\frac{\gamma_e}{\gamma_p}\right)}{1 + \frac{3k(1-\nu^2)}{k_b}\left(1 + \frac{\eta}{t}\right)}} \tag{87}$$

Again, for short overlaps for which $k \approx 1$, the maximum possible extent of plastic adhesive deformation (for isotropic adherends) is only one half as great as in the double-lap joint (Reference 12). This comparison and those preceding it are made with respect to isotropic adherends ($k_b = 1$ and $\lambda' = \lambda$) in order to compare the behavior of the two joint classes without adding complexities peculiar to a particular non-isotropic material.

In solving simultaneously equations (58), (77), (79) and (82), significant algebraic manipulation proves to be necessary. Since shear-stress governed failures are unusual even for metal adherends and rare for filamentary composite adherends, the remainder of this section on adhesive shear stresses is confined to isotropic adherends in order to simplify the procedures and remove one variable from the solution. The failure of single-lap joints between composite adherends is usually governed by peel stress considerations for thick adherends, so the extensional and bending stiffnesses of the adherends are uncoupled for

that problem, in Section 7. Adhesive shear failures of single-lap bonded joints are confined to thinner sections. For isotropic adherends ($k_b = 1$ and $\lambda' = \lambda$) it can be shown that, precisely,

$$\frac{\tau_{av}}{\tau_p}(\lambda\ell) = \frac{4K}{\left|1 + 3k(1-\nu^2)\left(1+\frac{\eta}{t}\right)\right|}\left[\tanh^2(\lambda d) + \frac{2\gamma_p}{K\gamma_e}\right]^{\frac{1}{2}} \tag{88}$$

$$= \frac{4K}{\left|1 + 3k(1-\nu^2)\left(1+\frac{\eta}{t}\right)\right|}\left[2\lambda\left(\frac{\ell - d}{2}\right) + \tanh(\lambda d)\right] \tag{89}$$

and that

$$\tanh^2(\lambda d) + \frac{2\gamma_p}{K\gamma_e} = \left\{\frac{1-K}{\dfrac{4K}{1 + 3k(1-\nu^2)\left(1+\frac{\eta}{t}\right)} - 1}\right\}^2 \left|\lambda d - \tanh(\lambda d)\right|^2 , \tag{90}$$

while

$$\lambda\ell = \lambda d + 2\lambda\left(\frac{\ell - d}{2}\right) = \left|\tanh^2(\lambda d) + \frac{2\gamma_p}{K\gamma_e}\right|^{\frac{1}{2}} + \lambda d - \tanh(\lambda d) \tag{91}$$

$$= \left\{\frac{\dfrac{4K}{1 + 3k(1-\nu^2)\ 1 + \frac{\eta}{t}} - K}{\dfrac{4K}{1 + 3k(1-\nu^2)\ 1 + \frac{\eta}{t}} - 1}\right\}[\lambda d - \tanh(\lambda d)] . \tag{92}$$

Given the correct value of k, one can assume a value of λd, compute K by means of equation (90), $\lambda\ell$ from equation (92), and $(\tau_{av}/\tau_p)\lambda\ell$ from equation (88). An iterative process must be used because of the indeterminacy of k:

$$k = 1/[1 + \frac{\xi\ell}{2} + \frac{1}{6}(\frac{\xi\ell}{2})^2] \qquad \text{in which} \qquad \xi^2 = \tau_{av}\ell/D . \tag{93}$$

Since a useful design chart is of the form load versus lap length with all other parameters held constant, it is desirable to non-dimensionalize the terms involved. Accordingly,

$$\left(\frac{\xi\ell}{2}\right)^2 = \left(\frac{\tau_{av}}{D}\right)\frac{\ell^2}{4} = \frac{\tau_{av}}{\tau_p}(\lambda\ell)(\lambda\ell)^2\frac{\tau_p}{4D\lambda^3} , \tag{94}$$

where $D = Et^3/[12(1-\nu^2)]$ is the bending stiffness of the adherend. The eccentricity parameter $\tau_p/4D\lambda^3$ * is found to range from 10^{-4} to 10^{-1} in the regime of practical concern. To reduce the number of variables involved, the approximation $[1 + (a/t)] \approx 1$ is utilized.

The adhesive shear stresses derived from the analysis above are developed on the assumption that the adherend still behaves elastically at the failure of the adhesive and that the adhesive fails in shear rather than in peel. The experimental evidence, on the other hand, indicates that significant adherend yielding frequently occurs prior to adhesive failure with metal adherends and that, for filamentary composite adherends, the failure is usually confined to the laminate(s) because it originated as the result of either transverse tension or the stretching and bending due to the eccentric load path. Such observations lead one to question the wisdom of interpreting test data on single-lap joints in terms of adhesive shear stresses. The same question may be raised about design except when using test data pertaining to the precise configuration involved. Nevertheless, since it is not possible to prove the universal impossibility of an adhesive shear failure in a single-lap joint, it is appropriate to illustrate the potential shear strengths of adhesive bonds. The computations were restricted to isotropic adherends because of the coupling between extensional and bending stiffnesses of the adherend(s). The solution is non-dimensionalized to minimize the number of graphs required. Figures 8 through 15 depict the potential adhesive shear strength of single-lap bonded joints. Figure 8 portrays, for a typical ductile adhesive, the effect of variation in adherend properties. It is apparent that higher adherend bending stiffnesses impose greater strain concentrations on the adhesive than do low bending stiffnesses. It is evident also that extremely great overlaps are required to approach the maximum (asymptotic) strength which is four times as great as that for joints of very short overlap. This phenomenon is quite diff-

---

* The eccentricity parameter $\tau_p/4D\lambda^3$ characterizes the decay rate of the influence of the eccentricity. The physical eccentricity is associated more with the inverse of this parameter. Consideration was given to using the inverse parameter, so that an increasing eccentricity would be associated with increasing values of the characterizing coefficient, but the fact that the eccentricity cannot range from zero to infinity led to the approach adopted here.

erent from that for double-lap joints in which only the adherend extensional stiffness (and not the bending stiffness) affects the potential bond shear strength, which does not increase steadily with increasingly long overlaps. Figure 9 illustrates the influence of the adhesive characteristics on the potential bond shear strength, which is seen to increase steadily with increasing adhesive plasticity. Just as for double-lap joints, the bond strength is related to the strain energy of the adhesive in shear. Figure 9 includes, for each adhesive plastic-to-elastic strain capability, the range of influence of the adherend properties. An assessment of the values of the physical quantities involved indicates that the full range of the eccentricity parameter (τ_y/Et^3) is encountered in practice and that there is essentially no difference in effect between unity and infinity for this parameter for the non-dimensionalized overlaps greater than those for which the adhesive behaves fully plastically throughout. Figures 10 to 15 present the adhesive bond potential shear strengths in non-dimensionalized form, for an adequate range of values of the parameters involved to encompass design practice.

For practical design purposes it is not necessary to construct the entire adhesive shear strength characteristic. It usually suffices to check that, for the given adherends, the potential bond shear strength at the transition from fully-plastic behavior exceeds the adherend strength for that particular overlap. The excess strength will be greater still for longer overlaps.

The adhesive shear stress analysis above pertains to tensile and to compressive lap shear. It accounts for the bending moments at the ends of the overlap which are responsible for much lower efficiencies than are developed on one side of a double-lap bonded joint. The in-plane shear loading of single-lap joints does not develop such eccentricities in the load path and is therefore covered by the double-lap joint analysis. Full details are to be found in Reference 12. Briefly, the normal adherend properties E are replaced by the shear properties G with the same form of differential equation governing the solution.

5. ADHESIVE PEEL STRESS DISTRIBUTIONS FOR BALANCED ADHERENDS

The analysis of peel stresses for double-lap adhesive-bonded joints in Reference 12 indicated that interlaminar tension was the dominant failure mode for thick composite adherends. Even higher peel stresses are induced for single-lap bonded joints, so it is appropriate to analyze these also. The tension stress in the adhesive is assumed to remain elastic for two reasons. First, for composite adherends, the adherend is much weaker in transverse tension than is the adhesive in peel. Consequently the adherend will fail as soon as the adhesive develops its peak peel stress in any one location (at the end(s) of the overlap) rather than holding on until the peak peel stress spreads over a greater area through yielding of the adhesive. Second, the adhesives are long-chain polymers and essentially incompressible. Therefore, the stiff in-plane constraints imposed on the adhesive film by the adjacent adherends effectively suppress any plastic deformation in the adhesive except at the periphery of the bond. Such phenomena are particularly difficult to account for analytically (and probably more difficult to quantify precisely by experiment), so it is sensible to start by seeking empirical correction factors to purely elastic analyses of the peel stress problem. If such correlation factors prove to be close to unity there is no need for a more elaborate analysis including plastic peel effects. Further support for the purely-elastic peel-stress approach derives from the fact that the behavior for composite adherends is governed not by the adhesive peel modulus alone but by an effective value including the effect of the finite stiffness of the proportionally much thicker adherends.

The analysis of peel stresses commences with the straightforward case of identical adherends, for which the differential equation governing the peel stress distribution along the joint is uncoupled from that pertaining to the shear stress distribution. The case of dissimilar adherends is covered in Section 8. The nomenclature and sign convention necessary for the present analysis are to be found in Figures 2 and 7. The basic equations are established in Section 2 above. From equations (13), (10), (11), (7) and (9) it can be shown that the peel stress equation is deduced by the following sequence.

$$\left(\frac{\eta}{E_c}\right)\frac{d^2\sigma_c}{ds^2} = \frac{d^2w_3}{ds^2} - \frac{d^2w_2}{ds^2} = -\frac{1}{D}(M_3 - M_2) = \frac{12(1-\nu^2)}{k_b E t^3}(M_3 - M_2) \qquad (95)$$

and

$$\left(\frac{k_b E t^3 \eta}{12(1-\nu^2)E_c}\right)\frac{d^3\sigma_c}{ds^3} = -(V_3 - V_2) \quad , \qquad (96)$$

whence

$$\frac{d^4\sigma_c}{ds^4} + 4\chi^4\sigma_c = 0 \qquad (97)$$

where

$$\chi^4 = \frac{E_c}{2\eta D} = \frac{6E_c(1-\nu^2)}{Et^3\eta k_b} \quad . \qquad (98)$$

This parameter is essentially the same as that for double-lap joints [equations (69) and (70) of Reference 12], just as was found for the parameter λ governing the shear stress distributions [see equations (25) and (26) here and equations (28) and (29) of Reference 12].

Symmetry of the peel stress distribution about the middle of the overlap for the identical adherends considered here reduces the solution of equation (97) to the form

$$\sigma_c = A\cos(\chi s)\cosh(\chi s) + B\sin(\chi s)\sinh(\chi s) \qquad (99)$$

when the origin of the s co-ordinate is now taken at the middle of the overlap. The boundary conditions determining the integration constants A and B are that there be zero resultant transverse force across the bond line, that is

$$\int_{-c}^{+c} \sigma_c ds = 0 \quad , \qquad (100)$$

and that the bending moment M_o is known, from Section 1, at the end of the joint. From equation (100), then,

$$A[\sin(\chi c)\cosh(\chi c) + \cos(\chi c)\sinh(\chi c)] + B[\sin(\chi c)\cosh(\chi c) - \cos(\chi c)\sinh(\chi c)] = 0, \qquad (101)$$

so that, for all but very short overlaps,

$$A[\sin(\chi c) + \cos(\chi c)] \simeq - B[\sin(\chi c) - \cos(\chi c)] \quad . \tag{102}$$

The simplification (102) follows from the approximation

$$\sinh(\chi c) \simeq \cosh(\chi c) \rightarrow \frac{1}{2} e^{(\chi c)} \tag{103}$$

for moderately long, or longer, overlaps. The incorporation of the bending moment condition can be understood from Figure 2. At $s = + c$,

$$M_2 \equiv 0 \qquad \text{and} \qquad M = M_o \quad , \tag{104}$$

with M_o being evaluated in equation (39). Now, from equations (13) and (10),

$$\frac{E_c M_o}{\eta D} \simeq \left.\frac{d^2\sigma_c}{ds^2}\right|_{+c} = - 2A\chi^2 \sin(\chi c)\sinh(\chi c) + 2B\chi^2 \cos(\chi c)\cosh(\chi c) \tag{105}$$

$$\simeq - \chi^2 e^{(\chi c)}[A \sin(\chi c) - B \cos(\chi c)] \quad . \tag{106}$$

Now, from equations (102) and (106),

$$A \sin(\chi c) - B \cos(\chi c) \simeq \frac{A}{[\sin(\chi c) - \cos(\chi c)]} \times$$

$$[\sin^2(\chi c) - \sin(\chi c)\cos(\chi c) + \sin(\chi c)\cos(\chi c) + \cos^2(\chi c)] \tag{107}$$

$$= A / [\sin(\chi c) - \cos(\chi c)] \tag{108}$$

$$= - E_c M_o / [\eta D \chi^2 e^{(\chi c)}] \quad . \tag{109}$$

Also,

$$\sigma_{c_{max}} \simeq \frac{1}{2} e^{(\chi c)}[A \cos(\chi c) + B \sin(\chi c)] \tag{110}$$

according to equation (99) and, from equation (102),

$$A \cos(\chi c) + B \sin(\chi c) \simeq \frac{A}{[\sin(\chi c) - \cos(\chi c)]} \times$$

$$[\sin(\chi c)\cos(\chi c) - \cos^2(\chi c) - \sin^2(\chi c) - \sin(\chi c)\cos(\chi c)] \tag{111}$$

$$= - A / [\sin(\chi c) - \cos(\chi c)] \quad . \tag{112}$$

Therefore, from equation (39),

$$\sigma_{c_{max}} = \frac{E_c}{2\eta} \frac{M_o}{D\chi^2} = \frac{E_c k}{2\eta D\chi^2} P \frac{t}{2}\left(1 + \frac{\eta}{t}\right) \tag{113}$$

or, in non-dimensionalized form,

$$\frac{\sigma_{c_{max}}}{\sigma_{av}} = k\left(1 + \frac{\eta}{t}\right)\left|\frac{3E_c(1-\nu^2)t}{2k_b En}\right|^{\frac{1}{2}} \quad . \tag{114}$$

The corresponding result for double-lap joints [equation (83) of Reference 12] shows both marked similarities and dissimilarities. For peel-stress governed failures of double-lap joints,

$$\frac{\sigma_{c_{max}}}{\tau_p} = \left|\frac{3E_c(1-\nu^2)t_o}{En}\right|^{\frac{1}{4}} \quad . \tag{115}$$

Essentially the same parameter ($E_c t/En$) governs the peel behavior of both joint classes, but single-lap joints are more sensitive to this effect because of the exponent 1/2 instead of 1/4. More importantly, the unsupported single-lap joint peel stresses are an order of magnitude higher than for double-lap joints between similar adherends. That this is so is evident from a comparison of the left-hand sides of equations (115) and (114). The double-lap peel stresses are non-dimensionalized with respect to the peak (plastic) adhesive shear stress while those for single-lap joints are expressed with respect to the very much higher average adherend stresses outside the joint. Furthermore, it is shown in Section 7 how any adherend stiffness imbalance increases the single-lap peel stresses still further.

Figure 16 depicts the solution of equations (114) and (39) computed for isotropic (metal) adherends. Two dominant influences are acting. The first is that very long overlaps can be employed successfully to minimize peel stresses regardless of all other factors. This is quite different from the double-lap joint behavior in which the overlap has essentially no influence on the peel stresses. The overlap length effect for single-lap joints is manifest through the parameter k in equation (114). The second major phenomenon is associated with both single- and double-lap joints and is that thicker adherends and/or stiffer (more brittle) adhesives aggravate the peel stress problem. A quantitative assessment of the data presented in Figure 16 shows that for aluminum alloys, for example, ℓ/t ratios in excess of 30 may be required to reduce the peel stress problem to a tolerable level, with even greater ℓ/t ratios required for thick adherends.

The influence of uncoupling the adherend bending and extensional stiffnesses of

advanced composite adherends is effected through the bending parameter k_b in equations (114) and (39). Laminates having those fibers aligned along the load direction near the outside of the adherend ($k_b > 1$) are less severely affected by peel stress problems than are the more flexible adherends with the same fibers grouped near the neutral axis of the laminate ($k_b < 1$). This distinction is pronounced only for thin laminates (of four plies or so) because the low interlaminar strength of composite resins precludes the bunching together of large numbers of plies having a common orientation with only a single matrix interface between such groups. In other words, a laminate such as $(0°_n/\pm 45°_n/0°_n)$ is prone to split apart at the changes in fiber orientation whereas the re-arrangement into the form $(0°/\pm 45°/0°)_n$ forms a structurally sound laminate. Because of this factor, major deviations from $k_b \approx 1$ are not practical for even moderately thick sections. The physical sources of these limitations are two-fold. In the first place, the widely dissimilar thermal coefficients of expansion can induce considerable residual stresses into a poorly designed laminate not having thoroughly interspersed cross-plies while the laminate is cooling down after curing at the normal elevated temperature. Secondly, resin matrices have relatively little strength in themselves and the application of mechanical loads to the same poorly conceived laminates tends to overload the few active interfaces for in-plane shear transfer.

The most important observations about peel stresses in single-lap adhesive-bonded joints are that they can be severe and are far more important than are the associated shear stresses. Also, very large ℓ/t ratios are needed to alleviate the problem.

6. JOINT EFFICIENCIES FOR BALANCED SINGLE-LAP JOINTS

The preceding analyses have established that, for unsupported single-lap adhesive-bonded joints, the joint (or the adherend immediately outside the overlap) cannot possibly be as strong as the potential strength far removed from the joint area. In other words, the joint efficiency of uniform-thickness single-lap structures is necessarily significantly less than unity. The other highlights of the analyses are the powerful influence of the ℓ/t ratio, the usually negligible impact of the adhesive shear stresses, and the change in mode of failure from failure of thin adherends just outside the joint because of combined direct and bending loads to failure of thick adherends due to peel or transverse tension stresses at the end(s) of the overlap. These various phenomena are illustrated in Figures 17 and 18 for aluminum adherends with representative 350 °F curing ductile and brittle adhesives. Figures 19 to 24 show the corresponding efficiencies for representative HTS graphite-epoxy laminates. The various material properties employed in preparing these graphs are recorded in Table I, and the digital computer program employed in their preparation is listed in the Appendix. (Strictly, the composite characteristics cannot be continuous for small numbers of plies of standard thickness in balanced laminates, and account should be taken of non-unity values of k_b for accurate design purposes. Inclusion of these considerations would tend to complicate and confuse the presentations of Figures 19 to 24, so they were omitted. Therefore, these figures should not be used for design purposes for very thin laminates.) These joint efficiency charts demonstrate how large overlaps and ductile adhesives minimize the structural efficiency loss caused by unsupported single-lap joints.

In addition to illustrating the extent of the single-lap joint problem, these same Figures 17 to 24 suggest a straightforward design technique to overcome (or at least minimize) the problems. The simple concept is illustrated in Figure 25 and would still be a considerable improvement even if the eccentricity were not minimized as shown by effecting a smooth joggle in the adherends. The application of this design technique to achieve adequate joint efficiencies is as follows. The first step starts either with a known load to be transmitted or specified adherends to be bonded. In either event, the joint load and

minimum adherend thickness far outside the joint can be established by neglecting the eccentricity in the load path. Then the charts are examined to find thicker adherends and an appropriate ℓ/t ratio which could carry the load so specified (with uniform thicker adherends inefficiently loaded outside the joint). To match the efficiencies of this thick joint and the thin adherends, it is simply necessary to effect a smooth transition as shown in Figure 25. That such a design technique is inevitably conservative with respect to the overlap area is readily confirmed by realizing that the more flexible adherends outside the joint will reduce the critical bending moment M_o below that associated with uniform thick adherends. On the other hand, equations (2) and (4) indicate that, no matter how long the transition between thicknesses is made, there will remain at least slight bending moments in the thin adherends outside the joint area. It would be a mistake not to allow for less than perfect efficiency outside the joint. However, arbitrarily accepting a maximum efficiency of say 70 to 80 per cent represents a very great improvement over the potential of 20 to 30 per cent without such stress concentration relief.

Figures 17 to 24 afford an interesting comparison with their counterparts [Figures 20 and 21 of Reference 12] for double-lap joints. There is simply no similarity other than that thick adherends cannot possibly be bonded together efficiently by uniform lap joints and that ductile adhesives are more efficient than brittle ones, both as regards shear stresses and peel stresses. Thin double-lap joints have a potential bond strength far in excess of the adherend strength. Also, the overlap length has no influence on double-lap joint strength once a relatively small minimum value necessary to develop the full strength has been exceeded. This indicates that the best way to deal with the problem of eccentricity in the load path of unsupported single-lap joints is to support them against rotation, thereby increasing the joint efficiency to approach that for half (one side) of a double-lap joint.

7. EFFECT OF ADHEREND STIFFNESS IMBALANCE ON ADHEREND FAILURES JUST OUTSIDE THE JOINT

As a result of any stiffness imbalance between the adherends it is obvious that the "thinner" adherend (of lower bending stiffness) will undergo greater transverse deflections than will the "thicker" adherend. The bending moments at each end of the joint will not be identical and a more general analysis than that used for identical adherends will be required. While an explicit analytical analysis proves to be quantitatively intractable, an iterative digital computer solution of the implicit equations can be achieved quite simply. The analyses above, together with the experimental evidence, have indicated the prime importance of the adherend bending stresses in determining the maximum joint load capacities, so these will be examined first.

The geometry and nomenclature pertaining to this analysis remain substantially as illustrated in Figure 2. It should be noted that, in general, the line of action of the applied loads intercepts the bond line eccentrically with respect to the center of the joint. While this problem could be analyzed with respect to any arbitrary reference axes, a careful choice of axes permits of a great simplification of the analysis. The location of the origin for the s co-ordinate is taken to be at that point O at which the bending moments in the adherends are zero: in other words, the line of action of the load passes through the "centroid" of the gross cross section. Whether O lies to the right or left of C, in Figure 26, is immaterial to the analysis. Fortunately it is established early in the analysis that, regardless of the joint geometry and material properties, O must lie within the lap region, between B and D. There proves to be no justification in considering a hypothetical situation in which $|e| \geq |c|$. The stiffness "centroid" lies between the centers of adherends 1 and 4 and it is relatively easily established that the transverse distance from the middle of adherend 1 is

$$EC_1 = \frac{\frac{1}{2}(t_1 + t_4 + 2t_i)}{\left(1 + \frac{E_1 t_1}{E_4 t_4}\right)} , \qquad (116)$$

while the transverse distance from the middle of adherend 4 is

$$EC_4 = \frac{\frac{1}{2}(t_1 + t_4 + 2\eta)}{\left(1 + \frac{E_4 t_4}{E_1 t_1}\right)} \tag{117}$$

The axial location of O with respect to the middle of the joint is arbitrarily identified by the (as yet unspecified) length e.

Throughout the adherend 1, the longitudinal stress resultant (force per unit lateral width) is uniform, at the value P. The stress couple M_1, per unit width, is then defined by the equilibrium equation

$$M_1 = P\left[\frac{(t_1 + t_4 + 2\eta)}{(\ell_1 + c + e)\left(1 + \frac{E_1 t_1}{E_4 t_4}\right)}\left(\frac{x_1}{2}\right) - w_1\right] \qquad \text{for } 0 \le x_1 \le \ell_1. \tag{118}$$

The classical theory for the infinitesimal bending of thin, cylindrically deformed plates then yields

$$\frac{d^2 w_1}{dx_1^2} = -\frac{M_1}{D_1} = -\frac{P}{D_1}\left[\frac{(t_1 + t_4 + 2\eta)}{(\ell_1 + c + e)\left(1 + \frac{E_1 t_1}{E_4 t_4}\right)}\left(\frac{x_1}{2}\right) - w_1\right] , \tag{119}$$

whence

$$w_1 = A_1 \cosh(\xi_1 x_1) + B_1 \sinh(\xi_1 x_1) + \frac{(t_1 + t_4 + 2\eta)}{(\ell_1 + c + e)\left(1 + \frac{E_1 t_1}{E_4 t_4}\right)}\left(\frac{x_1}{2}\right) , \tag{120}$$

where

$$(\xi_1)^2 = \frac{P}{D_1} = \frac{12P(1 - \nu_1^2)}{(k_b)_1 E_1 t_1^3} . \tag{121}$$

The assumption of negligible moment restraint at x = 0 (or, equivalently, that ℓ_1 is so large in comparison with c that the precise nature of the end conditions is immaterial) prescribes that

$$A_1 = 0 . \tag{122}$$

Similarly, for the other adherend, outside the joint,

$$M_4 = P\left[\frac{(t_1 + t_4 + 2\eta)}{(\ell_4 + c - e)\left(1 + \frac{E_4 t_4}{E_1 t_1}\right)}\left(\frac{x_4}{2}\right) - w_4\right] \qquad \text{for } -\ell_4 \le x_4 \le 0 \quad (123)$$

and

$$\frac{d^2 w_4}{dx_4^2} = -\frac{M_4}{D_4} = -\frac{P}{D_4}\left[\frac{(t_1 + t_4 + 2\eta)}{(\ell_4 + c - e)\left(1 + \frac{E_4 t_4}{E_1 t_1}\right)}\left(\frac{x_4}{2}\right) - w_4\right] , \quad (124)$$

whence

$$w_4 = B_4 \sinh(\xi_4 x_4) + \frac{(t_1 + t_4 + 2\eta)}{(\ell_4 + c - e)\left(1 + \frac{E_4 t_4}{E_1 t_1}\right)}\left(\frac{x_4}{2}\right) \quad (125)$$

where

$$(\xi_4)^2 = \frac{P}{D_4} = \frac{12P(1 - \nu_4^2)}{(k_b)_4 E_4 t_4^3} . \quad (126)$$

It is now possible to establish that $|e| < |c|$. The location O was defined as that point between A and E for which the bending moment is zero. Examination of equation (119) indicates that d^2w_1/dx_1^2 cannot be zero in the range $0 < x_1 \le \ell_1$. Hence the location of O must lie to the right of B. Likewise, d^2w_4/dx_4^2 cannot be zero in the range $-\ell_4 \le x_4 < 0$ so that O must lie to the left of D. Consequently, O must be located within the extent of the overlap.

The behavior of regions 2 and 3 (Figure 26) is governed by much the same equations as for balanced joints between identical adherends, equations (7) to (14). Due allowance must be given to the different thicknesses, however, so that

$$\left.\begin{aligned} \frac{dM_2}{ds} - V_2 + \tau\left(\frac{t_1 + \eta}{2}\right) &= 0 \\ \frac{dM_3}{ds} - V_3 + \tau\left(\frac{t_4 + \eta}{2}\right) &= 0 \end{aligned}\right\} , \quad (127)$$

$$\left.\begin{aligned} \frac{dT_2}{ds} + \tau &= 0 \\ \frac{dT_3}{ds} - \tau &= 0 \end{aligned}\right\} , \tag{128}$$

$$\left.\begin{aligned} \frac{dV_2}{ds} + \sigma_c &= 0 \\ \frac{dV_3}{ds} - \sigma_c &= 0 \end{aligned}\right\} , \tag{129}$$

$$\left.\begin{aligned} \frac{d^2w_2}{ds^2} &= -\frac{M_2}{D_1} = -\frac{12M_2(1-\nu_1^2)}{(k_b)_1 E_1 t_1^3} \\ \frac{d^2w_3}{ds^2} &= -\frac{M_3}{D_4} = -\frac{12M_3(1-\nu_4^2)}{(k_b)_4 E_4 t_4^3} \end{aligned}\right\} . \tag{130}$$

As in Section 2, it is necessary to use the evaluation techniques

$$\left.\begin{aligned} w_2 &= \tfrac{1}{2}(w_2 + w_3) + \tfrac{1}{2}(w_2 - w_3) \\ w_3 &= \tfrac{1}{2}(w_2 + w_3) - \tfrac{1}{2}(w_2 - w_3) \end{aligned}\right\} . \tag{131}$$

From the equations above,

$$\frac{d^2(w_2 + w_3)}{ds^2} = -\frac{M_2}{D_1} - \frac{M_3}{D_4} , \tag{132}$$

$$\frac{d^3(w_2 + w_3)}{ds^3} = -\frac{V_2}{D_1} + \frac{\tau}{D_1}\left[\frac{t_1 + \eta}{2}\right] - \frac{V_3}{D_4} + \frac{\tau}{D_4}\left[\frac{t_4 + \eta}{2}\right] , \tag{133}$$

$$\frac{d^4(w_2 + w_3)}{ds^4} = \frac{\sigma_c}{D_1} - \frac{\sigma_c}{D_4} + \left[\frac{t_1 + \eta}{2D_1} + \frac{t_4 + \eta}{2D_4}\right]\frac{d\tau}{ds} , \tag{134}$$

$$\frac{d^2(w_2 - w_3)}{ds^2} = -\frac{M_2}{D_1} + \frac{M_3}{D_4} , \tag{135}$$

and, since for an adhesive obeying a linear elastic law in tension (peeling)

$$\frac{\sigma_c}{E_c} = \frac{w_3 - w_2}{\eta} , \tag{136}$$

$$\frac{d^4(w_2 - w_3)}{ds^4} = -\left[\frac{1}{D_1} + \frac{1}{D_4}\right]\frac{E_c}{\eta}(w_2 - w_3) + \left[\frac{t_1 + \eta}{2D_1} - \frac{t_4 + \eta}{2D_4}\right]\frac{d\tau}{ds} \quad . \qquad (137)$$

A comparison of equations (134) and (137) with the corresponding equaticns (18) and (19) for balanced-stiffness adherends reveals that the imbalance couples the adhesive shear and peeling stresses, greatly complicating the analysis. In order to proceed explicitly, rather than implicitly (by numerical analyses), it proves convenient nct to attempt to satisfy the differential equation (134) for all values of s but to adopt, instead, an assumed solution with sufficient integration constants to satisfy the dominant boundary conditions at the ends of the joint. Such a procedure is analogous to the assumption of deflection modes in beam and plate theory when using the Ritz or Stodola methods. The simplest such solution is the polynomial

$$\tfrac{1}{2}(w_2 + w_3) \simeq A_{23}s^3 + B_{23}s^2 + C_{23}s + F_{23} \quad . \qquad (138)$$

The conditions $M_2 = M_3 \equiv 0$ at $s = 0$ permit the setting of

$$B_{23} = F_{23} = 0 \quad . \qquad (139)$$

As in Section 2, it is assumed that

$$\frac{dw_2}{ds} \simeq \frac{dw_3}{ds} \qquad \text{at} \quad s = -(c + e) \quad \text{and} \quad s = (c - e) \qquad (140)$$

but that the distinction between the second derivatives is vital since

$$\frac{d^2w_2}{ds^2} = -\frac{M_{o1}}{D_1} \quad , \quad \frac{d^2w_3}{ds^2} \equiv 0 \qquad \text{at } s = -(c + e) \qquad (141)$$

and

$$\frac{d^2w_3}{ds^2} = +\frac{M_{o4}}{D_4} \quad , \quad \frac{d^2w_2}{ds^2} \equiv 0 \qquad \text{at} \quad s = (c - e) \quad . \qquad (142)$$

(Note the sign convention for positive values of M_{04}). The pertinent boundary conditions prove to be, at $x_1 = \ell_1$, $s = -(c + e)$,

$$w_1 = B_1 \sinh(\xi_1\ell_1) + \left(\frac{t_1 + t_4 + 2\eta}{\ell_1 + c + e}\right)\frac{1}{\left(1 + \dfrac{E_1t_1}{E_4t_4}\right)}\left(\frac{\ell_1}{2}\right)$$

$$\simeq \tfrac{1}{2}(w_2 + w_3) = -A_{23}(c + e)^3 - C_{23}(c + e) \quad , \qquad (143)$$

$$\frac{dw_1}{dx_1} = B_1\xi_1 \cosh(\xi_1\ell_1) + \left(\frac{t_1 + t_4 + 2\eta}{\ell_1 + c + e}\right)\frac{1}{\left(1 + \frac{E_1t_1}{E_4t_4}\right)}\left(\frac{1}{2}\right)$$

$$\simeq \frac{1}{2}\frac{d(w_2 + w_3)}{ds} = 3A_{23}(c + e)^2 + C_{23} \quad , \tag{144}$$

$$\frac{d^2w_1}{dx_1^2} = -\frac{M_{o1}}{D_1} = B_1\xi_1^2 \sinh(\xi_1\ell_1)$$

$$= \frac{1}{2}\frac{d^2(w_2 + w_3)}{ds} + \frac{1}{2}\frac{d^2(w_2 - w_3)}{ds} = -6A_{23}(c + e) - \frac{M_{o1}}{2D} \tag{145}$$

and, for sufficiently large $(\xi_1\ell_1)$,

$$\sinh(\xi_1\ell_1) \simeq \cosh(\xi_1\ell_1) \simeq \frac{1}{2}e^{(\xi_1\ell_1)} \quad , \tag{146}$$

while, at $x_4 = -\ell_4$, $s = (c - e)$,

$$w_4 = -B_4 \sinh(\xi_4\ell_4) - \left(\frac{t_1 + t_4 + 2\eta}{\ell_4 + c - e}\right)\frac{1}{\left(1 + \frac{E_4t_4}{E_1t_1}\right)}\left(\frac{\ell_4}{2}\right)$$

$$\simeq \frac{1}{2}(w_2 + w_3) = A_{23}(c - e)^3 + C_{23}(c - e) \quad , \tag{147}$$

$$\frac{dw_4}{dx_4} = +B_4\xi_4 \cosh(\xi_4\ell_4) + \left(\frac{t_1 + t_4 + 2\eta}{\ell_4 + c - e}\right)\frac{1}{\left(1 + \frac{E_4t_4}{E_1t_1}\right)}\left(\frac{1}{2}\right)$$

$$\simeq \frac{1}{2}\frac{d(w_2 + w_3)}{ds} = 3A_{23}(c - e)^2 + C_{23} \quad , \tag{148}$$

$$\frac{d^2w_4}{dx_4^2} = +\frac{M_{o4}}{D_4} = -B_4\xi_4^2 \sinh(\xi_4\ell_4)$$

$$= \frac{1}{2}\frac{d^2(w_2 + w_3)}{ds^2} - \frac{1}{2}\frac{d^2(w_2 - w_3)}{ds^2} = 6A_{23}(c - e) + \frac{M_{o4}}{2D_4} \tag{149}$$

and, again, for sufficiently large $(\xi_4\ell_4)$,

$$\sinh(\xi_4\ell_4) \simeq \cosh(\xi_4\ell_4) \simeq \frac{1}{2}e^{(\xi_4\ell_4)} \quad . \tag{150}$$

According to the boundary conditions pertaining,

$$M_{o1}[1 + \xi_1(c + e) + \tfrac{1}{6}\xi_1^2(c + e)^2] = \frac{P}{2}\left[\frac{t_1 + t_4 + 2\eta}{1 + \dfrac{E_1 t_1}{E_4 t_4}}\right], \tag{151}$$

$$M_{o4}[1 + \xi_4(c - e) + \tfrac{1}{6}\xi_4^2(c - e)^2] = \frac{P}{2}\left[\frac{t_1 + t_4 + 2\eta}{1 + \dfrac{E_4 t_4}{E_1 t_1}}\right], \tag{152}$$

$$1 + \frac{e}{c} = \frac{2}{1 + \dfrac{M_{o4}}{D_4}\dfrac{D_1}{M_{o1}}}, \qquad 1 - \frac{e}{c} = \frac{2}{1 + \dfrac{M_{o1}}{D_1}\dfrac{D_4}{M_{o4}}}. \tag{153}$$

Dividing equation (151) by (152), it is found that

$$\frac{M_{o1}}{M_{o4}} = \left(\frac{E_4 t_4}{E_1 t_1}\right)\frac{\left\{1 + \xi_4 c\left[\dfrac{2}{1 + \dfrac{M_{o1}}{D_1}\dfrac{D_4}{M_{o4}}}\right] + \tfrac{1}{6}\xi_4^2 c^2\left[\dfrac{2}{1 + \dfrac{M_{o1}}{D_1}\dfrac{D_4}{M_{o4}}}\right]^2\right\}}{\left\{1 + \xi_1 c\left[\dfrac{2}{1 + \dfrac{M_{o4}}{D_4}\dfrac{D_1}{M_{o1}}}\right] + \tfrac{1}{6}\xi_1^2 c^2\left[\dfrac{2}{1 + \dfrac{M_{o4}}{D_4}\dfrac{D_1}{M_{o1}}}\right]^2\right\}}. \tag{154}$$

Equation (154) can be solved by iteration to determine M_{01}/M_{04} which then permits of the evaluation of e/c by means of equations (153), in turn leading to independent expressions for M_{01} and M_{04} from equations (151) and (152). Unfortunately, an explicit analytical resolution of M_{01} and M_{04} is not possible.

The programming of equations (151) to (154) is straightforward, even to extent of accounting for laminated composite adherends by including non-unity values of k_b. Once the bending moments M_{01} and M_{04} have been evaluated, the maximum adherend stress follows simply from equations (55) to (57) evaluated for the more critical adherend. For metal (isotropic) adherends, the thinner adherend is always more severely loaded than the thicker one. That this is so is apparent from equation (154). For low load intensities,

$$\frac{M_{o1}}{M_{o4}} \rightarrow \frac{E_4 t_4}{E_1 t_1} \qquad \text{for} \quad P \rightarrow 0 \quad , \tag{155}$$

so that the bending moments in the adherends at the ends of the joint are inversely proportional to the adherend extensional stiffnesses. Since the "thinner" adherend intrinsically has a lower bending stiffness than does the "thicker" adherend, this adherend imbalance imposes a severe stress concentration on the "thin" adherend, with respect to those bending stresses developed in a balanced joint. For filamentary composite adherends having markedly dissimilar values of the bending parameter k_b, it may be necessary to check each end of the joint separately to identify the more critical end, particularly if $k_b > 1$ for the thinner adherend and $k_b << 1$ for the thicker adherend.

Figure 27 depicts, in non-dimensionalized form, the strength degradation due to adherend stiffness imbalance for isotropic (metal) adherends. The failure mode considered is that of breaking the outermost "fiber" adjacent to the bond line at the end of the joint from which the thinner adherend extends. As is expected from the discussion above, any adherend stiffness imbalance is seen to significantly reduce further the joint efficiency. Just as in Figures 5 and 6, larger ℓ/t ratios minimize the strength loss by effectively reducing the eccentricity in the load path. For short overlaps, the joint strength is approximately proportional to the adherend stiffness ratio. That is, for a given short overlap, a joint with a stiffness imbalance ratio of 2:1 is about half as strong as one made out of two of the thinner adherends of the unbalanced joint. The reason why two thin adherends are stronger than one thin and one thicker adherend is that, in the former case, each adherend deflects the same amount under load to relieve the eccentricity while, for the latter, practically all of the distortion is concentrated at that end of the joint from which the thinner adherend extends.

For filamentary composite adherends, the value of the bending stiffness parameter $k_b = D / [Et^3/12(1-\nu^2)]$ must be accounted for also. Figure 28, for $k_b = 2.0$ and $k_b = 0.5$ shows how, just as for balanced joints, concentrating the bending material near the neutral axis is detrimental to joint strength. This figure may be compared with Figure 6 for $k_b = 1$.

An important conclusion from the analysis of unbalanced single-lap joints is that they are so much more inefficient than balanced single-lap joints that their use should be avoided. In any case, the thicker (and presumably stronger) adherend cannot accept any more load than is carried in the thinner adherend.

8. EFFECT OF ADHEREND STIFFNESS IMBALANCE ON PEEL (INTERLAMINAR TENSION) FAILURES AT END OF JOINT

The preceding section quantifies the loss of joint strength for potential failures in the adherend just outside the joint. For thicker adherends, peel failures of the adhesive or interlaminar tension failures of the adherend(s) are more likely. Any adherend stiffness imbalance also affects the adhesive shear stress distribution, as outlined below. However, this latter failure mode is improbable for real-life materials in joints of practical geometric dimensions, so the subject is not pursued in detail.

Proceeding from equations (127) through (130) and with equations (13) and (14), two coupled differential equations can be deduced for the adhesive shear and peel stress distributions, as follows. From the shear strain definition

$$\gamma = \frac{1}{\eta}(u_3 - u_2) \tag{156}$$

$$\frac{d\gamma}{ds} = \frac{1}{E_3 t_3 \eta}\left[T_3 - \frac{6(1-\nu_3^2)M_3}{(k_b)_3 t_3}\right] - \frac{1}{E_2 t_2 \eta}\left[T_2 + \frac{6(1-\nu_2^2)M_2}{(k_b)_2 t_2}\right] , \tag{157}$$

$$\frac{d^2\gamma}{ds^2} = \frac{1}{E_3 t_3 \eta}\left\{\tau - \frac{6(1-\nu_3^2)}{(k_b)_3 t_3}\left[V_3 - \tau\left(\frac{t_3+\eta}{2}\right)\right]\right\}$$

$$- \frac{1}{E_2 t_2 \eta}\left\{-\tau + \frac{6(1-\nu_2^2)}{(k_b)_2 t_2}\left[V_2 - \tau\left(\frac{t_2+\eta}{2}\right)\right]\right\} , \tag{158}$$

$$\frac{d^3\gamma}{ds^3} = \left\{\frac{1}{E_3 t_3 \eta}\left[1 + \frac{3(1-\nu_3^2)}{(k_b)_3}\left(1 + \frac{\eta}{t_3}\right)\right] + \frac{1}{E_2 t_2 \eta}\left[1 + \frac{3(1-\nu_2^2)}{(k_b)_2}\left(1 + \frac{\eta}{t_2}\right)\right]\right\}\frac{d\tau}{ds}$$

$$- \left\{\left(\frac{1}{E_3 t_3 \eta}\right)\left[\frac{6(1-\nu_3^2)}{(k_b)_3 t_3}\right] - \left(\frac{1}{E_2 t_2 \eta}\right)\left[\frac{6(1-\nu_2^2)}{(k_b)_2 t_2}\right]\right\}\sigma_c \tag{159}$$

and, for elastic adhesives,

$$\frac{d^3\gamma}{ds^3} = \frac{1}{G}\frac{d^3\tau}{ds^3} \tag{160}$$

Similarly, from the peel stress definition

$$\sigma_c = \frac{E_c}{\eta}(w_3 - w_2) \quad , \tag{161}$$

$$\left(\frac{\eta}{E_c}\right)\frac{d^2\sigma_c}{ds^2} = -\frac{M_3}{D_3} + \frac{M_2}{D_2} \quad , \tag{162}$$

$$\left(\frac{\eta}{E_c}\right)\frac{d^3\sigma_c}{ds^3} = -\frac{1}{D_3}\left[V_3 - \tau\left(\frac{t_3+\eta}{2}\right)\right] + \frac{1}{D_2}\left[V_2 - \tau\left(\frac{t_2+\eta}{2}\right)\right] \quad , \tag{163}$$

and

$$\left(\frac{\eta}{E_c}\right)\frac{d^4\sigma_c}{ds^4} + 12\left[\frac{(1-\nu_3^2)}{(k_b)_3E_3t_3^3} + \frac{(1-\nu_2^2)}{(k_b)_2E_2t_2^3}\right]\sigma_c = 6\left[\frac{(1-\nu_3^2)(1+\eta/t_3)}{(k_b)_3E_3t_3} - \frac{(1-\nu_2^2)(1+\eta/t_2)}{(k_b)_2E_2t_2}\right]\frac{d\tau}{ds} \quad . \tag{164}$$

Equations (159) and (164) are the coupled differential equations governing the adhesive stresses for arbitrary unsupported single-lap joints. Whenever the adherends are identical, the coupling terms drop out.

For the purely elastic material case, equation (164) can be employed to eliminate the derivatives of τ from equations (159) and (160), leading to a sixth-order differential equation in σ_c. Similarly, equations (159) and (160) permit the σ_c derivatives to be eliminated from equation (164), leading to a seventh-order differential equation in τ. For the plastic zones at the end(s) of the overlap, $d\tau/ds = 0$ and equation (164) then provides a solution for σ_c which can be substituted into equation (159) for the shear strain γ. Because of the coupling between the adhesive stresses, the general solution involves matching a large number of boundary conditions to determine the 13 integration constants. This must be done not only at the ends of the overlap but also at any transition from elastic to plastic behavior within the adhesive.

An approximate simpler solution is available for the peel stresses (but not for the shear stresses) in an unbalanced single-lap joint by recognizing that, for practically all good structural adhesives, the shear stress is in the plastic state for one or both end zones and that it is there that the only severe peel stresses are developed. With reference to equation (164), then, an approximate solution for the adhesive peel stresses follows from

$$\frac{d^4\sigma_c}{ds^4} + 12\frac{E_c}{\eta}\left[\frac{(1-\nu_3^2)}{(k_b)_3E_3t_3^3} + \frac{(1-\nu_2^2)}{(k_b)_2E_2t_2^3}\right]\sigma_c \simeq 0 \qquad (165)$$

as

$$\sigma_c = A\cos(\chi s)\cosh(\chi s) + B\sin(\chi s)\sinh(\chi s) + C\cos(\chi s)\sinh(\chi s) + D\sin(\chi s)\cosh(\chi s) \qquad (166)$$

where, here,

$$\chi^4 = \frac{E_c}{4\eta}\left[\frac{1}{D_1} + \frac{1}{D_4}\right] = \frac{3E_c}{\eta}\left[\frac{(1-\nu_4^2)}{(k_b)_4E_4t_4^3} + \frac{(1-\nu_1^2)}{(k_b)_1E_1t_1^3}\right] . \qquad (167)$$

The boundary conditions determining the integration constants in equation (166) include

$$\int_{-c}^{+c}\sigma_c\,ds \equiv 0 , \qquad (168)$$

whence

$$A[\sin(\chi c)\cosh(\chi c) + \cos(\chi c)\sinh(\chi c)] + B[\sin(\chi c)\cosh(\chi c) - \cos(\chi c)\sinh(\chi c)] = 0 . \qquad (169)$$

Just as in the analysis of peel stresses in balanced joints, the approximations

$$\sinh(\chi c) \simeq \cosh(\chi c) \rightarrow \frac{1}{2}e^{(\chi c)} \qquad (170)$$

are employed for joints of practical geometry. Consequently

$$A[\sin(\chi c) + \cos(\chi c)] + B[\sin(\chi c) - \cos(\chi c)] \simeq 0 . \qquad (171)$$

In order to derive an explicit solution for the critical peel stress, it is necessary to derive an equation in the other two integration constants, C and D in equation (166), which is equivalent to equation (171). The procedure is as follows. Reference to Figure 26 reveals that, for an unbalanced joint, the bending moments in the adherends are zero at a distance $e \leq c$ off the middle of the overlap. The eccentricity e is evaluated in equations (153) as

$$\frac{e}{c} = \frac{\left(\frac{M_{o1}}{D_1}\frac{D_4}{M_{o4}} - \frac{M_{o4}}{D_4}\frac{D_1}{M_{o1}}\right)}{\left(2 + \frac{M_{o4}}{D_4}\frac{D_1}{M_{o1}} + \frac{M_{o1}}{D_1}\frac{D_4}{M_{o4}}\right)} = \frac{\left(\frac{M_{o1}}{D_1} - \frac{M_{o4}}{D_4}\right)}{\left(\frac{M_{o1}}{D_1} + \frac{M_{o4}}{D_4}\right)} . \qquad (172)$$

Since there is no transverse shear stress across the adherends at s = e, it is necessary that

$$\int_{e}^{c} \sigma_c \, ds = 0 \quad \text{and} \quad \int_{-c}^{e} \sigma_c \, ds = 0 \; . \tag{173}$$

In terms of equation (166), then,

$$\begin{aligned} &A[\sin(\chi c)\cosh(\chi c) + \cos(\chi c)\sinh(\chi c) - \sin(\chi e)\cosh(\chi e) - \cos(\chi e)\sinh(\chi e)] \\ &+ B[\sin(\chi c)\cosh(\chi c) - \cos(\chi c)\sinh(\chi c) - \sin(\chi e)\cosh(\chi e) + \cos(\chi e)\sinh(\chi e)] \\ &+ C[\sin(\chi c)\sinh(\chi c) + \cos(\chi c)\cosh(\chi c) - \sin(\chi e)\sinh(\chi e) - \cos(\chi e)\cosh(\chi e)] \\ &+ D[\sin(\chi c)\sinh(\chi c) - \cos(\chi c)\cosh(\chi c) - \sin(\chi e)\sinh(\chi e) + \cos(\chi e)\cosh(\chi e)] \\ &= 0 \end{aligned} \tag{174}$$

and

$$\begin{aligned} &A[\sin(\chi e)\cosh(\chi e) + \cos(\chi e)\sinh(\chi e) + \sin(\chi c)\cosh(\chi c) + \cos(\chi c)\sinh(\chi c)] \\ &+ B[\sin(\chi e)\cosh(\chi e) - \cos(\chi e)\sinh(\chi e) + \sin(\chi c)\cosh(\chi c) - \cos(\chi c)\sinh(\chi c)] \\ &+ C[\sin(\chi e)\sinh(\chi e) + \cos(\chi e)\cosh(\chi e) - \sin(\chi c)\sinh(\chi c) - \cos(\chi c)\cosh(\chi c)] \\ &+ D[\sin(\chi e)\sinh(\chi e) - \cos(\chi e)\cosh(\chi e) - \sin(\chi c)\sinh(\chi c) + \cos(\chi c)\cosh(\chi c)] \\ &= 0 \; . \end{aligned} \tag{175}$$

Equation (169) results from the addition of equations (174) and (175). Their subtraction leads to

$$\begin{aligned} &C[\sin(\chi c)\sinh(\chi c) + \cos(\chi c)\cosh(\chi c)] + D[\sin(\chi c)\sinh(\chi c) - \cos(\chi c)\cosh(\chi c)] \\ &- A[\sin(\chi e)\cosh(\chi e) + \cos(\chi e)\sinh(\chi e)] - B[\sin(\chi e)\cosh(\chi e) - \cos(\chi e)\sinh(\chi e)] \\ &- C[\sin(\chi e)\sinh(\chi e) + \cos(\chi e)\cosh(\chi e)] - D[\sin(\chi e)\sinh(\chi e) - \cos(\chi e)\cosh(\chi e)] \\ &= 0 \end{aligned} \tag{176}$$

Strictly speaking, no further simplification of equation (176) is possible. However, subject to the usual practical constraints of small adherend stiffness imbalance ($e \approx 0$) and large overlap to minimize the structural joint inefficiency, one may set

$$C[\sin(\chi c) + \cos(\chi c)] + D[\sin(\chi c) - \cos(\chi c)] \approx 0 \tag{177}$$

to provide consistency with equation (171). Subject to the exclusion of short overlaps and severe stiffness imbalances between the adherends, the analysis

proceeds, as follows, from equation (162). With reference to Figure 26, at the left-hand side of the joint

$$\frac{E_c}{n}\frac{M_{o1}}{D_1}\frac{1}{\frac{1}{2}\chi^2 e^{(\chi c)}} \simeq -2(A - C)\sin(\chi c) + 2(B - D)\cos(\chi c) \qquad (178)$$

while, at the right-hand end,

$$\frac{E_c}{n}\frac{M_{o4}}{D_4}\frac{1}{\frac{1}{2}\chi^2 e^{(\chi c)}} \simeq -2(A + C)\sin(\chi c) + 2(B + D)\cos(\chi c) \quad . \qquad (179)$$

Similarly, from equations (166) and (170), at the left-hand end of the joint

$$\sigma_c \simeq \frac{1}{2} e^{(\chi c)}[(A - C)\cos(\chi c) + (B - D)\sin(\chi c)] \qquad (180)$$

while, at the right-hand end,

$$\sigma_c \simeq \frac{1}{2} e^{(\chi c)}[(A + C)\cos(\chi c) + (B + D)\sin(\chi c)] \quad . \qquad (181)$$

Equations (171) and (177) enable the direct expression of the σ's in terms of the M_o's by elimination of the integration constants A to D. Adding together and subtracting, in turn, equations (178) and (179) provides

$$\frac{2E_c}{n\chi^2 e^{(\chi c)}}\left[\frac{M_{o1}}{D_1} + \frac{M_{o4}}{D_4}\right] = -4A\sin(\chi c) + 4B\cos(\chi c) \qquad (182)$$

and

$$\frac{2E_c}{n\chi^2 e^{(\chi c)}}\left[\frac{M_{o1}}{D_1} - \frac{M_{o4}}{D_4}\right] = 4C\sin(\chi c) - 4D\cos(\chi c) \quad . \qquad (183)$$

Equations (171) and (177) may be re-arranged in the form

$$A\cos(\chi c) + B\sin(\chi c) = -A\sin(\chi c) + B\cos(\chi c) \qquad (184)$$

and

$$C\cos(\chi c) + D\sin(\chi c) = -C\sin(\chi c) + D\cos(\chi c) \quad . \qquad (185)$$

It then follows from equations (178) to (183) that, at the left-hand end of the joint,

$$\sigma_c \simeq \frac{E_c}{2n}\frac{M_{o1}}{D_1\chi^2} \qquad (186)$$

while, at the right-hand end,

$$\sigma_c = \frac{E_c}{2n} \frac{M_{o4}}{D_4 X^2} \quad . \tag{187}$$

The critical end of the joint in peel (interlaminar tension) is the same end as that which is critical for bending. Any adherend stiffness imbalance is seen to aggravate the peel stress problem.

The bending moments M_{o1} and M_{o4} are derived as explained in the preceding section. Equations (186) and (187) may be re-expressed in non-dimensionalized form. In the event that the adherend 1 end of the joint is more critical, at the end $s = -c$,

$$\frac{\sigma_{peel}}{(\sigma_{avg})_1} = k_1 \left\{ \frac{3(1-\nu_1^2)E_c t_1 \left(1 + \frac{n}{t_1}\right)^2}{E_1 n \left[1 + \frac{(k_b)_1 E_1 t_1^3 (1-\nu_4^2)}{(k_b)_4 E_4 t_4^3 (1-\nu_1^2)}\right]} \right\}^{\frac{1}{2}} , \tag{188}$$

in which

$$k_1 = \frac{2M_{o1}}{Pt_1\left(1 + \frac{n}{t_1}\right)} = \frac{1}{1 + \xi_1 c + \frac{1}{6}(\xi_1 c)^2} \quad . \tag{189}$$

In the event that the adherend 4 end of the joint ($s = +c$) is the more critical, the subscripts 1 and 4 are to be interchanged. Equation (188) includes the influence of filamentary composite adherends as well as of adherend stiffness imbalance. As explained above, its use should be restricted to small adherend mismatches and those other curves deduced from it and shown in Figure 29 are indicative of the trend in behavior, rather than of precise values for large mismatches. Because of the severe peel stresses predicted for short overlaps and widely dissimilar adherends, the associated joint strengths will be intolerably small, even when computed more accurately.

9. EFFECT OF THERMAL MISMATCH BETWEEN ADHERENDS

When a single-lap bonded joint in which the adherends have different coefficients of thermal expansion is operated at a temperature different from that at which the adhesive is cured, there are initial curvatures due to locked-in strains. These influence the already eccentric load path and thereby change the bending moments at the ends of the joint which, in turn, affect the adhesive shear and peel stress distributions. The joint load capacity is usually decreased since one end of the joint is rendered more critical than the other. The analytical formulation of this problem is straightforward, following the approach adopted in Reference 12. However, since it is not possible to obtain explicit expressions (which would be valid for all geometries outside the joint) for the bending moments M_{01} and M_{04} at the ends of the joint, each individual case must be solved by iteration (preferably on a digital computer). Therefore the practical utility of such an analysis as a design technique is severely limited, so the analysis is not developed here. Instead, a qualitative description of the various factors interacting is provided in Figure 30. The eccentricity in the load path is influenced by the length of adherends outside the joint. This is evident from the upper part of Figure 30, and is the reason for the comment above that no explicit expressions could be obtained for M_{01} and M_{04} independently of the geometry outside the joint. It is evident from the lower illustration in Figure 30 that, in the absence of any stiffness imbalance between the adherends, the thermal mismatch has increased the bending moment in the adherend of lower coefficient of thermal expansion (which is usually the composite end of a composite-to-metal joint) whenever the operating temperature is less than the adhesive curing temperature, which is usually the situation prevailing. The influence of this initial curvature and increased bending moment is to alleviate the load carried at the other end of the joint, thereby decreasing the joint efficiency with respect to a balanced joint. This reduction applies to all three possible modes of failure.

10. PARAMETRIC EFFECTS

The analyses of Sections 2, 3 and 4 have established that the plastic behavior of most good structural adhesives in shear is so significant that, usually, joint failure is initiated in the adherend(s) just outside the joint. Three separate analysis techniques have been prepared for: (1) the bond shear strength, on the assumption that the adherends behave linearly elastically and that the peel strength is greater than the shear strength, (2) the bending failure of the adherend under the eccentric load path, assuming adequate bond shear and peel strengths, and (3) the peel failure of adhesive (for metal adherends) or the transverse tension failure of the laminates (for filamentary composite adherends) under the assumption of adequate adherend strength and adhesive shear strength. In the case of adhesive failure with metal adherends, there is probably an interaction between peel and shear failures over a small range of thicknesses. The theories do not account for this interaction and represent the asymptotic behavior when one case or other dominates. Likewise, for highly ductile adhesives, the yielding of metal adherends just outside the joint does not constitute immediate failure the way it does for brittle adhesives. Some increase in load capacity remains, even though the structure has been permanently deformed. The analyses established also that longer overlaps enhanced the joint efficiency significantly, that tough ductile adhesives produced much stronger joints than the stronger more brittle variety, and that the combination of unbalanced adherends degraded the joint strength to below that which would be obtained using two adherends each the same as the thinner (weaker) of the unbalanced combination.

Figure 31 provides a comparison of the relative strengths of ductile and brittle adhesives with the strength of 0.060 inch thick aluminum adherends. The adherend yield line is derived on the assumption that the adhesive bond has adequate strength while the potential adhesive shear strengths are based on the assumption that the adherends had the same modulus E but a much greater ultimate strength than they actually possess in order to eliminate from the analysis the effects of adherend yielding. Naturally there can be no failures observed above the ultimate strength cut-off at 42 kips per inch. Even though the brittle adhesive has a much higher peak shear stress (10,000 psi) than does the ductile

adhesive (4,500 psi), the former is seem to produce a much weaker joint owing to its lack of ductility. While the perfectly brittle adhesive ($\gamma_p/\gamma_e = 0$) shown is of comparable strength with the yield strength of the adherend, this is only because of the artificial exclusion of the small ductility that even brittle adhesives possess. While small, this ductility is sufficient to ensure that, for 0.060 inch thick aluminum adherends at least, that real structural adhesives are never responsible for initiating failure, provided that the overlap exceeds a certain minimum (0.33 inch in the case shown in Figure 31). Once the adherend bending moment has been relieved by yielding, the adherend capability is increased to its ultimate strength, so it is the bond which is observed to fail. Depending on the amount of adhesive ductility present, failure of the adhesive will occur somewhere between the formation of the plastic hinge (yielding on only the adhesive side of the adherend) and the gross yielding of the entire thickness. The yielding at the end of the joint exceeds the adhesive shear or peel strain capacity locally and the adhesive fractures progressively as the effective overlap decreases. Consequently, with reference to Figure 31, all test results will be bounded within the triangle formed by the adherend yield strength (or ultimate load) on top, the adherend proportional limit load (formation of plastic hinge) below, and the adhesive shear or peel characteristic to the left for short overlaps. The most ductile adhesives will develop strengths approaching the ultimate adherend strengths while the very brittle adhesives will barely exceed the adherend plastic hinge formation. The only exceptions to this rule fall in the class of the non-structural sealants specifically formulated to break apart easily for inspection or repair and which serve only as a sealant. Even the better room-temperature curing two-part part epoxies survive until after the adherend yields unless an excessively thick glue line (or inadequate overlap) is responsible for a greater moment M_o than would be associated with a 0.005 inch thick standard bond line.

Figure 31 is prepared specifically for a single adherend thickness. Figure 32 presents the joint loads at the formation of the plastic hinges for a range of aluminum adherend thicknesses. The adherend limit loads shown are, strictly speaking, proportional limits and may well exceed two thirds of the ultimate capacity. It should be remembered also that, just because failure is induced by the adherend, it does not follow that the joint efficiency is at its maximum. Just as shown in Figure 32, strength increases are to be obtained by

increasing the overlap until the asymptotic limit (shown for thin adherends) is attained.

A further variable to be considered is that of the adherend material and modulus. Figure 33 reveals how those adherends with high strength and modulus (such as steel) exhibit both higher potential bond shear strengths and adherend plastic hinge formation loads. This explains a well-known phenomenon according to which a given adhesive will develop higher single-lap shear values with steel or titanium adherends than with aluminum. This is not due to better adhesion at all, as is well recognized for titanium (which is very difficult to bond to well), but simply to the different elasto-mechanical properties. Likewise, a thicker adherend of the same material also appears to enhance the bond strength, as shown in Figure 32.

11. JOINT EFFICIENCY CHARTS FOR SINGLE-LAP JOINTS

The analyses performed above can be employed in the generation of joint efficiency diagrams. A computer program has been prepared in the Appendix for unsupported single-lap joints between identical adherends. Sample outputs have been illustrated for commonly used areospace materials. The computer program has been prepared for arbitrary materials but the joint efficiency charts (Figures 17 to 24) have been restricted to room-temperature performance of a single example of the best of the 350 °F curing ductile and brittle adhesives. The joint strengths follow from the joint efficiencies (or, more sensibly, inefficiencies since they must inevitably be less than unity for practical joint proportions) by multiplying the basic adherend strength $F_{tu}t$ by the efficiency. An example of this is provided in Figure 34. The material properties used in preparing these charts are recorded in Table 1. The adhesives have not been identified because the effective peel properties of constrained adhesive films have not yet been measured sufficienctly precisely. Also, the very thin composite adherends do not reflect the discrete limitations on balanced laminate thicknesses derivable from a particular ply thickness. Similarly, the effect of stacking sequence ($k_b \neq 1$) has been omitted to clarify the presentation. Certain trends are evident from these charts. In the first place, the very powerful role of the ℓ/t ratio in minimizing the inherent inefficiency of the joint is quite apparent. Next, the severe limitations imposed on filamentary composites by the low interlaminar shear srtengths are exemplified. This problem is seen to become progressively more acute as the adherend thickness is increased. Indeed, for any given ℓ/t ratio, the peel (interlaminar tension) problem imposes a rapid degradation in joint strength beyond some defined overlap. Adhesive shear failures are seen to have surprisingly little effect on the predicted joint strengths. Adhesive shear failures are shown, in Figures 17 to 24 and 34 to be limited to two characteristic zones. The first is for short overlaps and high strength adherend materials while the second is for thick adherends with sufficiently long overlaps to alleviate the peel stress problem. Other than these situations, adherend bending governs the thinner adherends and peel stresses the thicker adherends.

Caution should be exercised in attempting to extrapolate these diagrams to thin

adherends and short overlaps because of two simplifications incorporated in the computer program. The adhesive peel stresses induce transverse strains in the adjacent adherends which, in turn, influence the bending moments set up in the adherends. To account for this effect precisely one would have to relax the simplifiying assumption that the adhesive stresses do not vary through the thickness. To do so would result in considerable analytical complexities including an increase in the degree of the governing differential equations. Instead, the following simple technique has been adopted to account for this factor in an approximate manner. A constant thickness of the adherend three times as thick as the adhesive layer has been considered affected by the peel stresses on each side of the adhesive layer. Therefore, the effective peel modulus of the joint is given by

$$\frac{1}{E_c'} = \frac{1}{E_c} + \frac{6}{E_n} \quad . \tag{190}$$

Obviously this approximation becomes questionable as the adherend thickness approaches the adhesive thickness. The number 6 above was selected after trial runs with 2 because it gives predictions in better accord with the standard lap-shear data. Drastic changes in this constant (as from 2 to 6) effect only a few per cent change in joint efficiency, so a precise determination may be unnecessary. The second limitation on the computer program restricts it from applying to such geometries as the half-inch thick single-lap specimen now used to derive experimental stress-strain curves. This limitation derives from equation (35) and prevents the solution from applying to short overlaps with essentially uniform shear stress. Such a restriction is not considered excessive, however, because structural joints, as distinct from purely experimental joints always employ much greater ℓ/t ratios.

These joint efficiency charts elucidate the inherently low efficiency of unsupported single-lap joints and the motivation for providing a moment-resistant support to improve efficiency.

12. THE STANDARD HALF-INCH SINGLE-LAP JOINT TEST

Over the years a tremendous number of the standard tensile lap shear tests (ASTM # D-1002) have been performed by many organizations in the mistaken belief that the failure load was in some way related to the shear strength of the adhesive being tested. The purpose of this section is to debunk that myth once and for all. This is not to imply that the test should be discarded, because there is no other test which, in a single measurement, obtains so inexpensively a simultaneous assessment of all sorts of adhesive properties. A decrease in any one property reduces the failure load of the joint, even if the property responsible cannot be identified. It is a fine screening and quality control specimen, but the hypothetical shear stress deduced by dividing the failure load by the bond area has no merit in any rational design process. Indeed, the peel stress influences this failure more than does the shear stress. The failure in the standard lap-shear test is almost invariably initiated by yielding of the aluminum adherends just outside the joint. The strength obtained is shown in Figure 5 to have a markedly non-linear dependence on the ℓ/t ratio as well as separately on the adherend thickness. The failure loads simply do not scale up proportionally with the bond area, even if one ignores the problem of the adhesive layer thickness not scaling up in proportion to the other dimensions.

As a quantitative verification of this criticism of using single-lap shear data for design purposes, consider the case of FM-47. This vinyl-phenolic highly-ductile adhesive as known to develop a peak shear stress of 10,000 to 12,000 psi at 75 °F when characterized by a torsion-ring experiment. Yet lap-shear tests on 0.5 inch overlaps of 0.064 inch thick 2024-T3 aluminum alloy exhibit only 4,800 psi "shear" stress at failure. This value is observed to be raised to 8,000 psi for 0.064 inch 301 half-hard stainless steel adherends with half-inch overlap single-lap tests. It is evident, therefore, that the standard half-inch single-lap tensile shear tests do not characterize adhesive shear stress in a quantitative manner. They serve merely to separate brittle from ductile adhesives.

With reference to the lower left corner of Figure 33, and proceeding upwards along the half-inch overlap line, it is clear that 3000 psi average shear stress marks the transition at the formation of the plastic hinge. That is to say that any adhesive developing significantly more than 3000 psi on this test for 7075-T6 aluminum (or somewhat less for 2024-T3 which yields at a much lower stress) inevitably has significant "plasticity" so that the maximum overlap at which the adhesive remains fully-plastic throughout is in excess of 0.5 inch. Those adhesives developing significantly less than 3000 psi with this test must inevitably be so brittle as not to permit even the low joint efficiency of the adherend (34 per cent) to be developed in unsupported single-lap joints. Subject to the exclusion of those cases requiring high-temperature operating environments, which exclude the use of ductile adhesives, all of the best structural adhesives employed in the commercial aircraft inductry (operating requirements from -67 °F to +160 °F) exceed 4000 psi on the standard single-lap tensile shear test, yet most of these have a maximum shear stress of less than 7000 psi when measured with a torsion-ring or thick-adherend specimen.

Figure 32 should suffice to prove the unreliability of designing in terms of an "allowable" average shear stress and a bond area. The fully-plastic adhesive failure line shown corresponds to the true material maximum shear stress of 4500 psi. Suppose an arbitrary lower design stress of 2000 psi were to be specified. This would appear as a radial line from the origin through the point (ℓ = 5 inch, P = 10,000 kips per inch). Any design on the 2000 psi line which was below the true adhesive strength line (governed by adherend bending in the cases shown) would represent a realizable situation but, anywhere to the right of the intersection of those lines, an overestimate of the joint strength would result. For example, for ℓ = 5 inch, the average shear stress actually developable on a 0.080 inch thick adherend is just less than 1000 psi. Figure 33 illustrates these radial constant average stress lines. Figure 33 also demonstrates how an "allowable" adhesive shear stress value mysteriously changes with the material from which the adherends are made. There is just no rational basis for design in terms of load equal to bond area multiplied by standard single-lap shear stress (or any other uniform allowable shear stress for that matter), and this widespread practice should be discontinued. Probably the only things that have saved major problems with such an approach are the arbitrarily low (1000 to 1500 psi) "allowables" which have been established for bonding and that most

aerospace bonding with single- or double-lap joints is confined to thin sheets well within the true capabilities of the adhesive when its plastic behavior is considered.

In any case, the present approach of designing in terms of elastic-plastic stress-strain adhesive characteristics in adhesive shear and of including distinct peel-stress phenomena does permit bonded joint design to be placed on a rational basis.

13. CONCLUSIONS

Iterative closed-form analytical solutions for single-lap adhesive-bonded joints have been derived which account explicitly for adhesive plasticity, and adherend stiffness imbalance. Three distinct failure modes are covered: adherend failure induced by bending due to the eccentric load path, peel (or transverse tension) failure, and shear failure of the adhesive. Somewhat surprisingly, in view of the basic shear nature of the applied load, the latter failure mode is rare for real materials in joints of practical proportions. Joint inefficiency charts have been prepared for representative material combinations. These emphasize how a drastic efficiency reduction is imposed by the eccentricity in the load path and that, beyond a certain thickness (for each ℓ/t ratio), peel failures of the adhesive or interlaminar tension failures of the laminated adherend result in even less efficient utilization of the adherend material.

A technique is described for alleviating the eccentricity problems which is particularly suited to filamentary composite adherends. This involves the judicious build-up of the laminate in the overlap area.

Because the transverse deflections of unsupported single-lap joints induce significant bending stresses in the adherend, thereby limiting the average stress capability, it is recommended that good design practice should provide moment restraint to minimize the transverse deflections. In such a case, the simpler analysis for one side of a double-lap joint applies.

While the single-lap joint can be a useful and inexpensive quality control test, it represents a very poor approach to generating design data. The reasons why it is poor are that joint strengths do not scale up linearly with the bond area and that predominantly adhesive shear failures are just as rare with single-lap structural joints as they are with test specimens.

REFERENCES

1. Goland. M. and Reissner, E., "The Stresses in Cemented Joints," J. Appl. Mech. 11, A17-A27 (1944).

2. Hahn, K., "Photostress Investigation of Bonded Lap Joints," Part I - Theoretical Analysis, Douglas Aircraft Co., Research Report SM-40001, (1960).

3. Hahn, K., "Stress Distribution in Adherends of Bonded Lap Joints," Part I - Theoretical Analysis and Part II - Analysis of Experimental Data (with Computer Program in Appendix), Douglas Aircraft Co., Research Report SM-40010, (1961).

4. Hahn, K. F. and Fouser, D. F., "Methods for Determining Stress Distribution in Adherends and Adhesives," Symposium on Adhesives for Structural Applications, (Ed. Bodnar, M. J.), pp. 25-29, Picatinny Arsenal 1961, Inter-Science, (1962).

5. Kuenzi, E. W. and Stevens, G. H., "Determination of Mechanical Properties of Adhesives for Use in the Design of Bonded Joints," U.S. Forest Service Research Note FPL-011, September 1963.

6. Kutscha, D. and Hofer, K. E. Jr., "Feasibility of Joining Advanced Composite Flight Vehicle Structures," IIT Research Institute, Technical Report AFML-TR-68-391, January 1969.

7. Kutscha, D., "Mechanics of Adhesive Bonded Lap-Type Joints: Survey and Review," Technical Report AFML-TDR-64-298, Forest Products Laboratory, December 1964.

8. Grimes, G. C., Calcote, L. R., Wah, T. et al., "The Development of Non-Linear Analysis Methods for Bonded Joints and Advanced Filamentary Composite Structures," SouthWest Research Institute, R&D Interim Technical Report No. 1, August 1969.

9. Dickson, J. N., Hsu, T. M., and McKinney, J. M., "Development of an Understanding of the Fatigue Phenomena of Bonded and Bolted Joints in Advanced Filamentray Composite Materials," Lockheed-Georgia Co., Technical Report AFFDL-TR-72-64, Volume 1, June 1972.

10. Goodwin, J. F., "Research on Thermomechanical Analysis of Brazed or Bonded Structural Joints," FAA, USAF, NASA Contract Technical Report ASD-TDR-63-447, Douglas Aircraft Co., September 1963.

11. Hart-Smith, L. J., "The Strength of Adhesive-Bonded Double-Lap Joints, " Douglas Aircraft Co., IRAD Technical Report MDC-J0367, November 1969.

12. Hart-Smith, L. J., "Adhesive-Bonded Double-Lap Joints," Douglas Aircraft Co., NASA Langley Contract Report CR-112235, January 1973.

13. Hart-Smith, L. J., "The Strength of Adhesive-Bonded Single-Lap Joints," Douglas Aircraft Co., IRAD Technical Report MDC-J0742, April 1970.

TABLE I. MATERIAL PROPERTIES FOR FIGURES 17 TO 24 AND 34

7075-T6 ALUMINUM ALLOY:

$E = 10.3 \times 10^6$ psi, $F_{ty} = 70$ ksi, $F_{tu} = 80$ ksi.

HIGH-STRENGTH GRAPHITE-EPOXY:

$(0°/+45°/90°/-45°)_s$ pattern:

$E_L^t = 8.0 \times 10^6$ psi, $E_N^t = 1.7 \times 10^6$ psi,
$F_L^{tu} = 69$ ksi, $F_N^{tu} = 8$ ksi,

$(0°/+45°/0°/-45°)_s$ pattern:

$E_L^t = 11.9 \times 10^6$ psi, $E_N^t = 1.7 \times 10^6$ psi,
$F_L^{tu} = 103$ ksi, $F_N^{tu} = 8$ ksi,

$(0°)$ unidirectional laminate:

$E_L^t = 21.0 \times 10^6$ psi, $E_N^t = 1.7 \times 10^6$ psi,
$F_L^{tu} = 180$ ksi, $F_N^{tu} = 8$ ksi,

(in which the subscript N refers to properties in the thickness direction).

DUCTILE ADHESIVE:

$\tau_p = 6$ ksi, $\eta = 0.005$ in., $\gamma_p/\gamma_e = 20$, $\eta(\frac{1}{2}\gamma_e + \gamma_p) = 0.0102$ in.,
$E_c \simeq 500$ ksi, $\sigma_{c_{max}} \simeq 10$ ksi.

BRITTLE ADHESIVE:

$\tau_p = 9$ ksi, $\eta = 0.005$ in., $\gamma_p/\gamma_e = 1.5$, $\eta(\frac{1}{2}\gamma_e + \gamma_p) = 0.00042$ in.,
$E_c \simeq 1500$ ksi, $\sigma_{c_{max}} \simeq 17$ ksi.

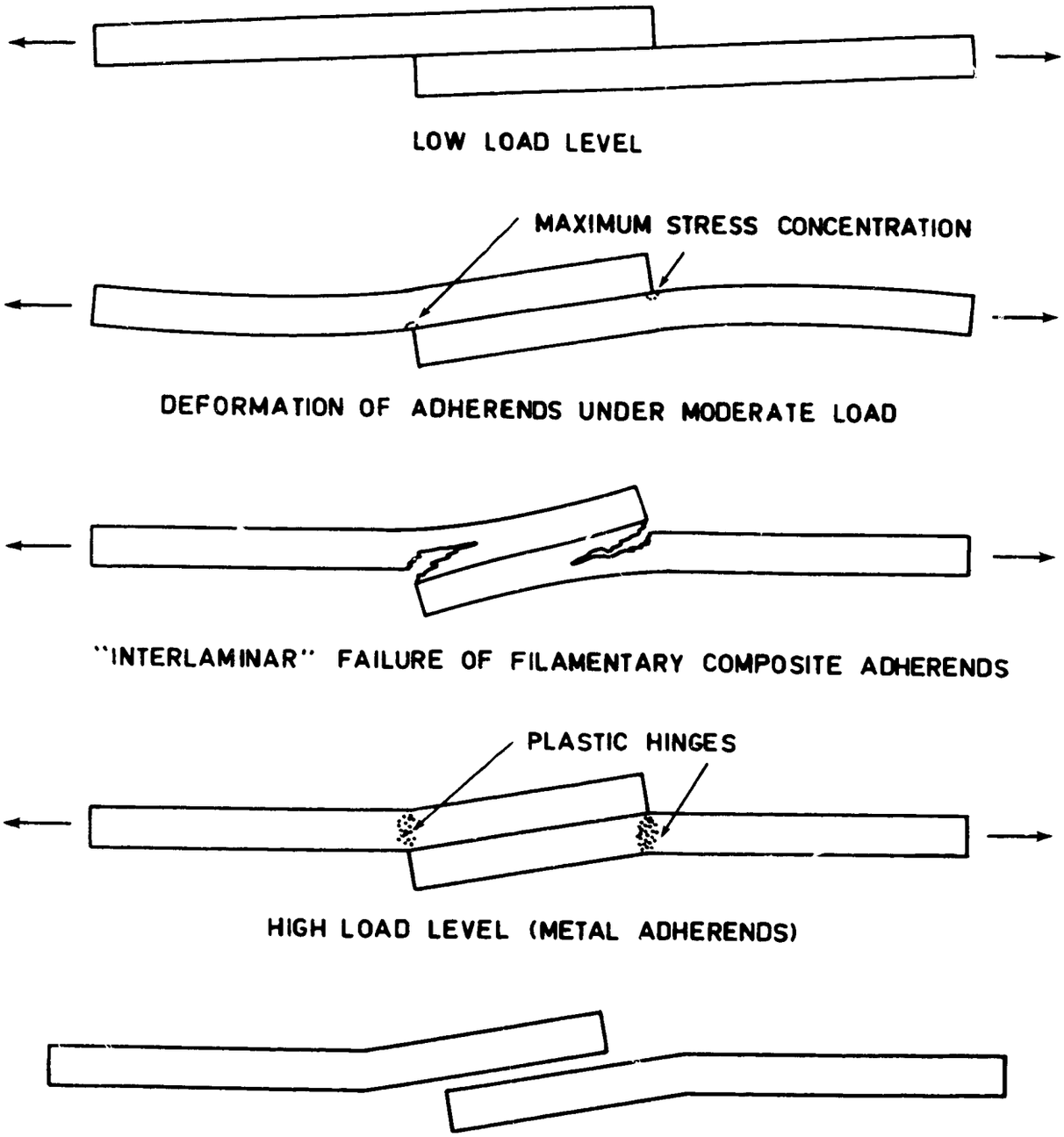

FIGURE 1. FAILURE OF SINGLE-LAP BONDED JOINTS WITH BRITTLE AND WITH YIELDING ADHERENDS

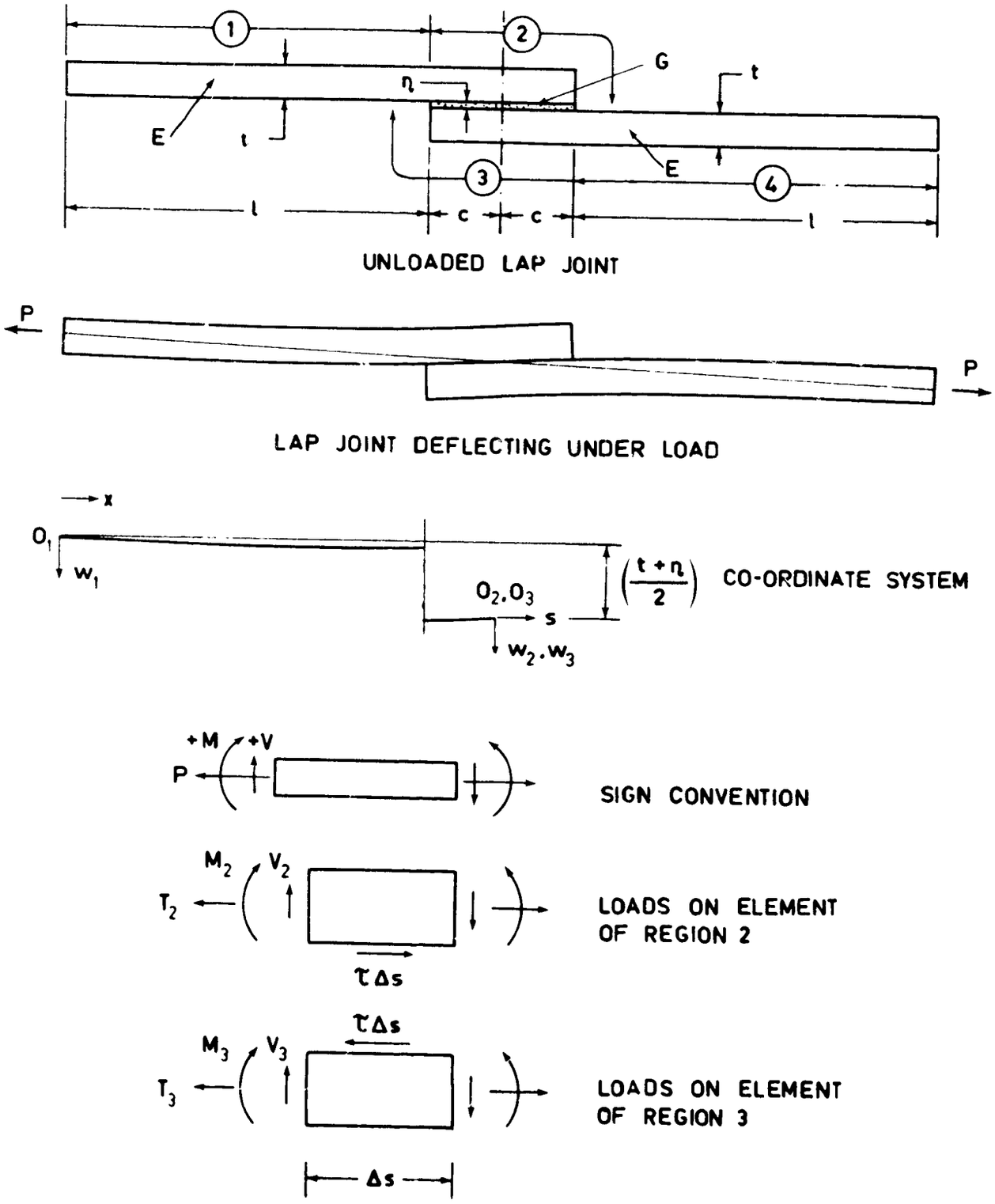

FIGURE 2. CO-ORDINATE SYSTEM AND DEFORMATIONS IN BALANCED SINGLE-LAP BONDED JOINTS

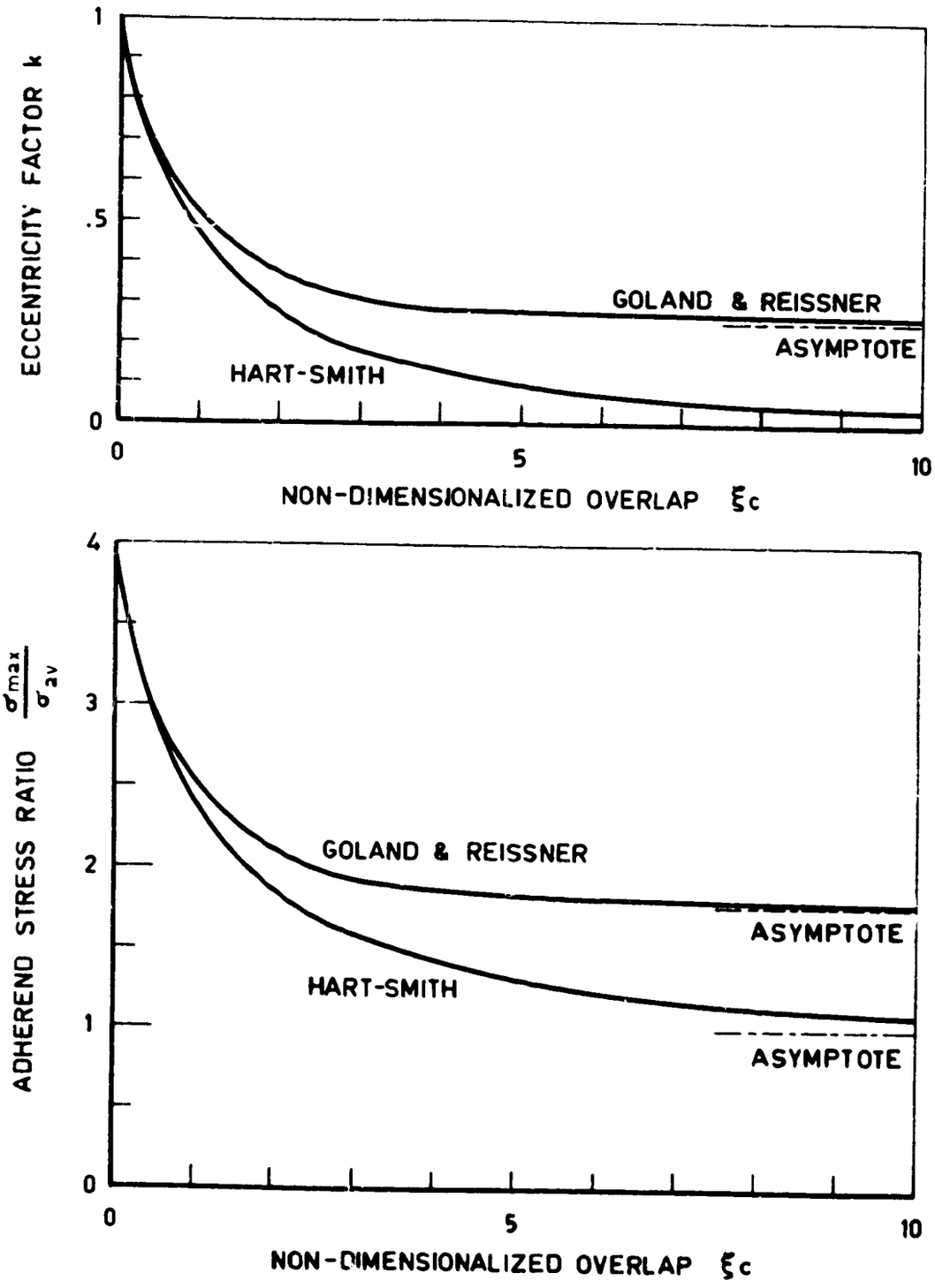

FIGURE 3. COMPARISON BETWEEN PRESENT SOLUTION FOR ADHEREND STRESSES AND THAT OF GOLAND AND REISSNER

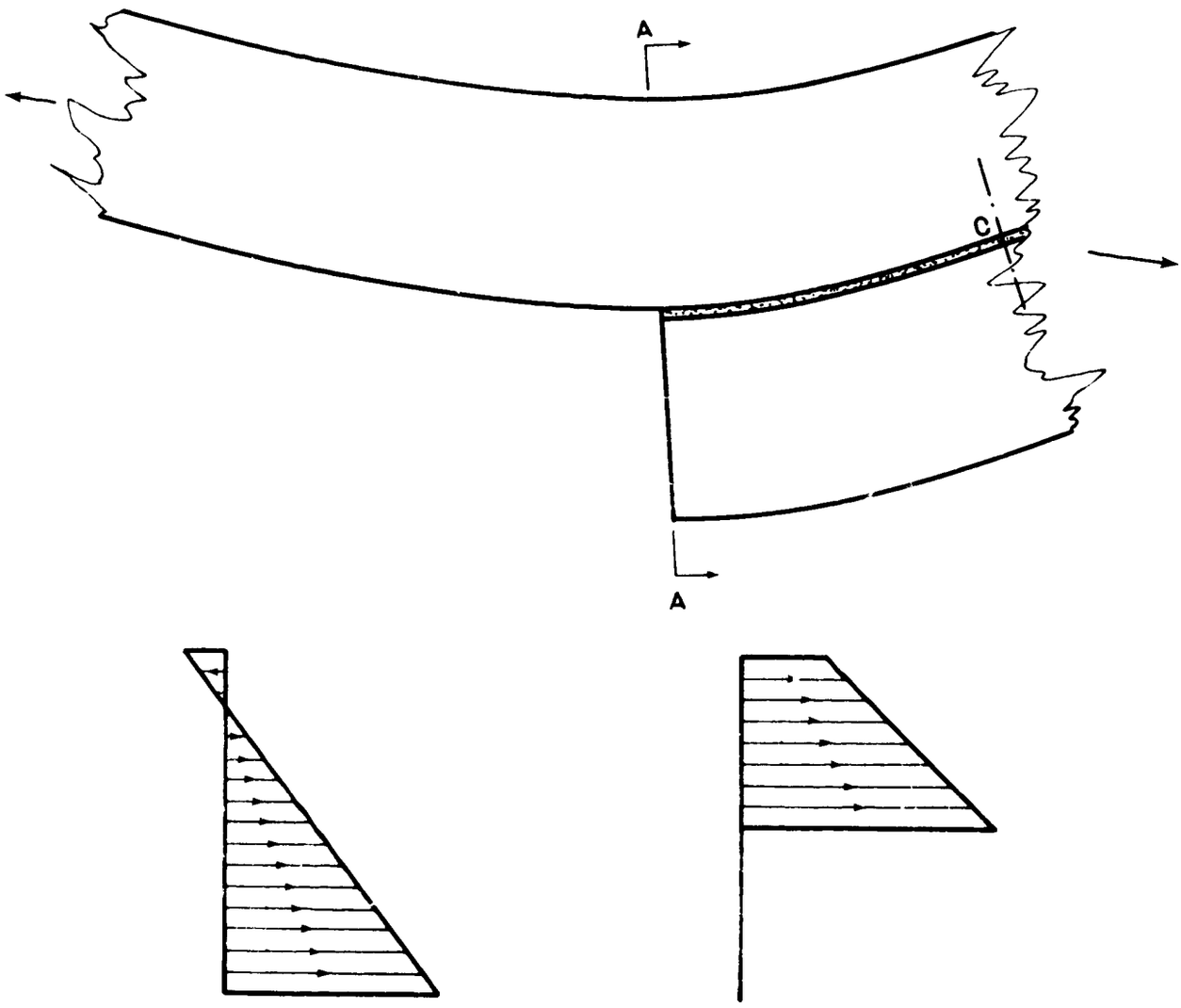

STRESS DISTRIBUTION
ON SECTION A-A
ADOPTED BY
GOLAND AND REISSNER

STRESS DISTRIBUTION
ON SECTION A-A
ASSUMED IN
PRESENT ANALYSIS

FIGURE 4. EXPLANATION OF FALLACY IN GOLAND AND REISSNER ANALYSIS

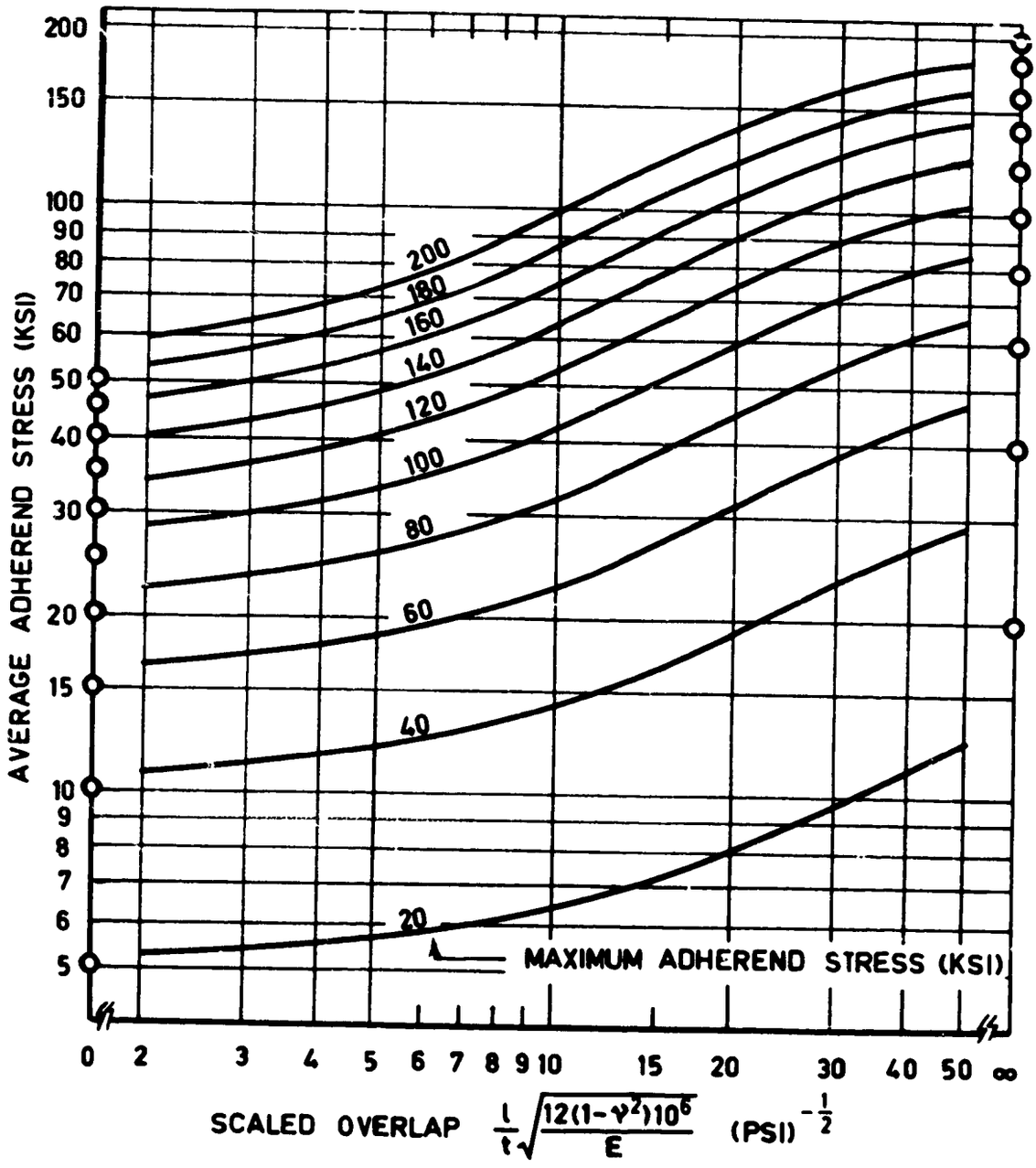

FIGURE 5. ADHEREND LIMIT LOADS FOR BALANCED SINGLE-LAP JOINTS

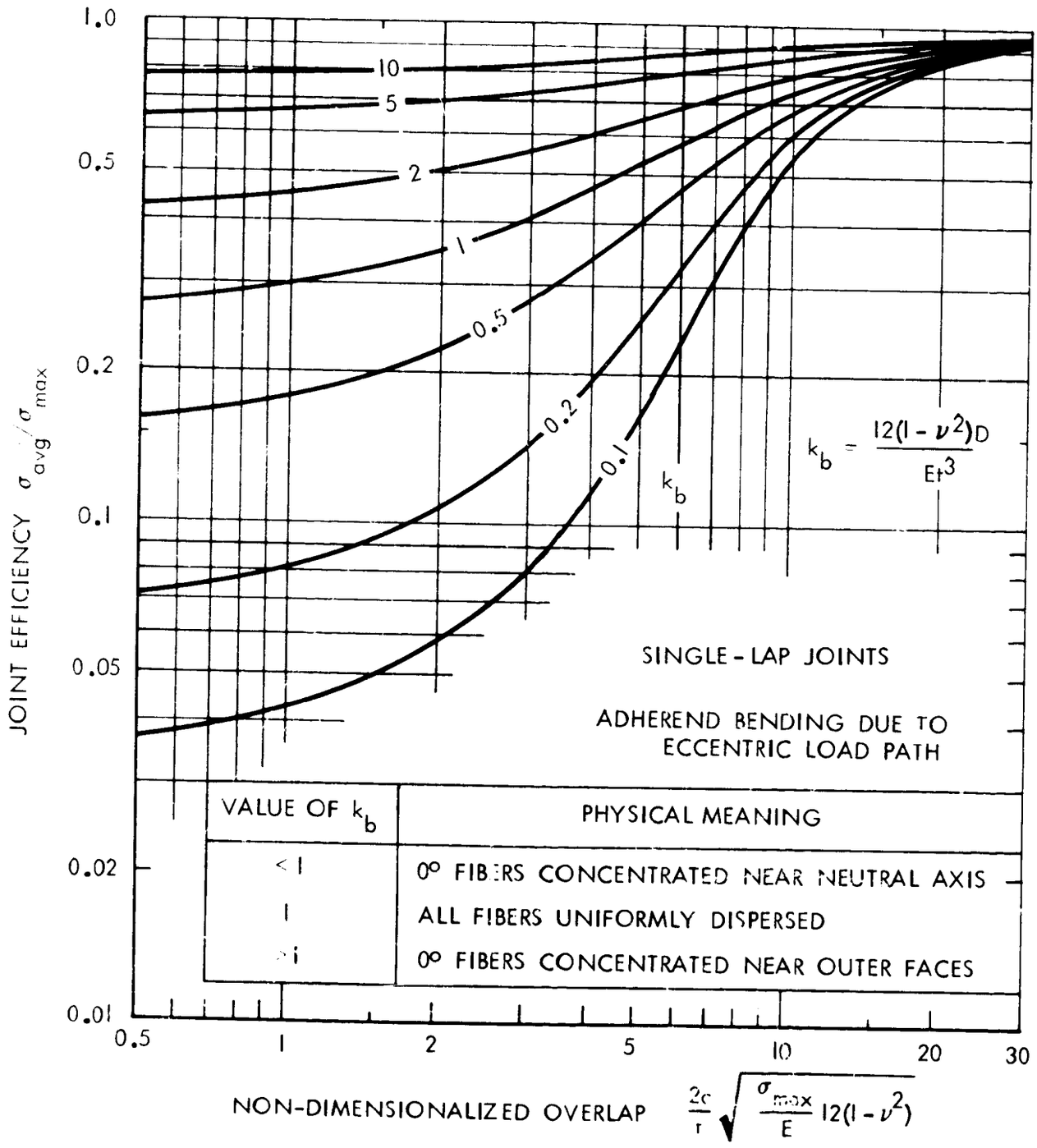

FIGURE 6. INFLUENCE OF PLY STACKING SEQUENCE IN COMPOSITE LAMINATES ON ADHEREND BENDING STRENGTH OF BALANCED SINGLE-LAP JOINTS

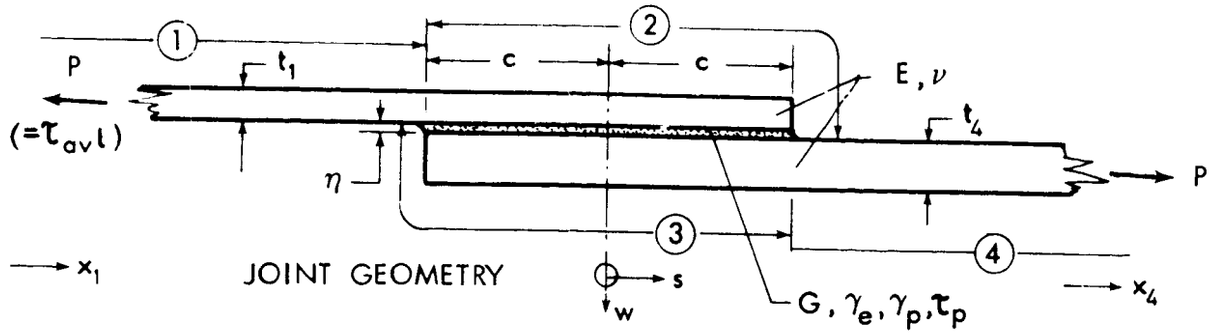

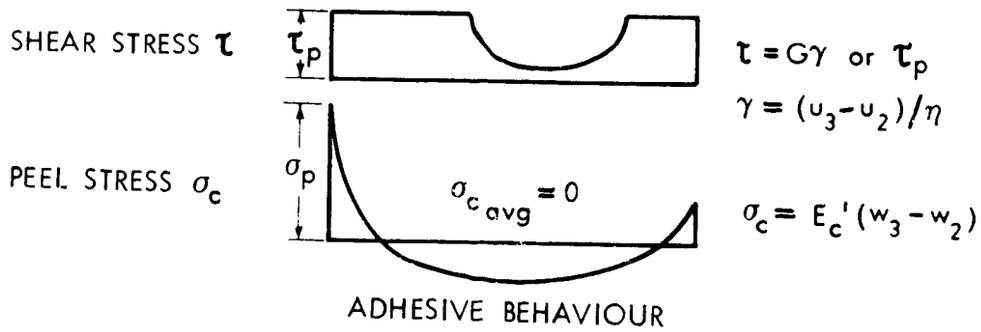

ADHESIVE BEHAVIOUR

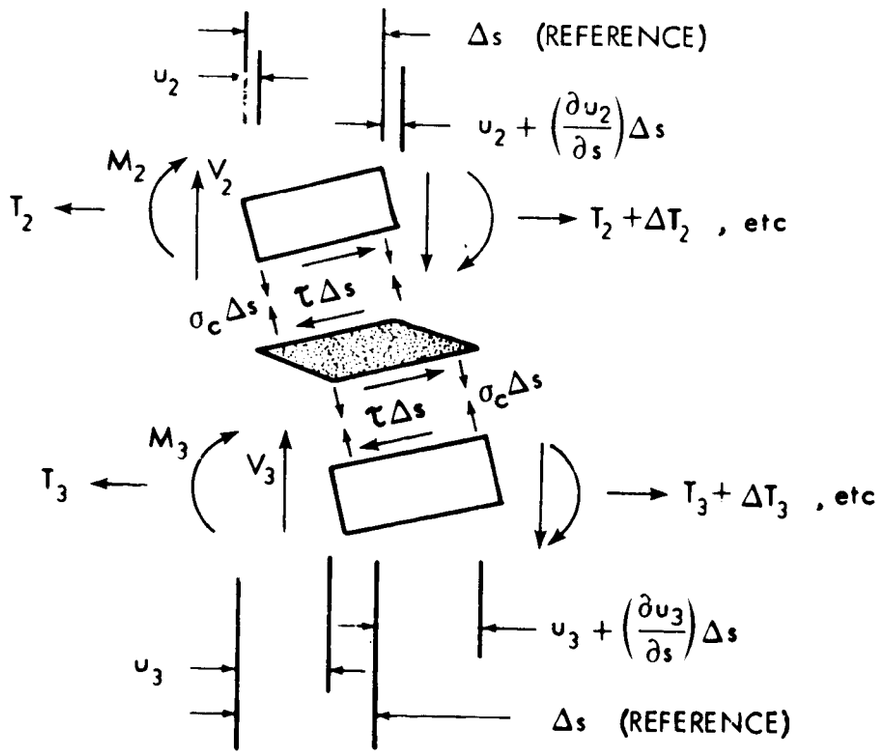

DISPLACEMENTS AND ELEMENT LOADS

FIGURE 7. GEOMETRY, NOMENCLATURE AND MATHEMATICAL MODEL FOR ANALYSIS OF UNBALANCED SINGLE-LAP JOINTS

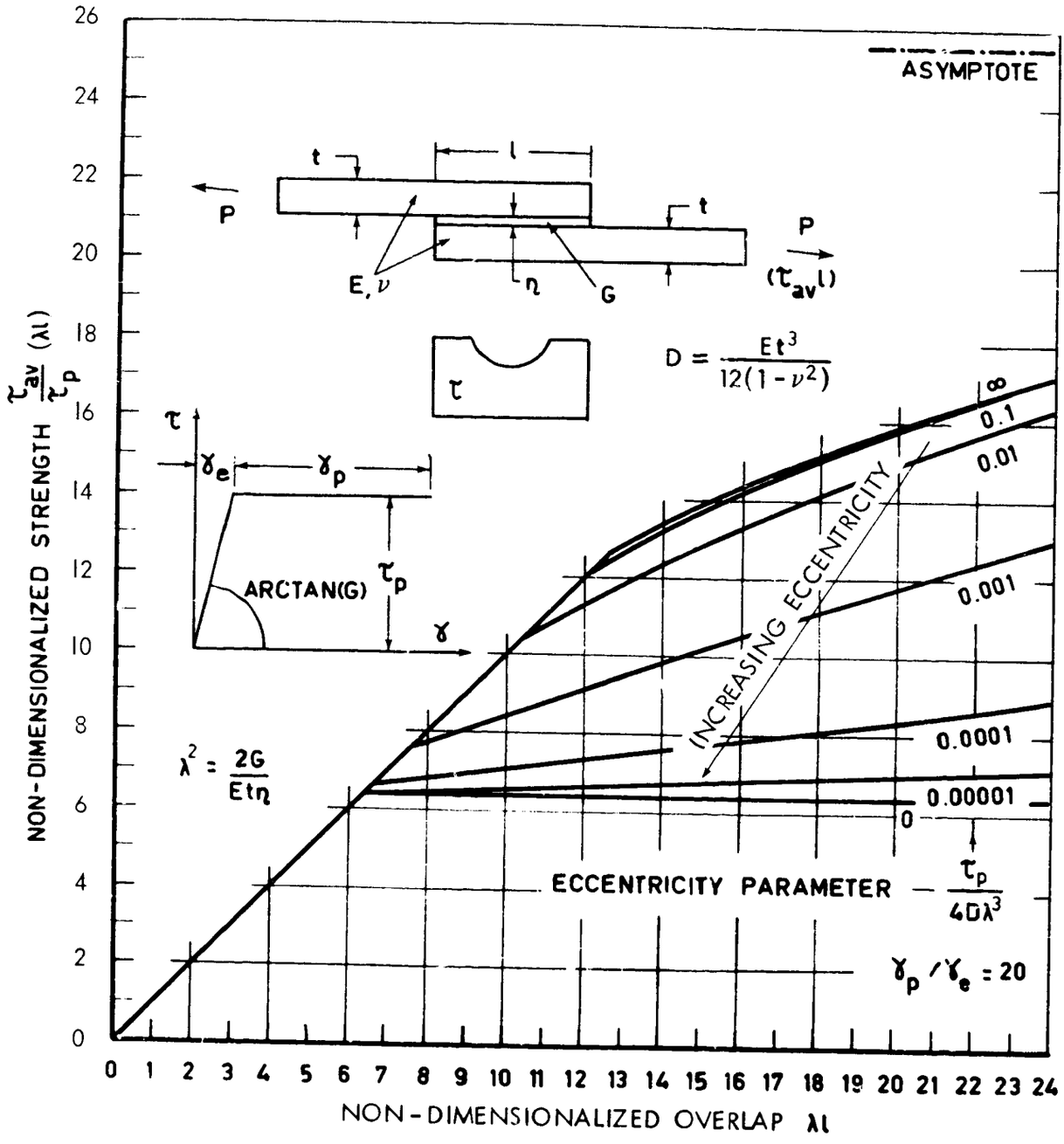

FIGURE 8. INFLUENCE OF ADHEREND PROPERTIES ON SHEAR STRENGTH OF SINGLE-LAP BONDED JOINTS

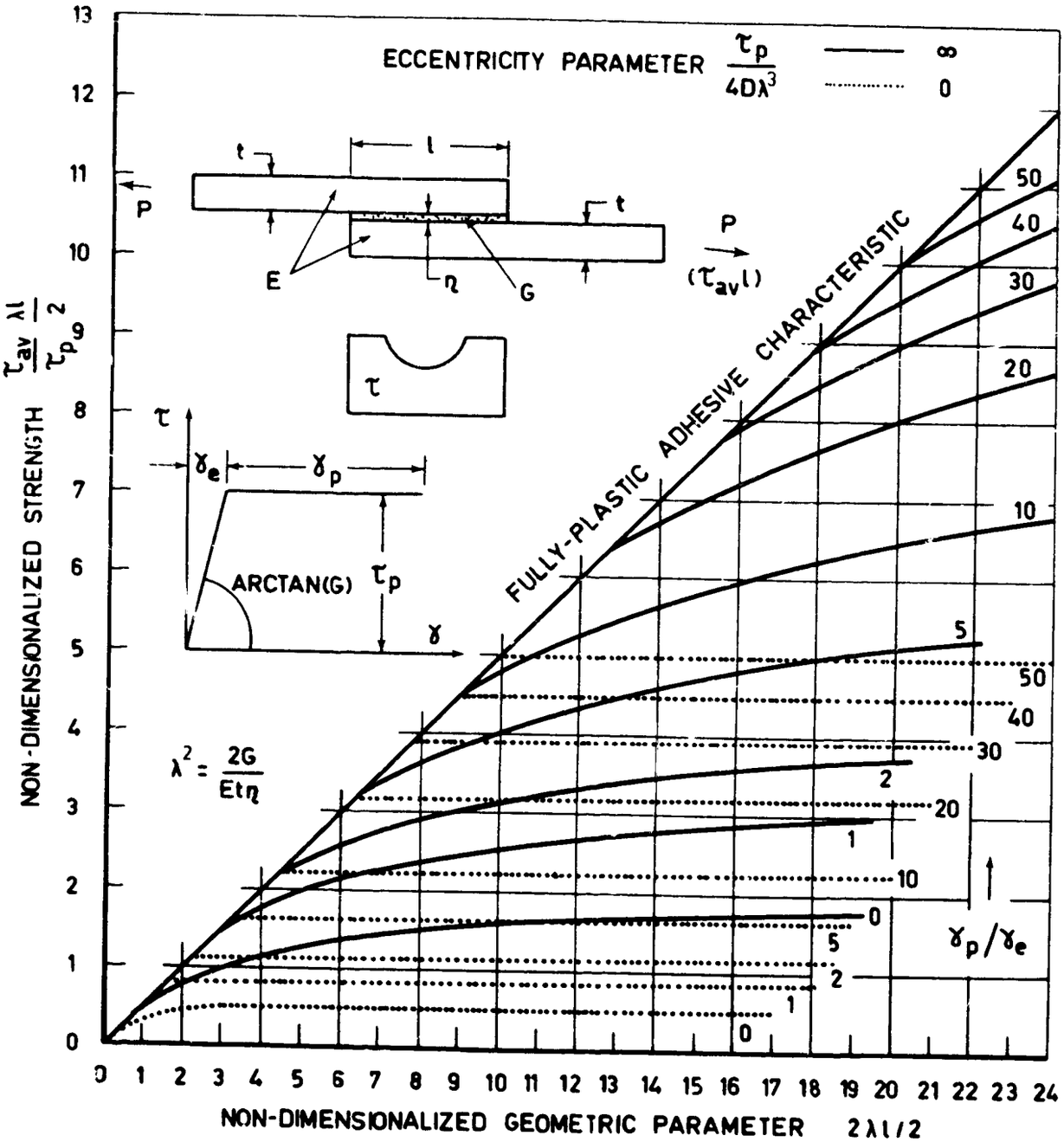

FIGURE 9. INFLUENCE OF ADHESIVE PROPERTIES ON SHEAR STRENGTH OF SINGLE-LAP BONDED JOINTS

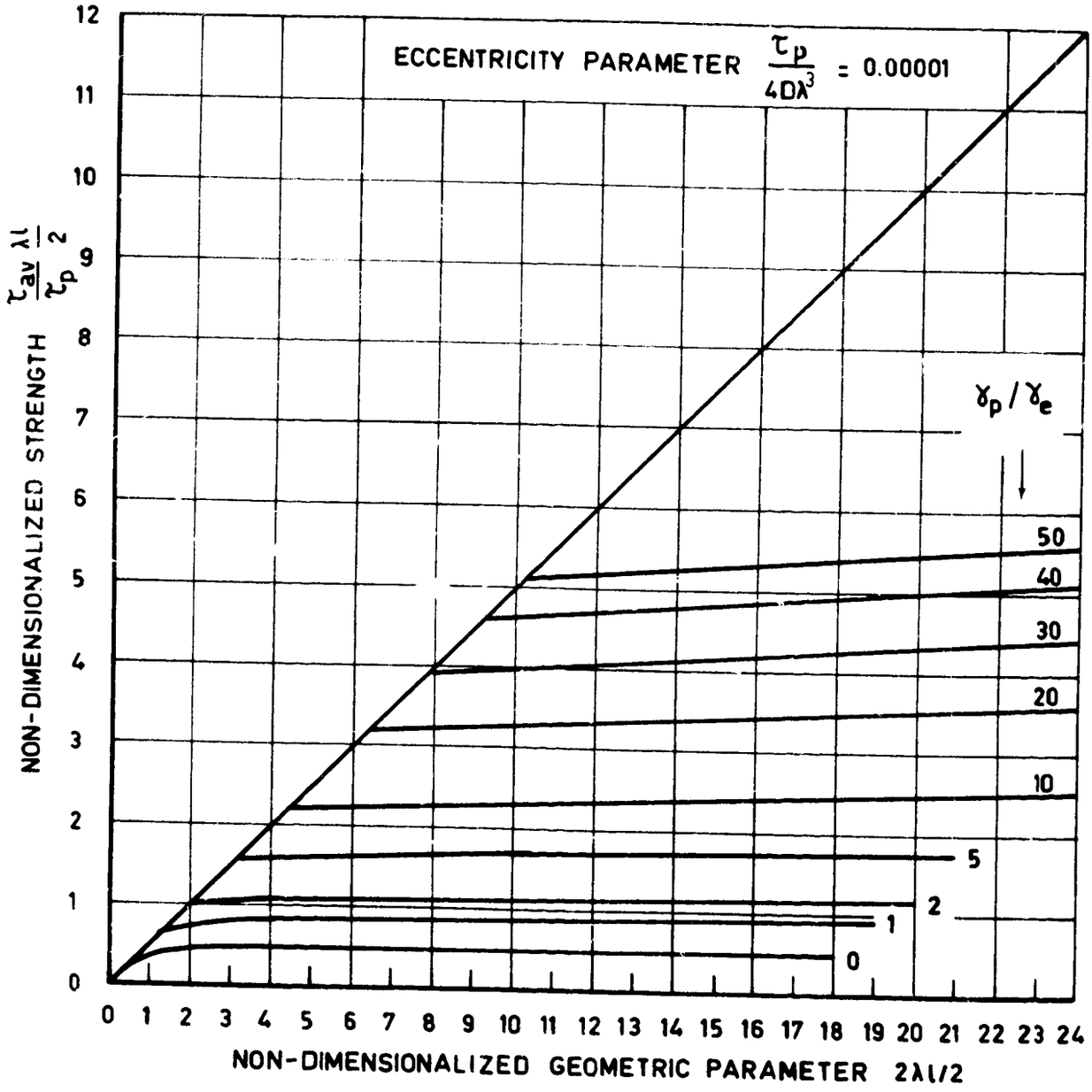

FIGURE 10. NON-DIMENSIONALIZED ADHESIVE BOND SHEAR STRENGTHS FOR SINGLE-LAP BONDED JOINTS

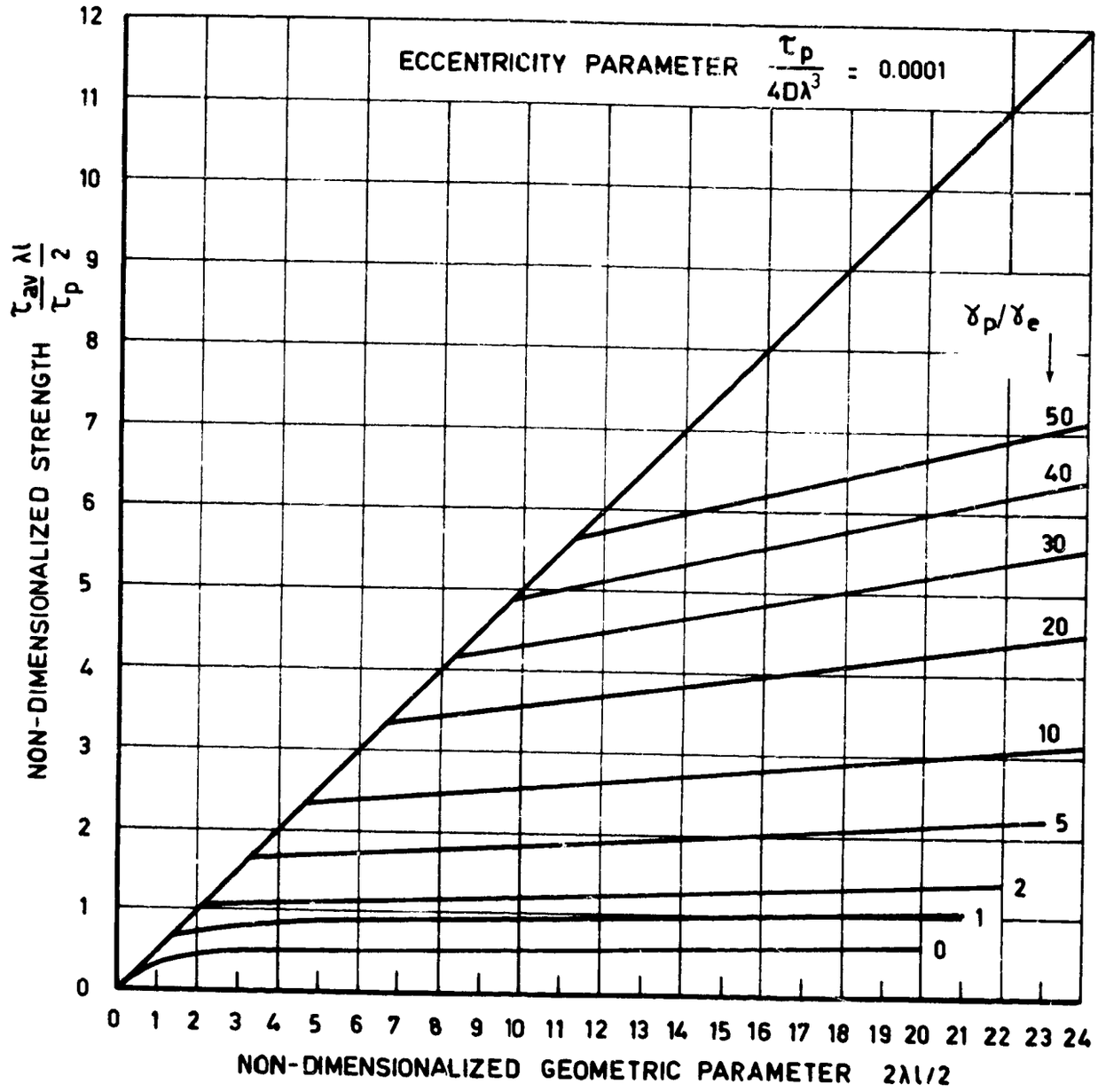

FIGURE 11. NON-DIMENSIONALIZED ADHESIVE BOND SHEAR STRENGTHS FOR SINGLE-LAP BONDED JOINTS

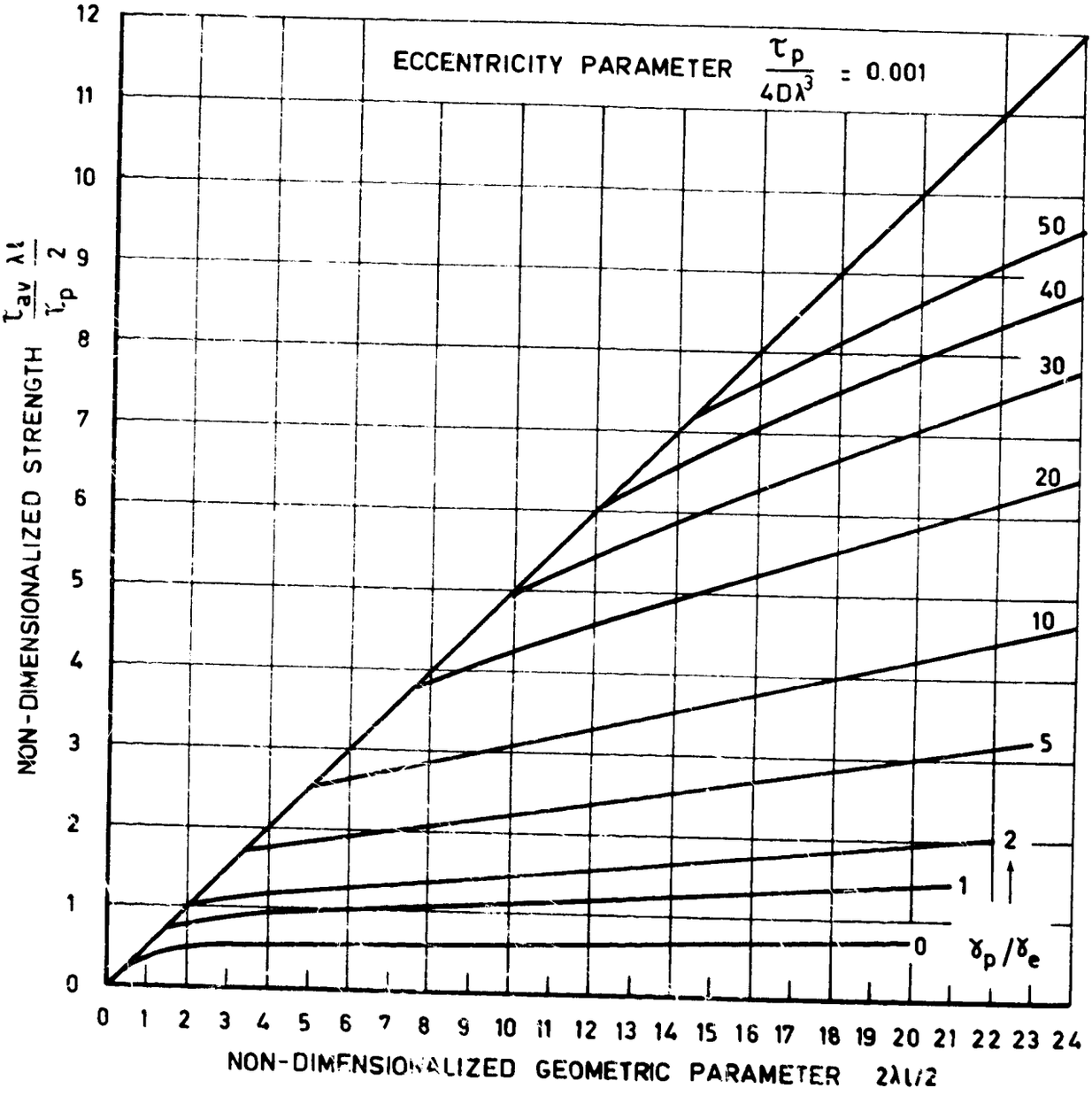

FIGURE 12. NON-DIMENSIONALIZED ADHESIVE BOND SHEAR STRENGTHS FOR SINGLE-LAP BONDED JOINTS

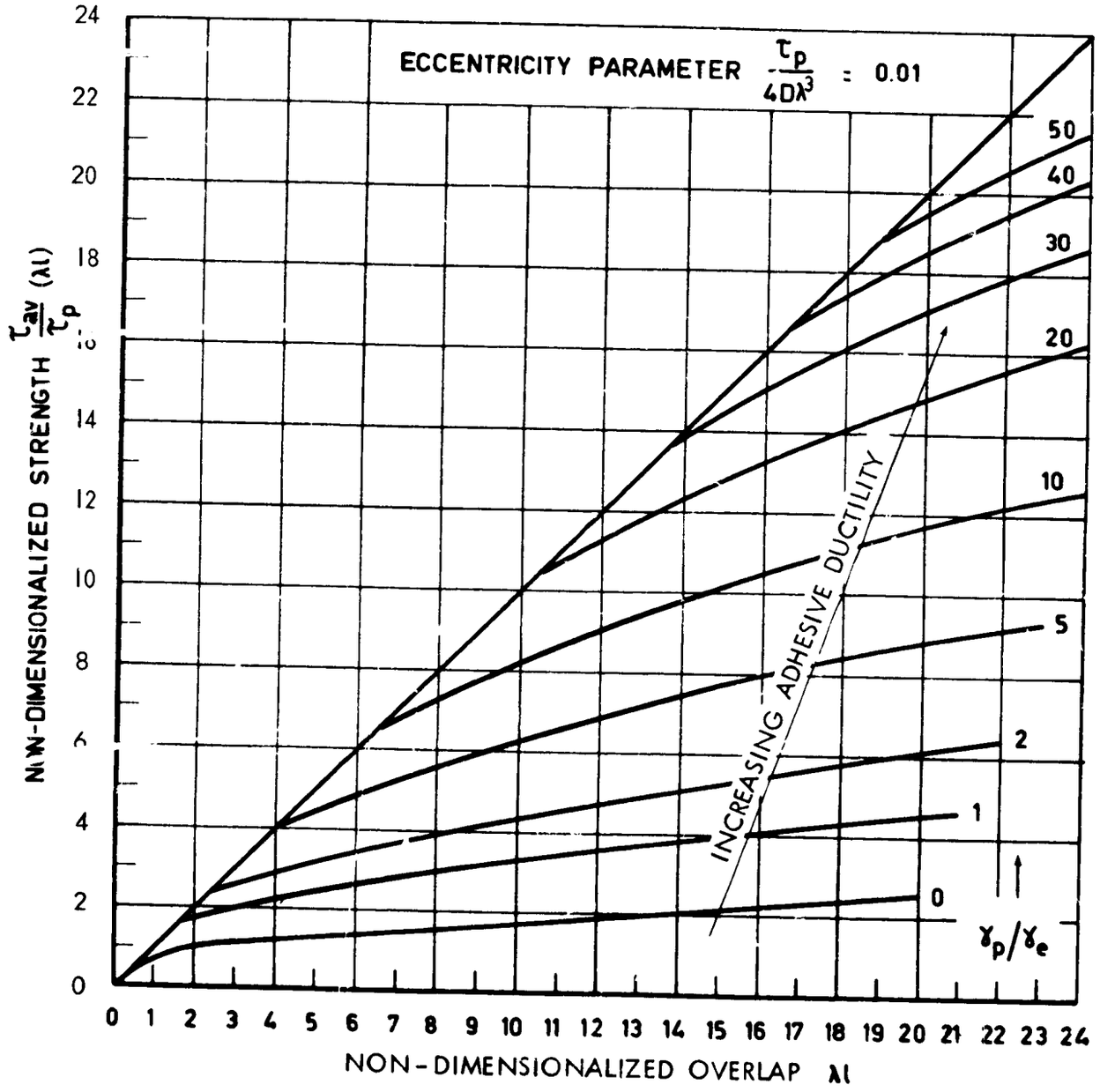

FIGURE 13. NON-DIMENSIONALIZED ADHESIVE BOND SHEAR STRENGTHS FOR SINGLE-LAP BONDED JOINTS

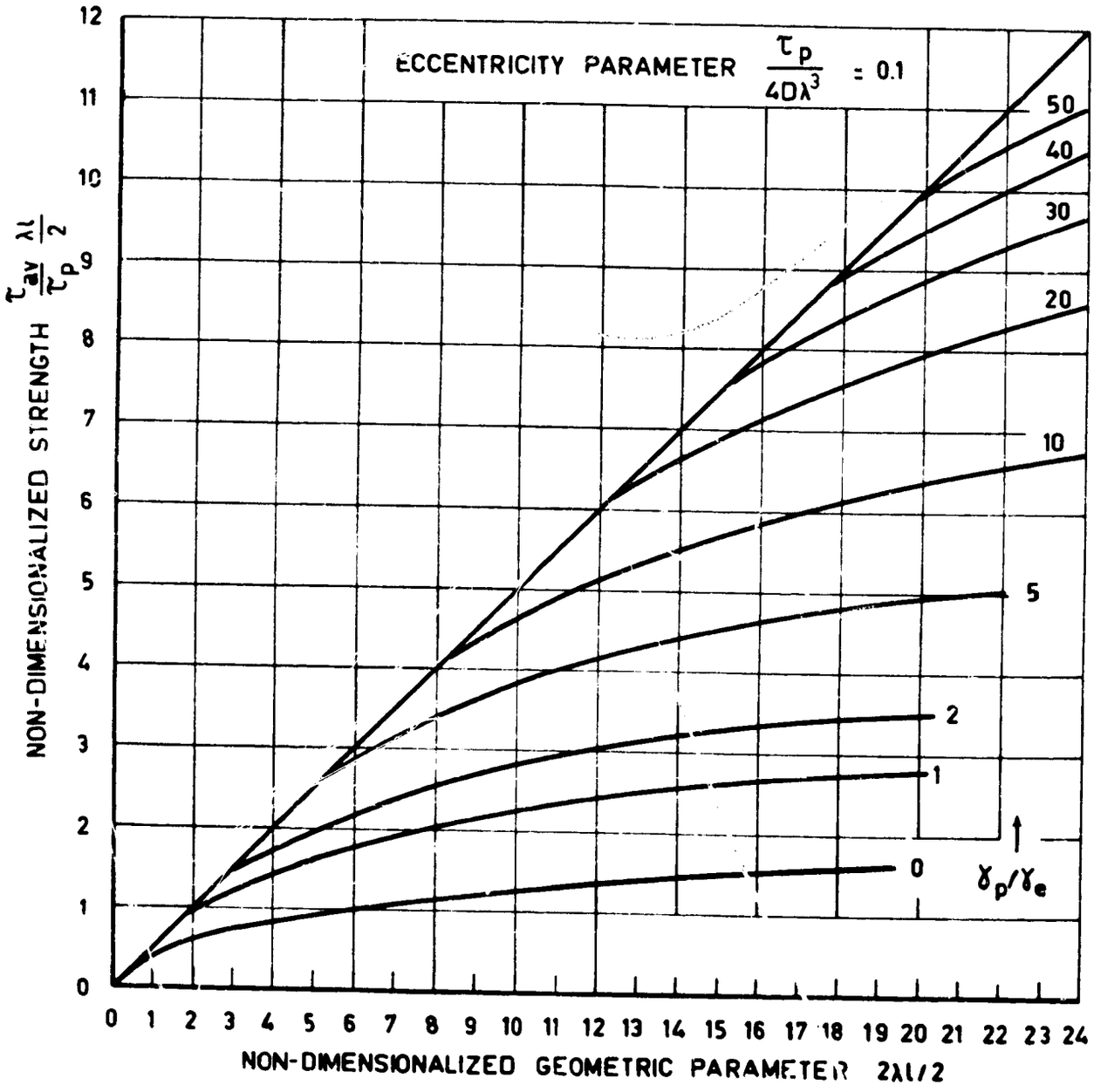

FIGURE 14. NON-DIMENSIONALIZED ADHESIVE BOND SHEAR STRENGTHS FOR SINGLE-LAP BONDED JOINTS

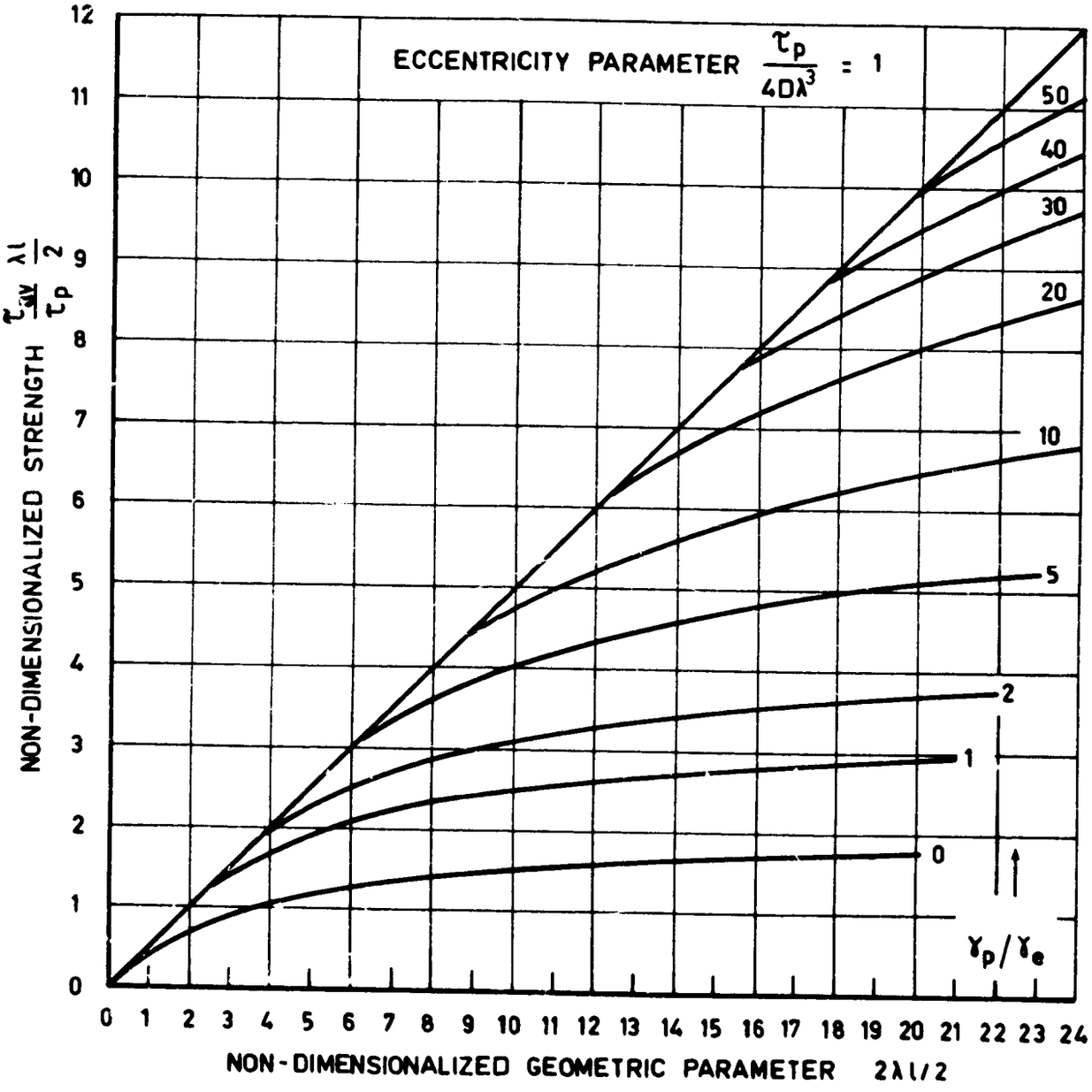

FIGURE 15. NON-DIMENSIONALIZED ADHESIVE BOND SHEAR STRENGTHS FOR SINGLE-LAP BONDED JOINTS

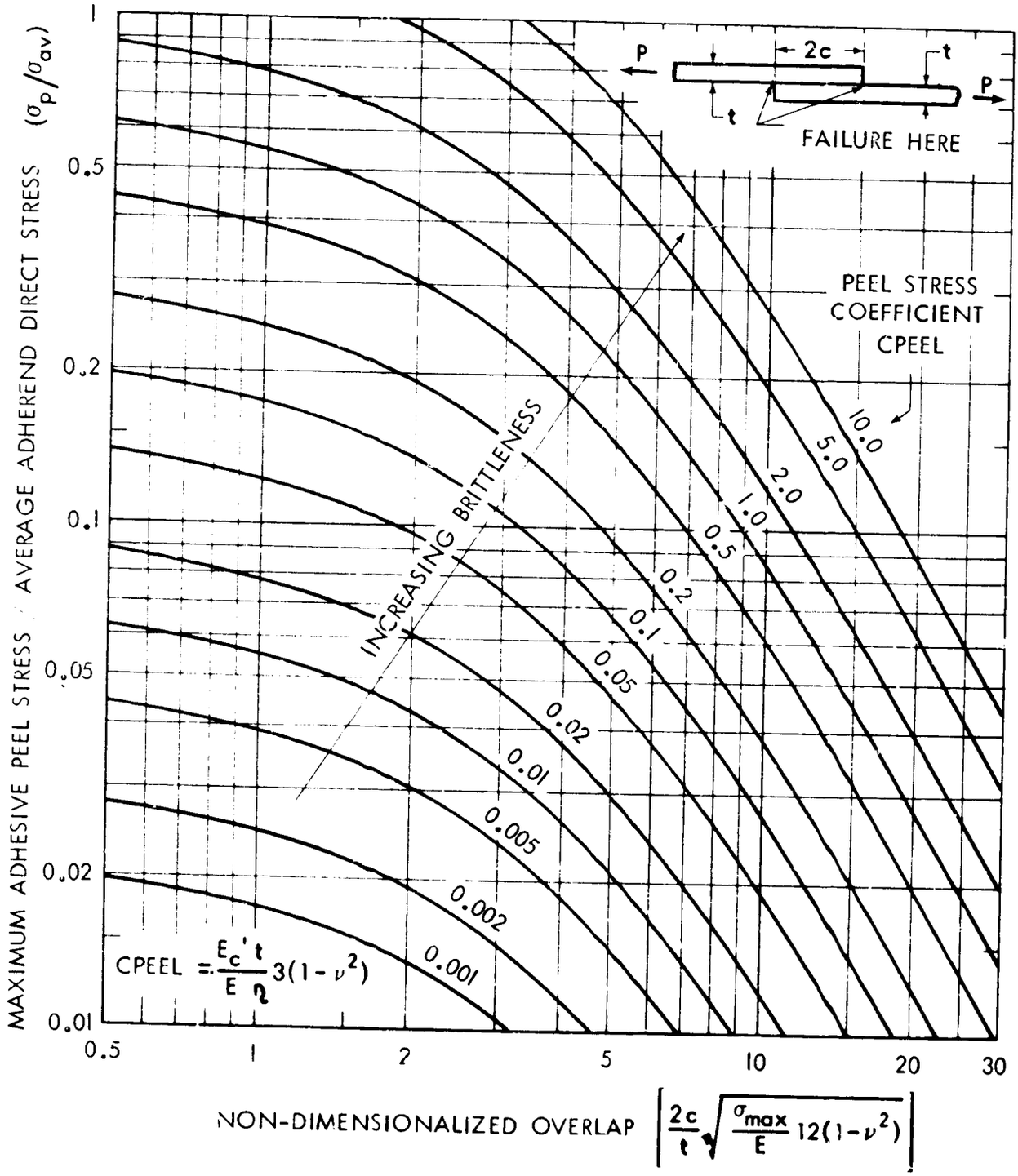

FIGURE 16. PEEL STRESSES IN BALANCED SINGLE-LAP JOINTS

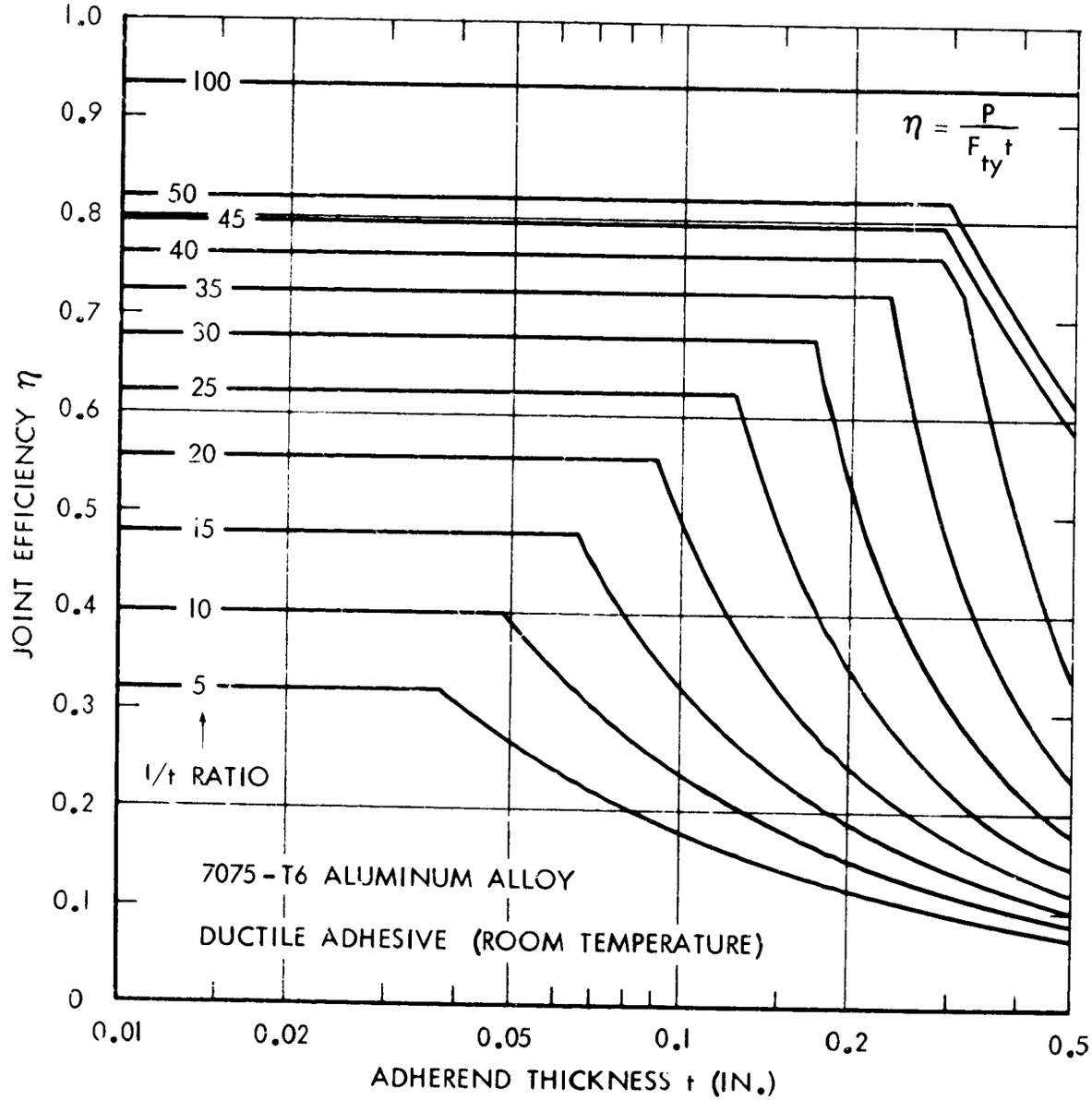

FIGURE 17. JOINT EFFICIENCY CHART FOR SINGLE-LAP METAL JOINTS

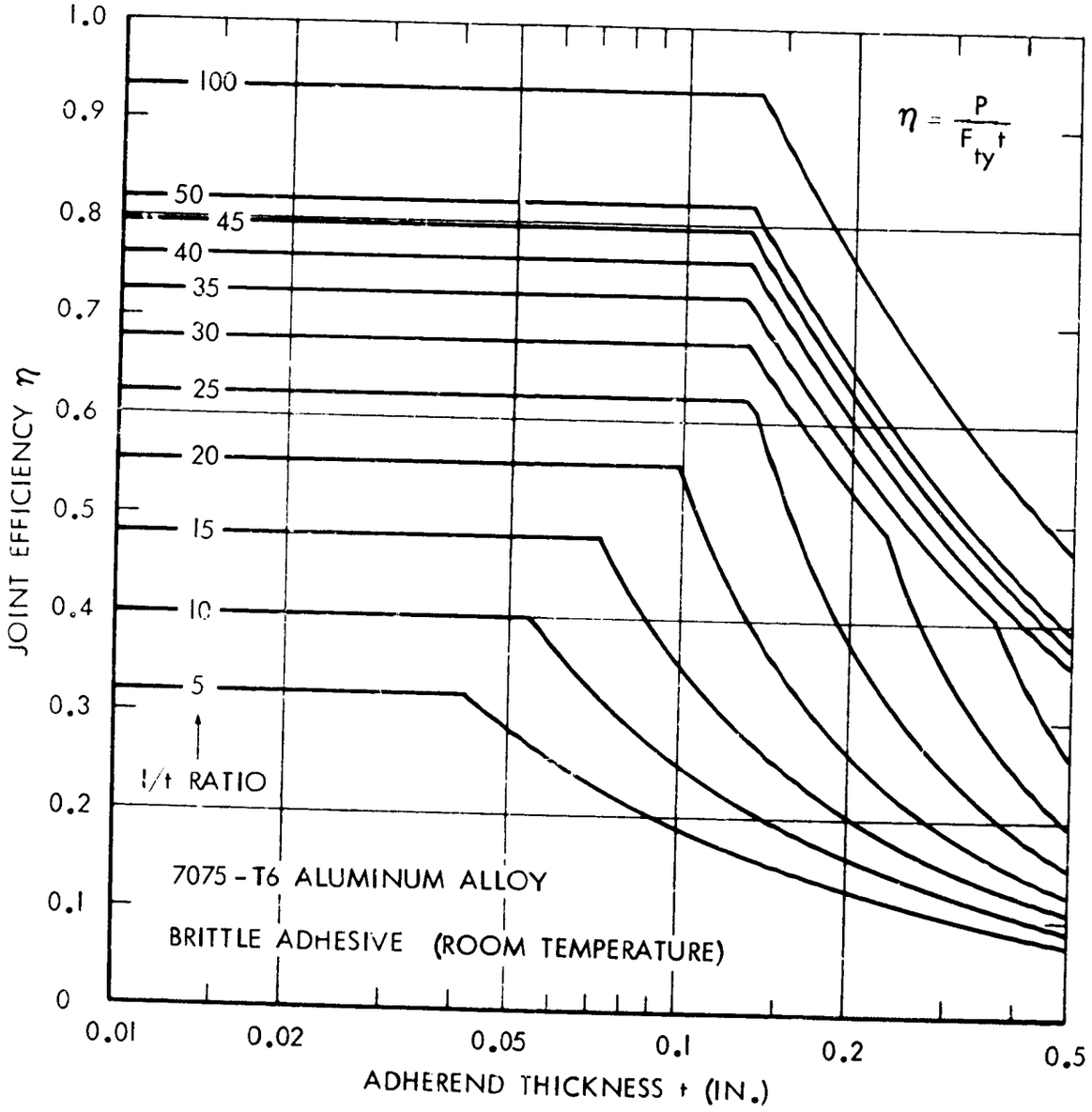

FIGURE 18. JOINT EFFICIENCY CHART FOR SINGLE-LAP METAL JOINTS

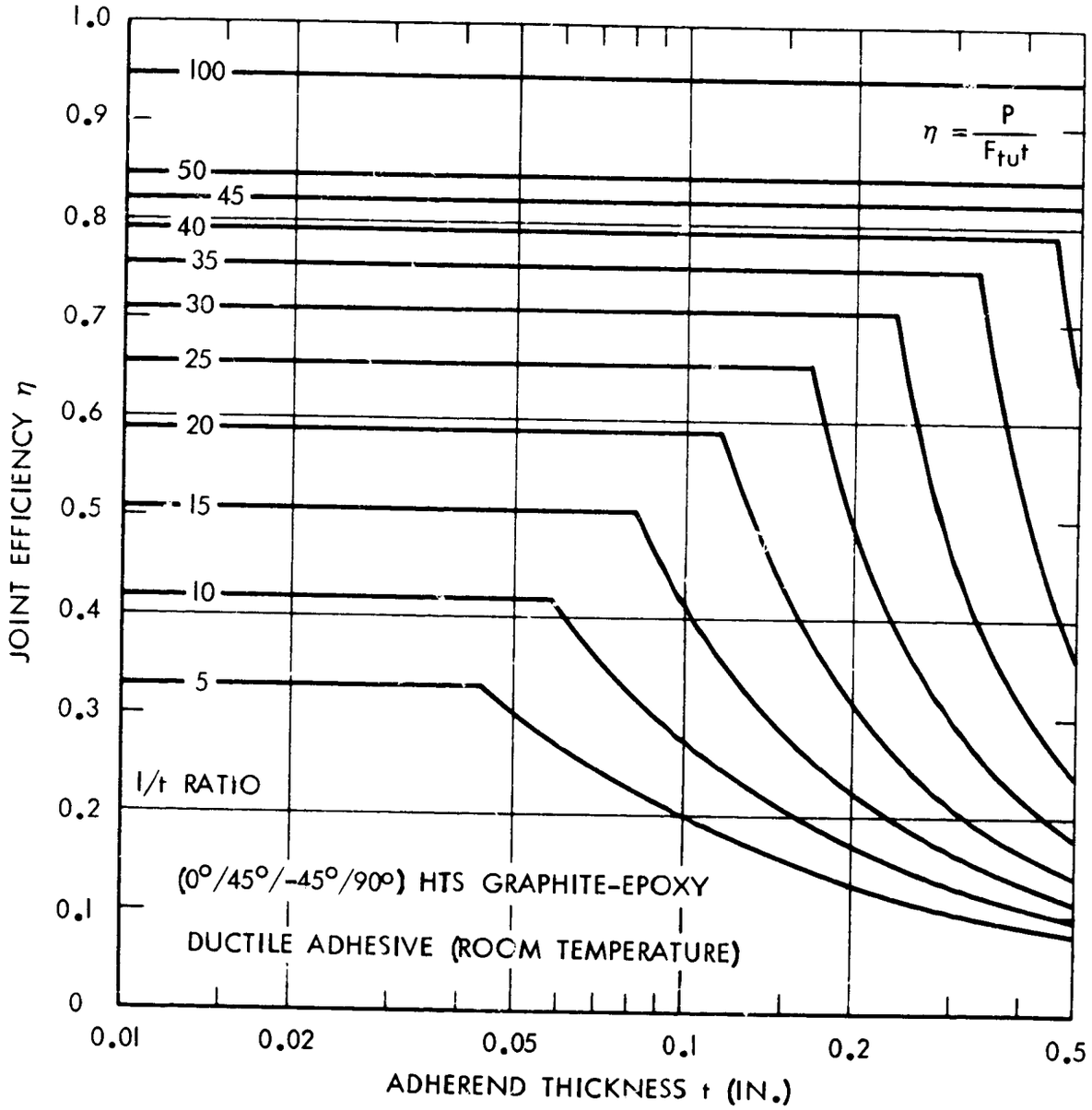

FIGURE 19. JOINT EFFICIENCY CHART FOR SINGLE-LAP COMPOSITE JOINTS

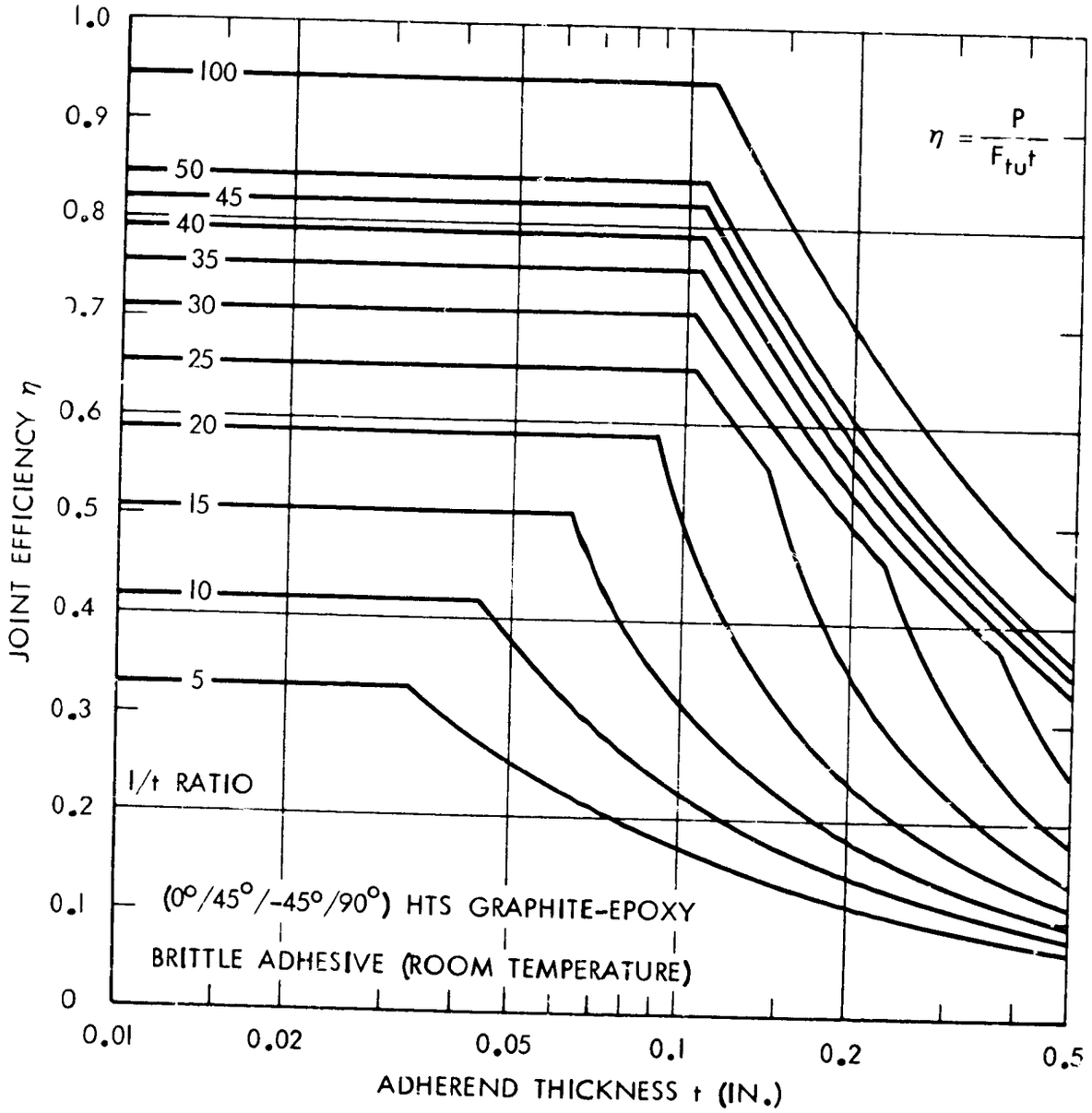

FIGURE 20. JOINT EFFICIENCY CHART FOR SINGLE-LAP COMPOSITE JOINTS

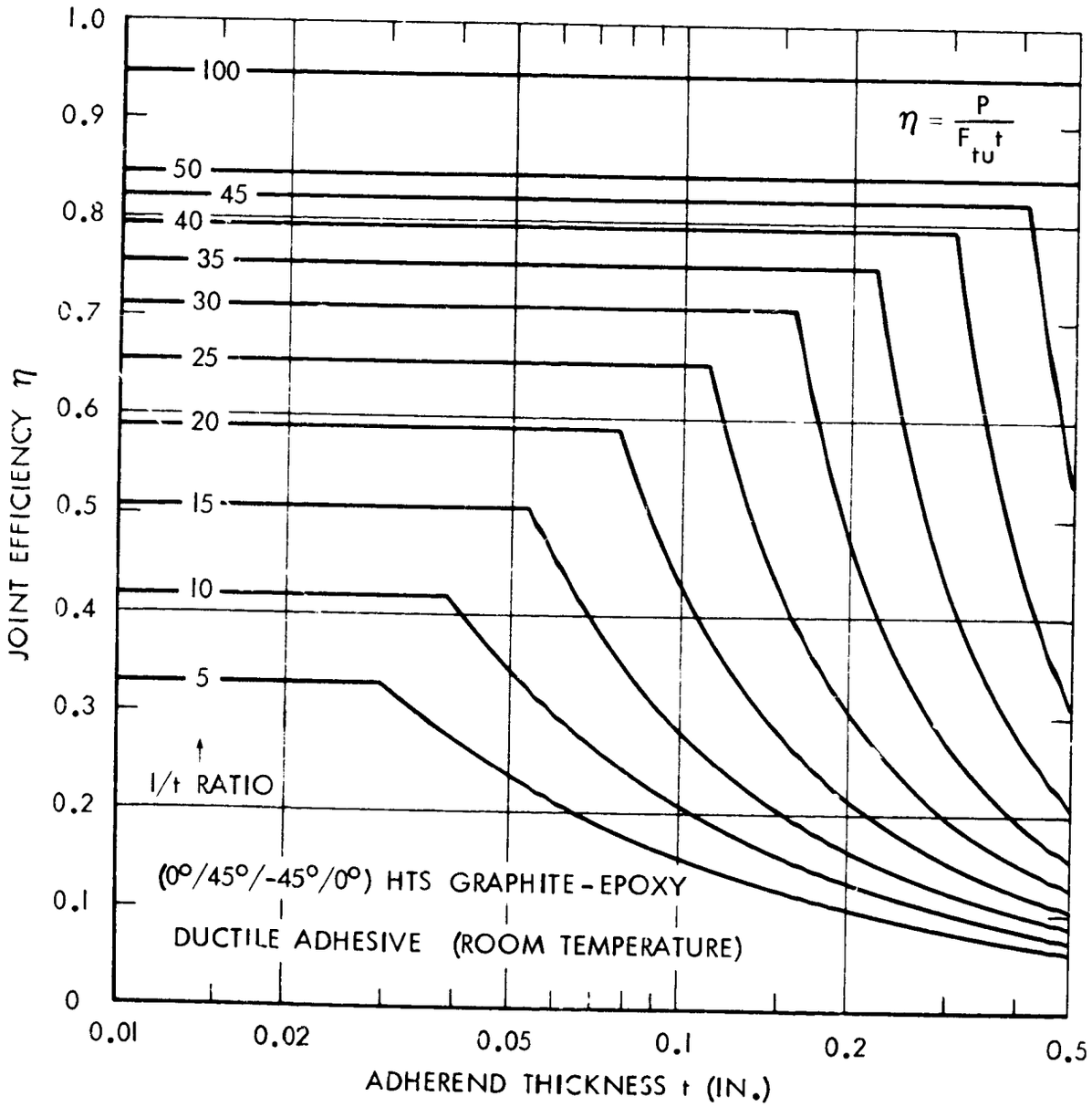

FIGURE 21. JOINT EFFICIENCY CHART FOR SINGLE-LAP COMPOSITE JOINTS

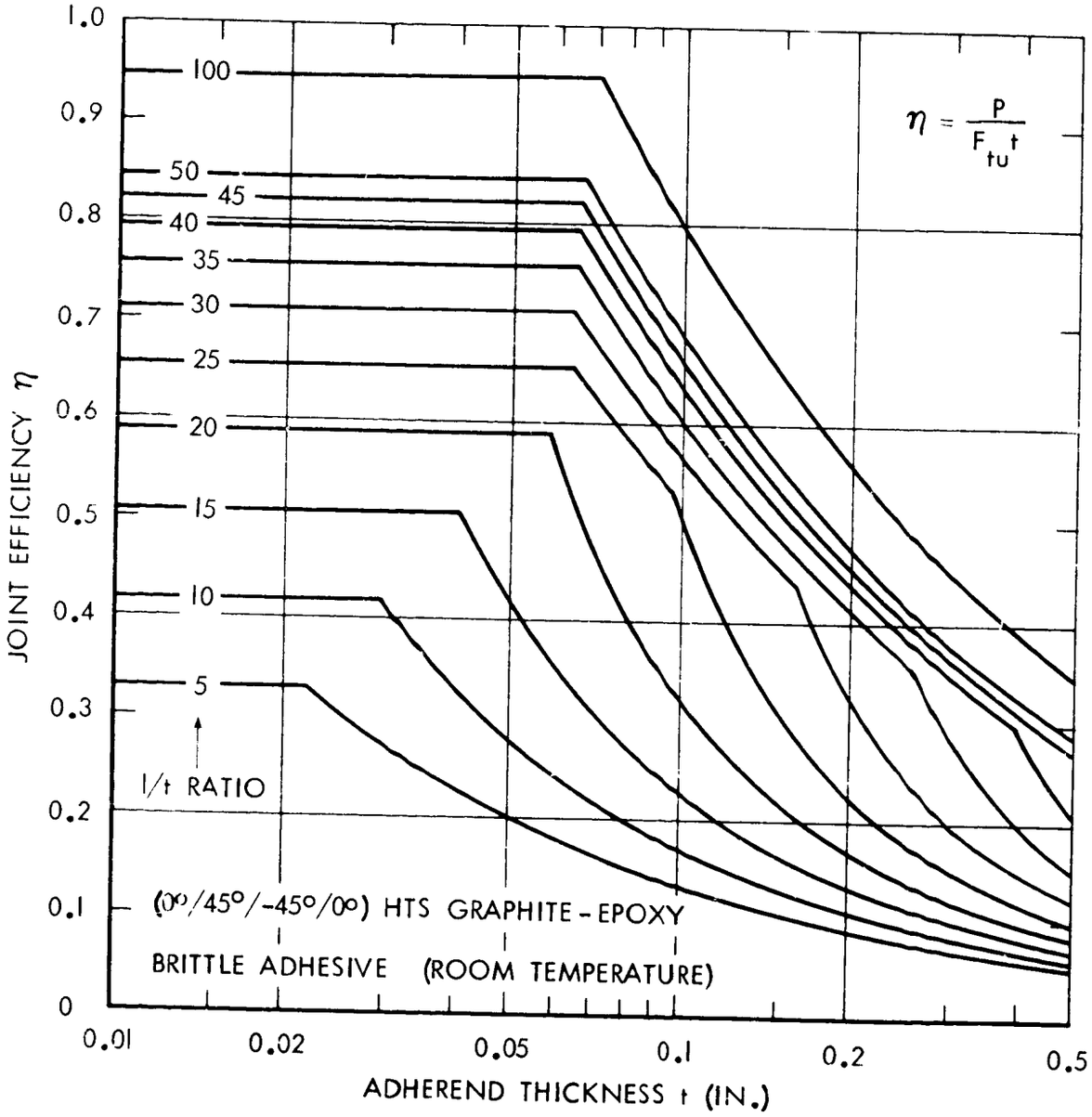

FIGURE 22. JOINT EFFICIENCY CHART FOR SINGLE-LAP COMPOSITE JOINTS

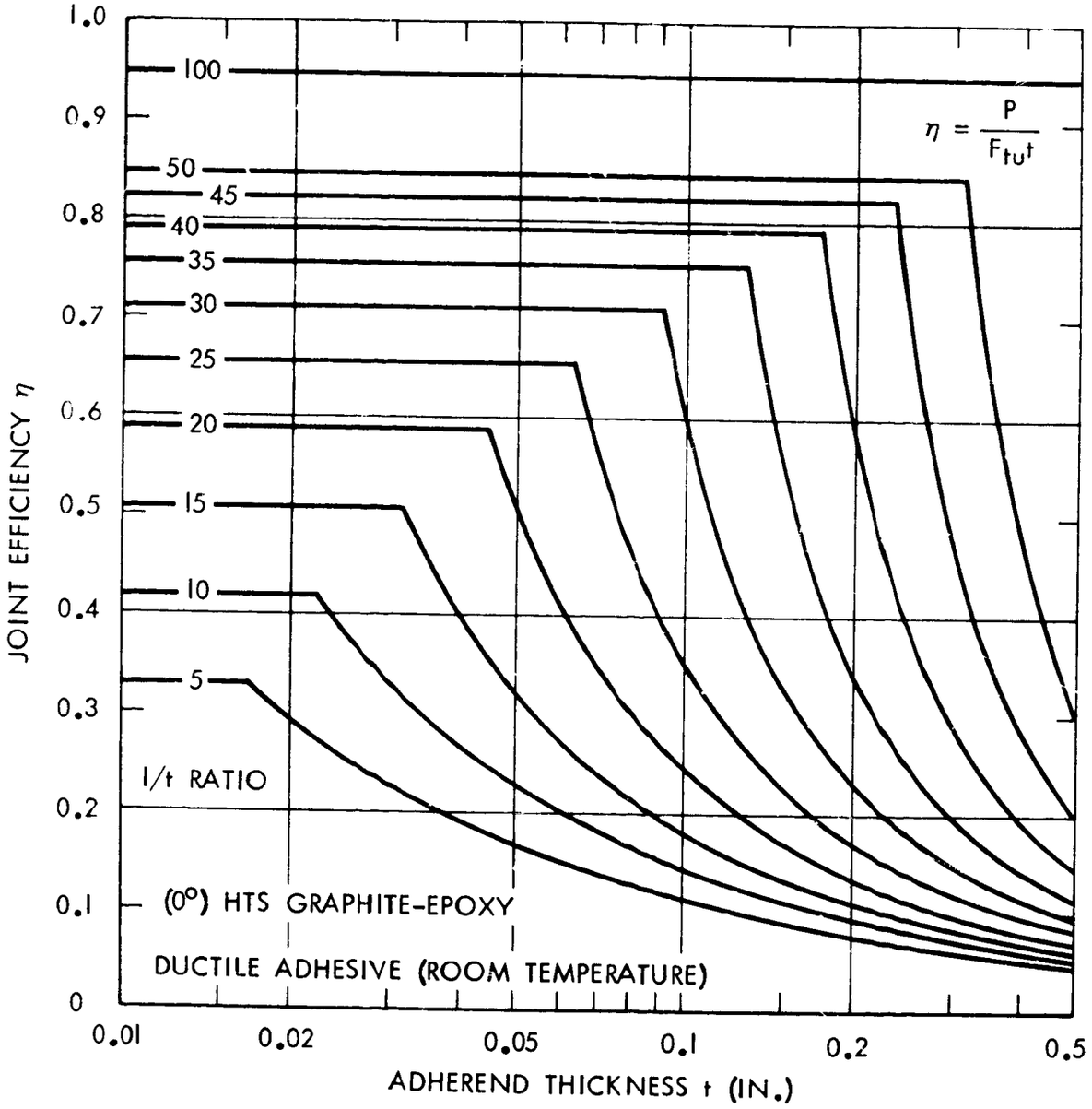

FIGURE 23. JOINT EFFICIENCY CHART FOR SINGLE-LAP COMPOSITE JOINTS

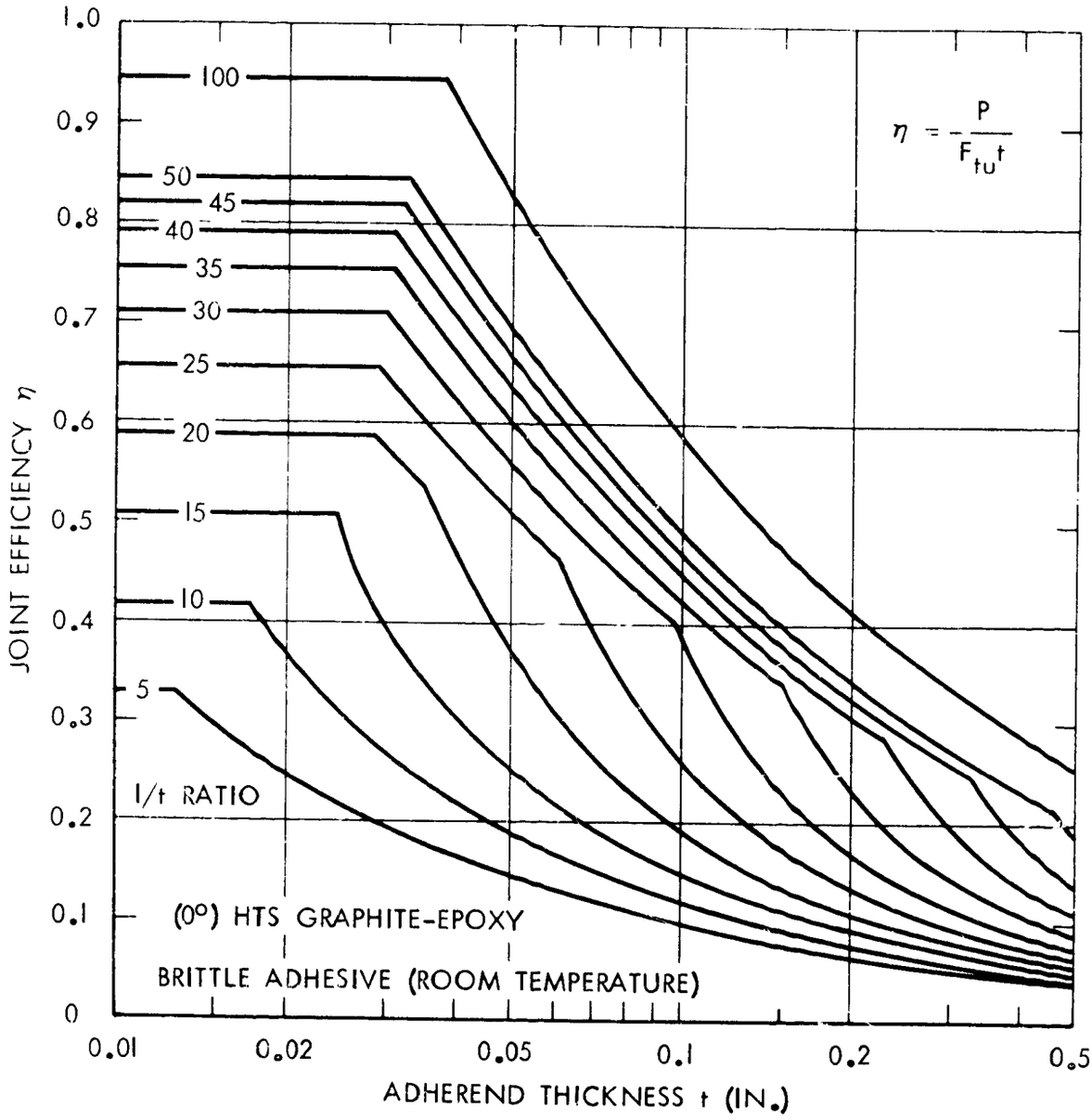

FIGURE 24. JOINT EFFICIENCY CHART FOR SINGLE-LAP COMPOSITE JOINTS

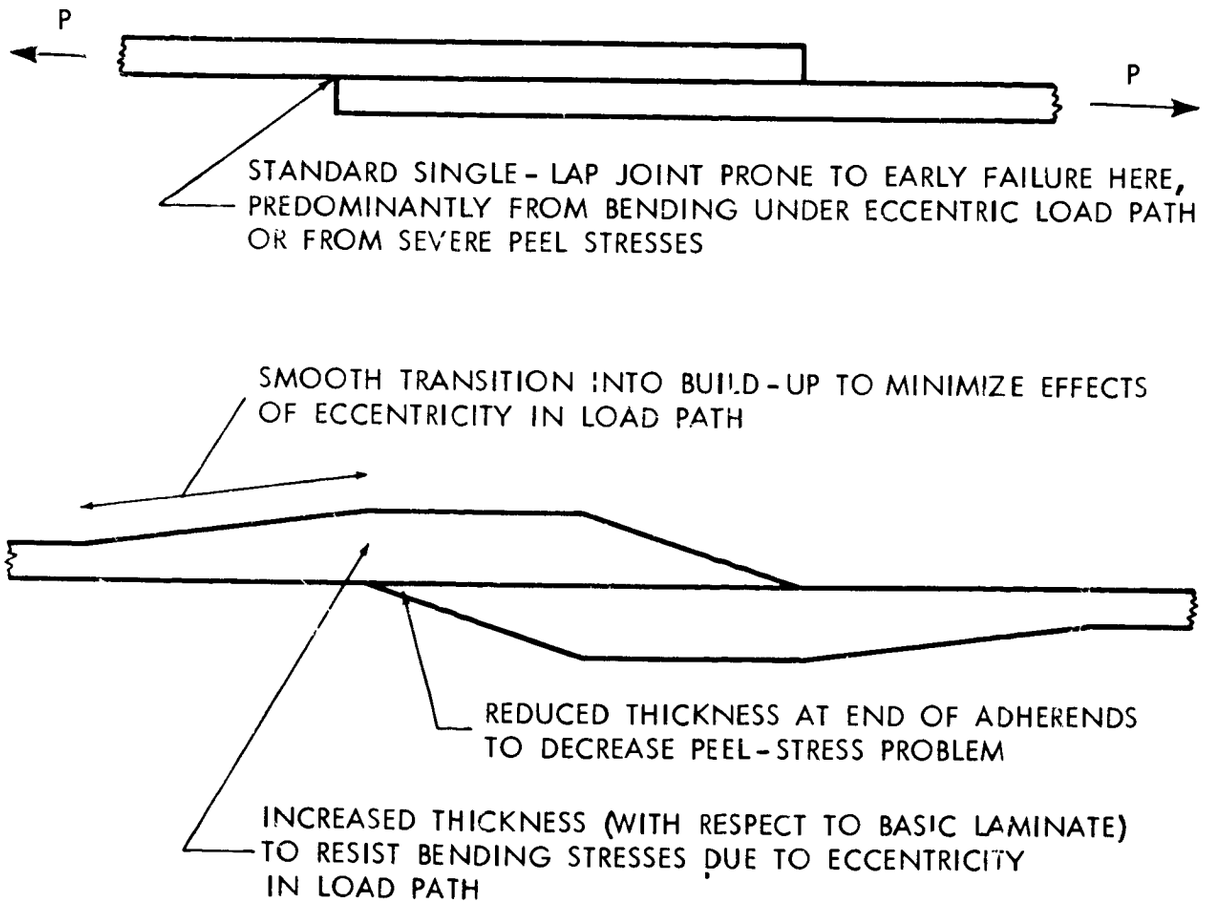

FIGURE 25. REDUCTION IN INEFFICIENCY OF UNSUPPORTED SINGLE-LAP JOINTS

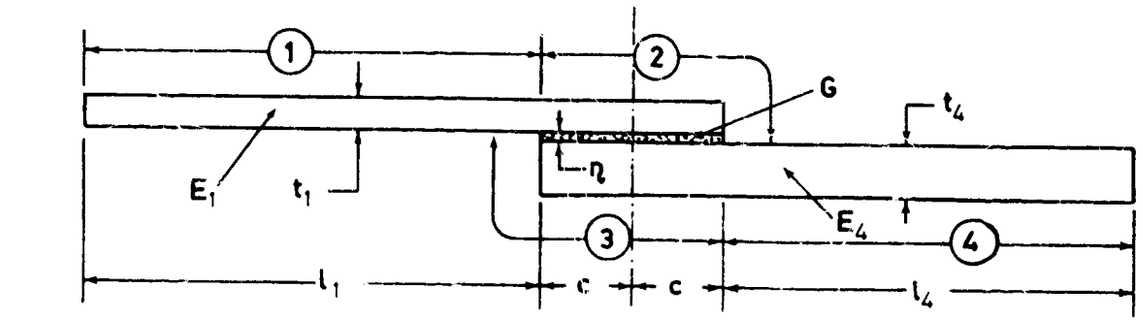

UNLOADED LAP JOINT

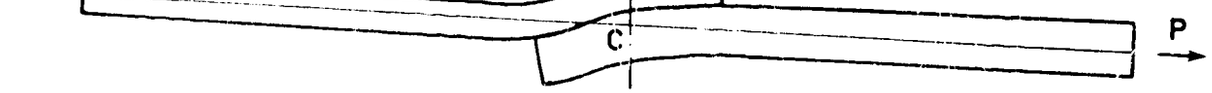

LAP JOINT DEFLECTING UNDER LOAD

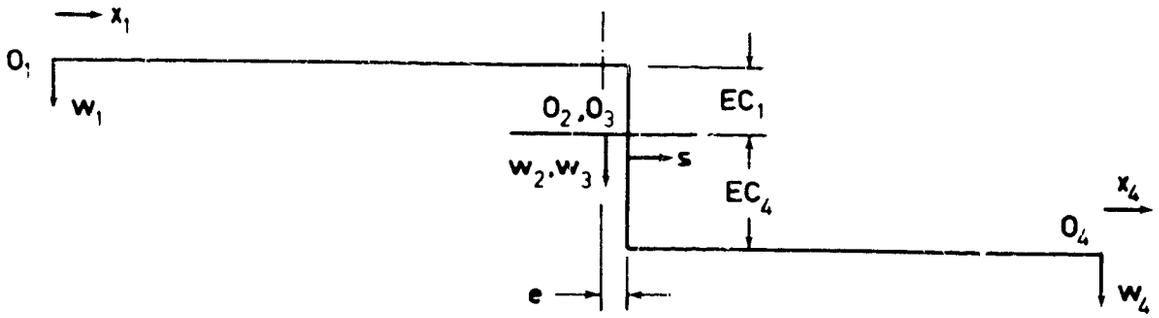

CO-ORDINATE SYSTEM

FIGURE 26. CO-ORDINATE SYSTEM FOR UNBALANCED SINGLE-LAP JOINTS

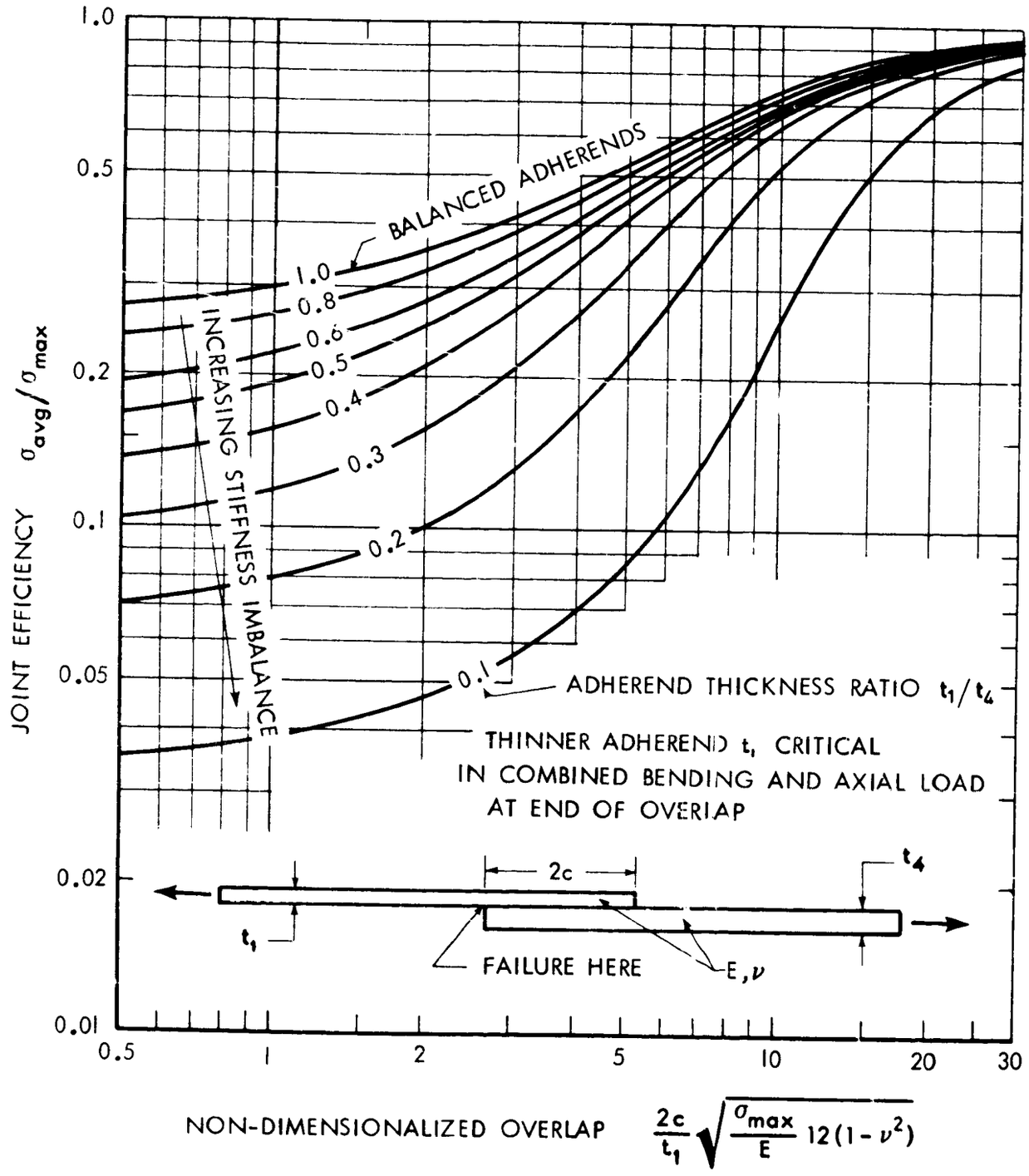

FIGURE 27. EFFECT OF ADHEREND STIFFNESS IMBALANCE ON ADHEREND BENDING STRENGTH OF SINGLE-LAP BONDED JOINTS

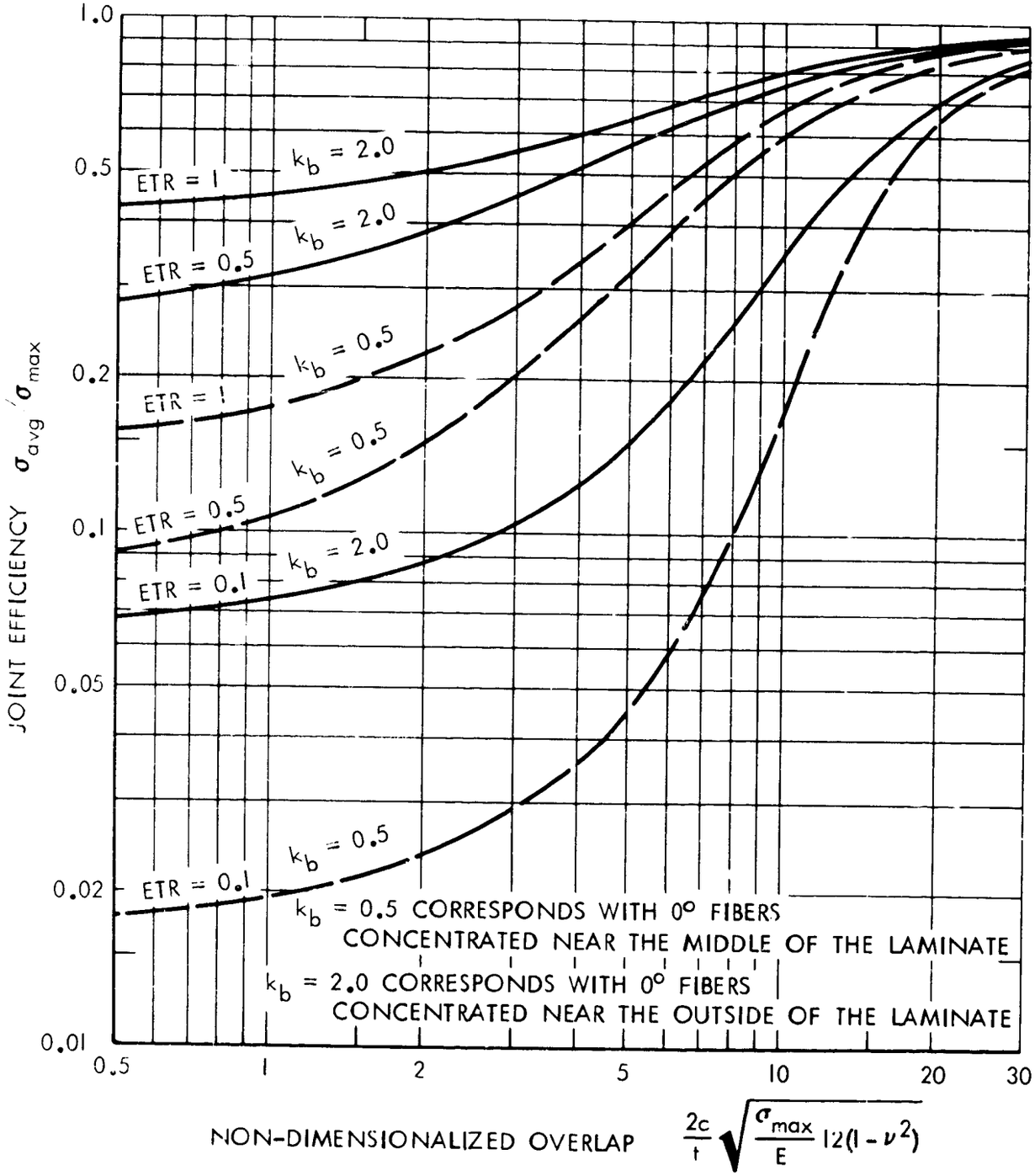

FIGURE 28. EFFECT OF FIBER STACKING SEQUENCE ON ADHEREND BENDING STRENGTH OF UNBALANCED COMPOSITE SINGLE-LAP JOINTS

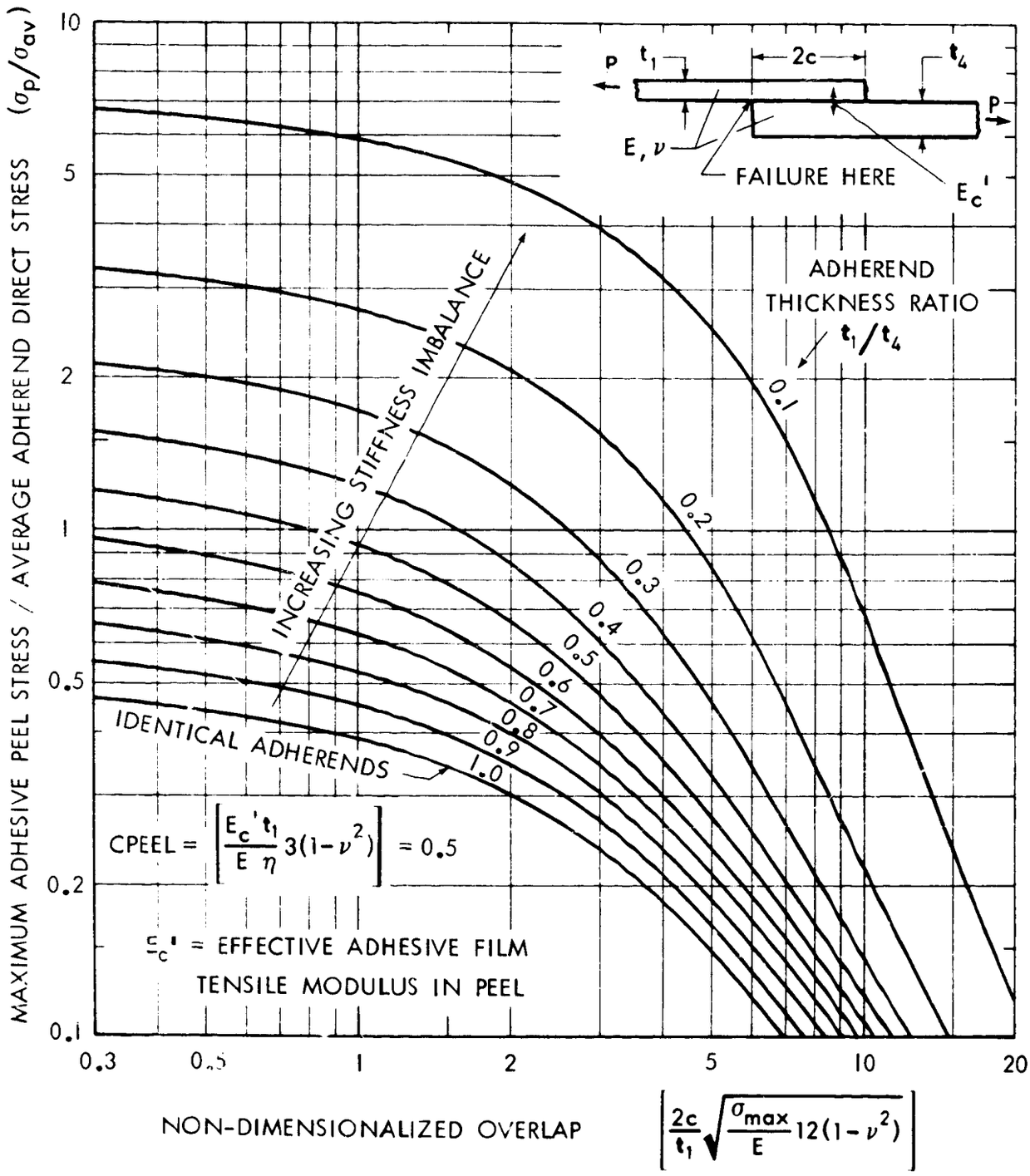

FIGURE 29. EFFECT OF ADHEREND STIFFNESS IMBALANCE ON PEEL STRESSES IN SINGLE-LAP BONDED JOINTS

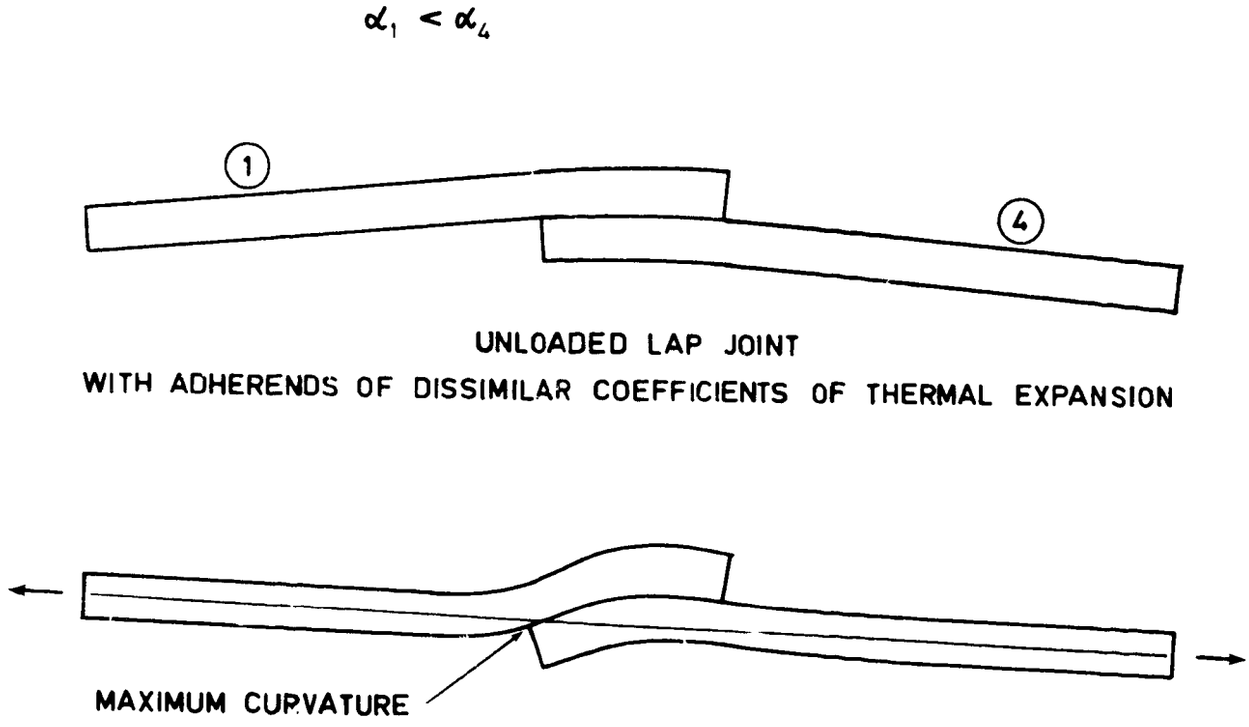

FIGURE 30. EFFECT OF ADHEREND THERMAL MISMATCH ON SINGLE-LAP BONDED JOINTS

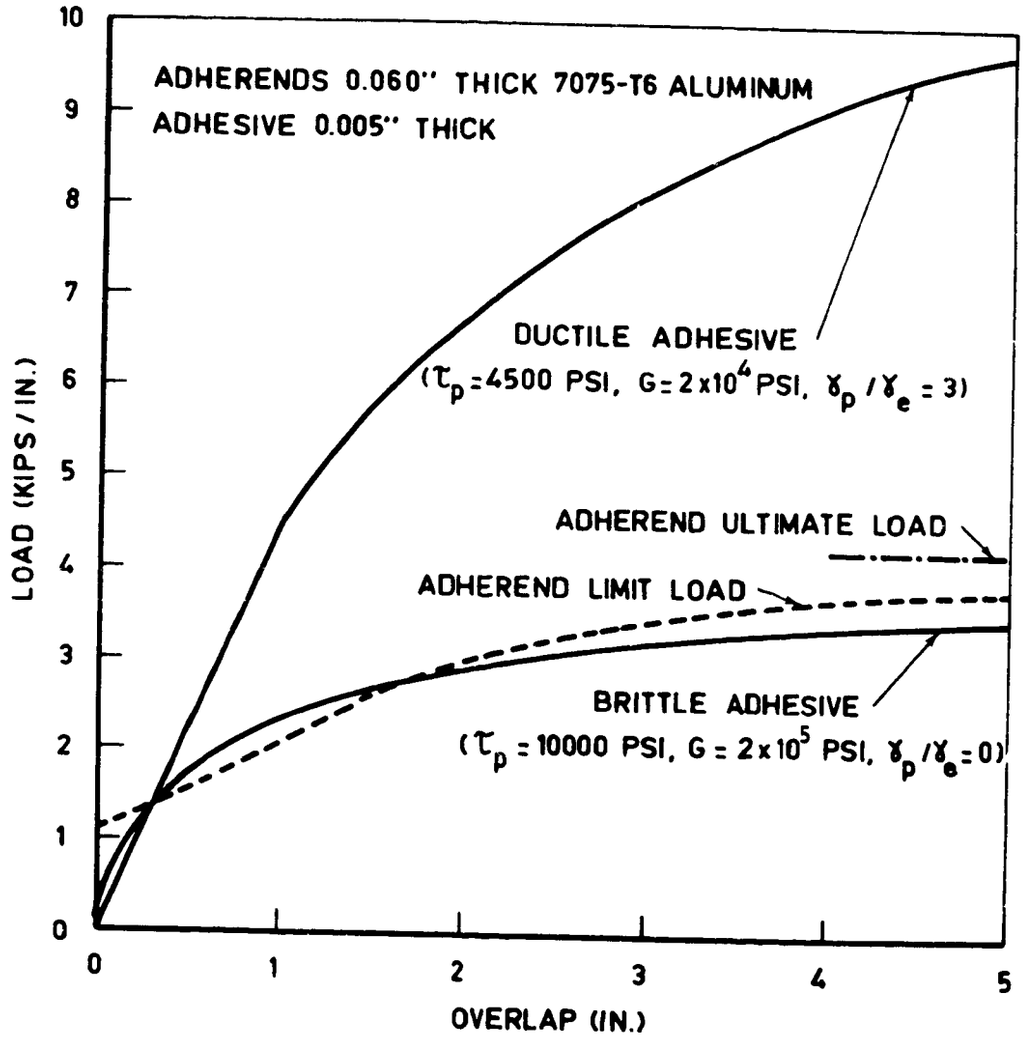

FIGURE 31. COMPARISON OF ADHESIVE AND ADHEREND STRENGTHS FOR SINGLE-LAP BONDED JOINTS

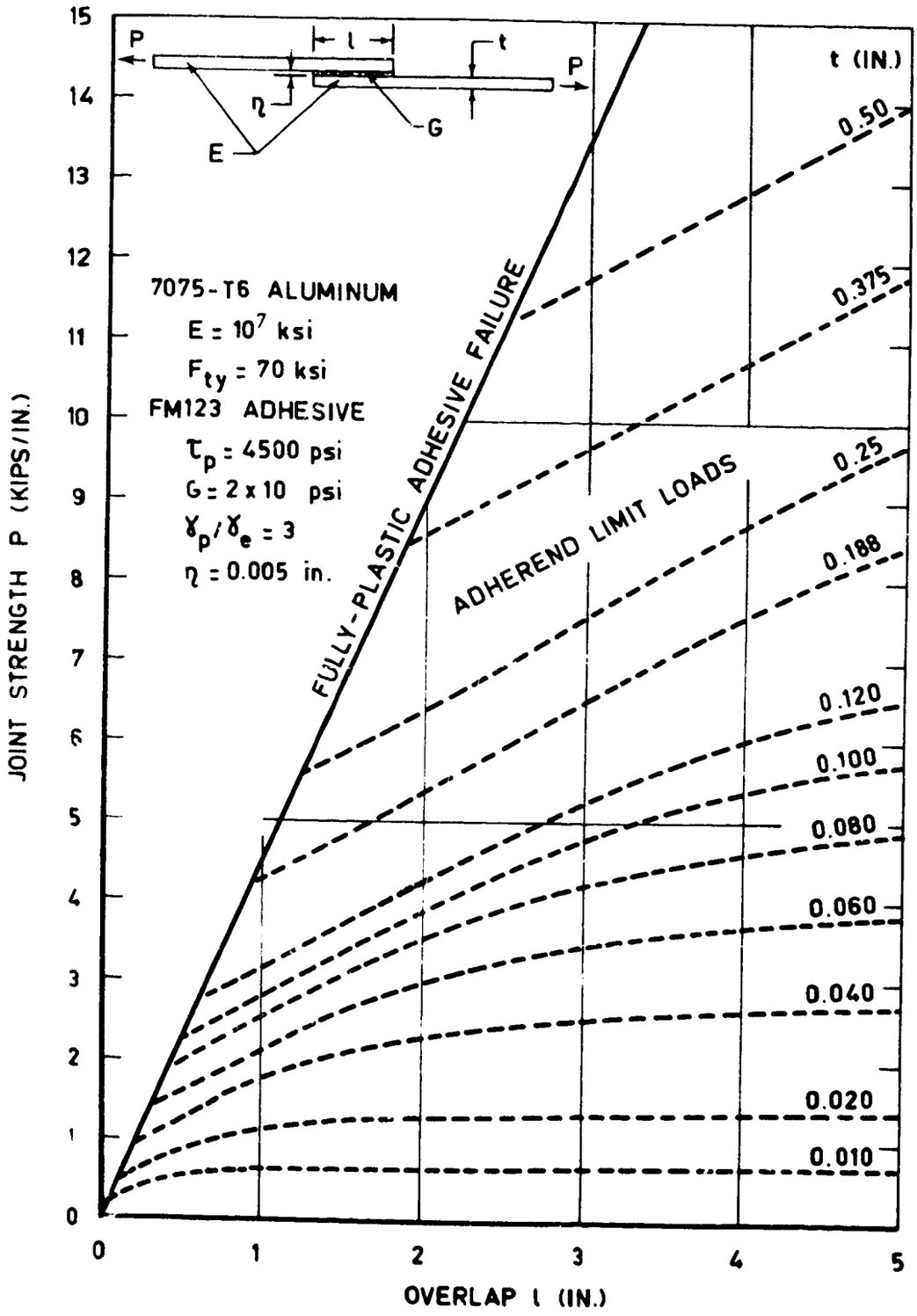

FIGURE 32. FORMATION OF PLASTIC HINGES DUE TO ECCENTRIC LOAD PATH FOR SINGLE-LAP BONDED JOINTS

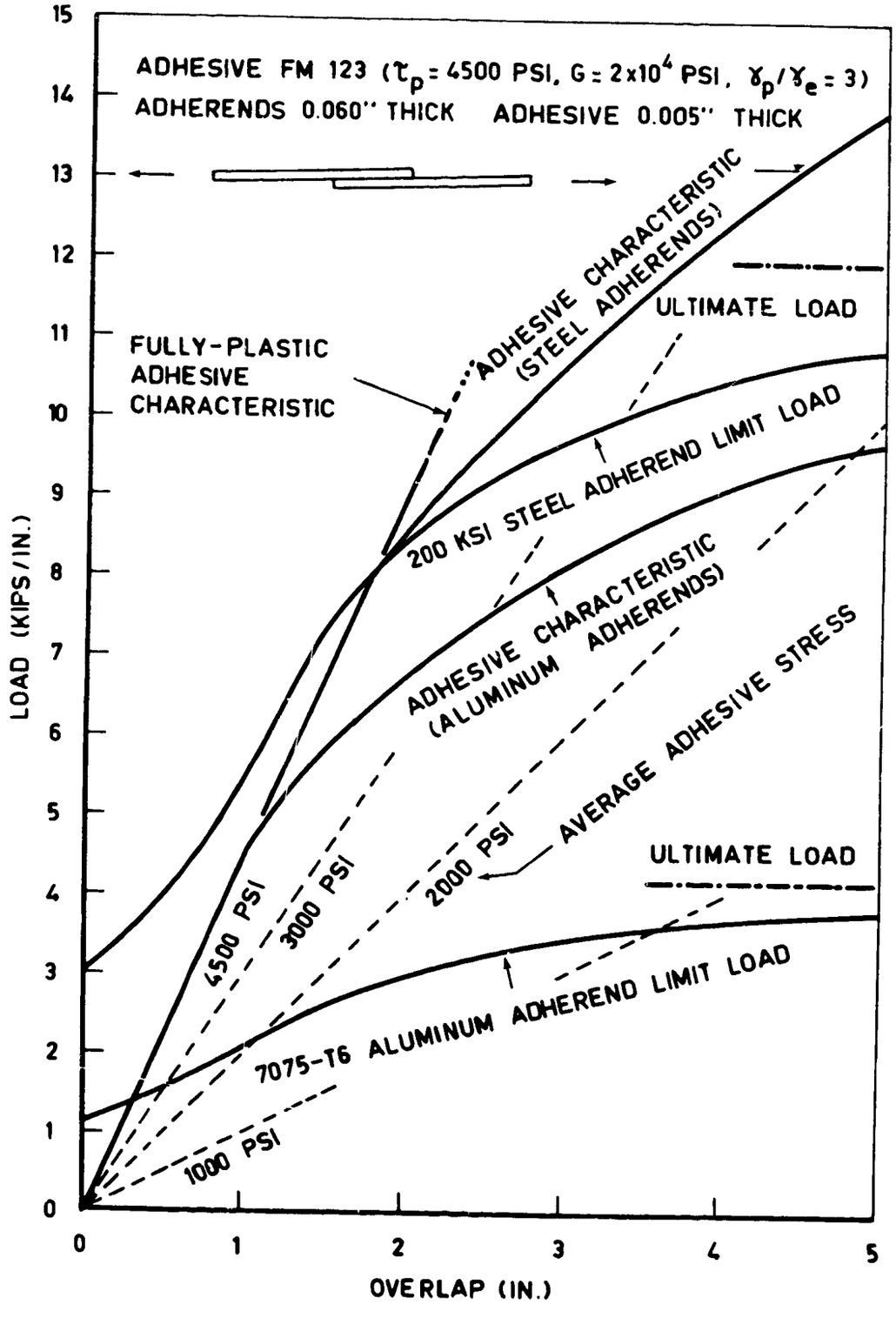

FIGURE 33. INFLUENCE OF ADHEREND MATERIAL ON SINGLE-LAP BONDED JOINTS

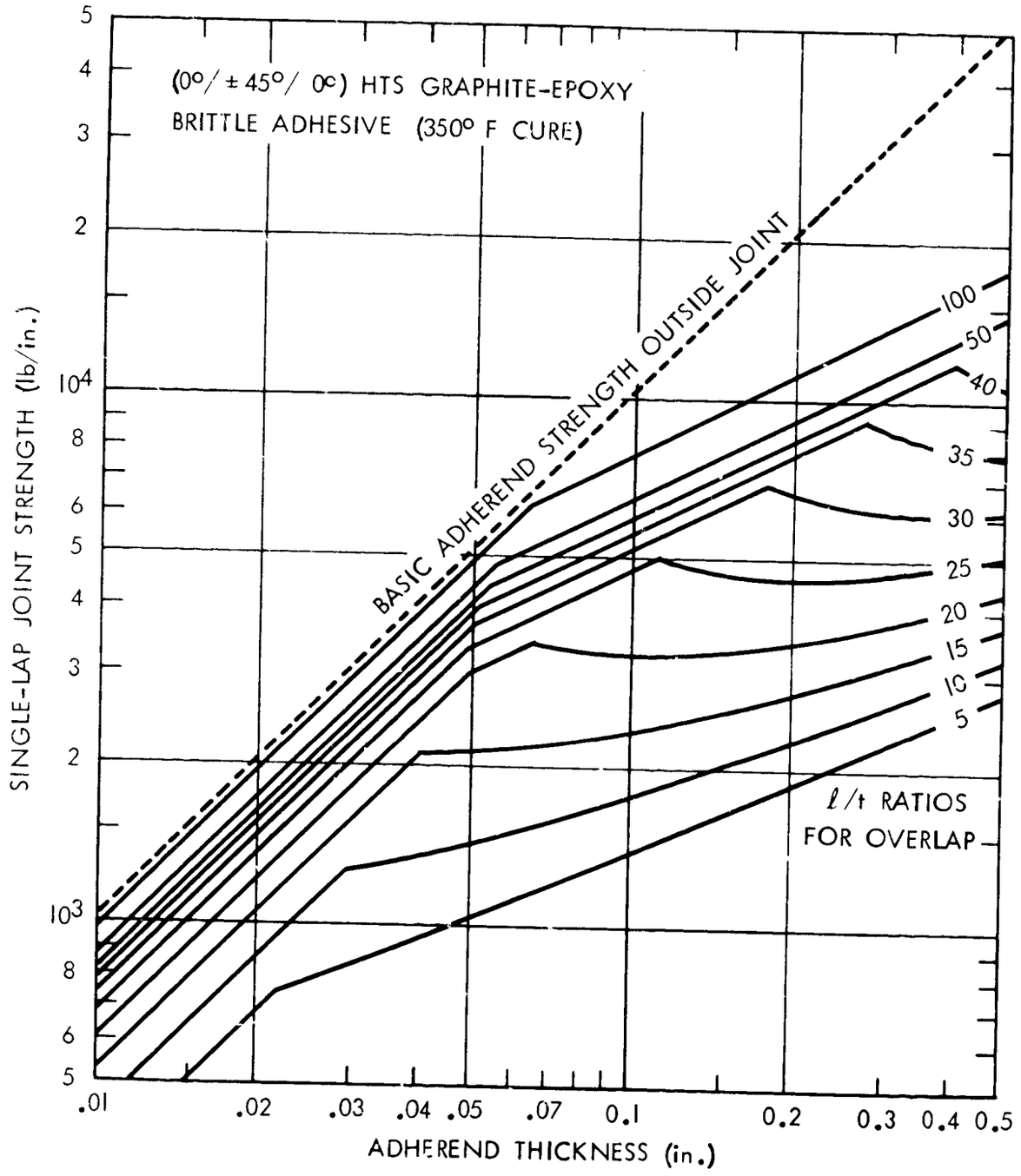

FIGURE 34. JOINT STRENGTH OF COMPOSITE SINGLE-LAP ADHESIVE-BONDED JOINTS, SHOWING INTERACTION OF THREE FAILURE MODES

APPENDIX

Computer Program A4EA for Strengths of Single-Lap Adhesive-Bonded Joints

A Fortran IV digital computer program has been prepared and checked out for solving those equations in the body of the report pertaining to joints between identical adherends. Each of the three potential failure modes is analyzed and printed out separately. This permits the strength margins of the stronger modes to be evaluated with respect to the governing (weakest) failure mode. The complete listing follows, along with sample output pages. The format of the input data is discussed below.

While other computer programs were prepared for unbalanced single-lap joints also, these are not reported here because of the intolerably low efficiencies of unsupported single-lap joints in structural applications. For unbalanced joints the efficiencies are lower still. Sample solutions prepared from the unreported computer programs are included in the report and serve to illustrate the effect of adherend dissimilarity on the joint strength.

The input data necessary to operate the A4EA computer program is as follows:

CARD 1:

FORMAT (I2)

NICNT = Number of material combinations to be read in.

CARD 2:

FORMAT (5F10.1)

AKB = Bending stiffness parameter $D / \{Et^3/[12(1-\nu^2)]\}$.
This factor serves to uncouple the bending and extensional stiffnesses for filamentary composites and has the value unity for metals.

EYOUNG = Young's modulus for the adherend, in the in-plane direction of the applied load.

IGMAX = Ultimate (or allowable) maximum stress in adherend.
The values F_{tu} or F_{cu} are used, depending on the direction of application of the load.

POISSN = In-plane Poisson's ratio associated with Young's modulus above.

ETRNSV = Transverse tension modulus of adherends.

For filamentary composites, this differs significantly from the in-plane values (which are largely fiber-controlled) because of the proportionally greater influence of the matrix.

CARD 3:

FORMAT (6F12.4)

G = Shear modulus for adhesive film.

Use actual value for elastic solution and equivalent elastic value based on matching strain energy for elastic-plastic solutions.

GAMMAR = γ_p/γ_e = Ratio of plastic to equivalent elastic adhesive shear strains. Value of zero is set for elastic case because plastic strain is defined to exclude the initial elastic increment.

ETA = Adhesive layer thickness.

TAUMAX = Maximum (plastic) adhesive shear stress.

PEELSG = Limiting peel strength, being the weaker of the adhesive peel stress (under the constraint of the adjacent adherends) and the interlaminar tension strength of a laminated adherend.

EPEEL = Modulus of adhesive layer in peel (under the constraint of the adjacent adherends).

CARDS 4, 4A, 4B, etc.:

FORMAT (12F6.3)

THICKN = Thickness of adherend.

Program is presently set up to read 17 thicknesses and there are dependent do-loops set to the same number. Alterations are straightforward but the number appears in a variety of places other than just input, output, and dimension statements.

CARDS 5, 5A, 5B, etc.:

FORMAT (11F6.1)

OLOVTH = ℓ/t ratio for joint.

Program is presently set to operate with 11 ℓ/t ratios. Simple changes to program will be necessary to operate with a different number, just as for THICKN. Note, however, that an increase in the number of OLOVTH is limited by the page width, while THICKN is listed

vertically and not subjected to such a severe limit.

The output of program A4EA is presented in sets of six pages, the first three in terms of joint strength per unit width and the last three in terms of the corresponding joint efficiencies by dividing throughout by the basic adherend strength. The entries in the output tables are self explanatory and each failure mode is identified in the caption.

In the event that the joint strength is not limited by the adherend bending strength but rather by the adhesive shear or peel strength, an iterative technique is used to adjust the load downwards in order to compute the actual bending moment at the end of the overlap instead of the maximum of which the adherends are capable. This refinement increases the predicted failure load which is, in all cases, critically dependent upon the estimate of the bending moment M_o.

The iteration sequences established in this program have been demonstrated to be convergent. Other possible re-arrangements of the equations do not lead to convergent sequences, so re-arrangement of the computational equations is not recommended. The input and output format and/or the units employed may be modified readily by the user to suit his specific requirements.

```
CDECK A4EA                                                                      A4EA0010
C  SINGLE-LAP ADHESIVE-BONDED JOINTS                                           A4EA0020
C  JOINT EFFICIENCY COMPUTATIONS                                               A4EA0030
C  DIMENSIONAL SOLUTION FOR BALANCED ADHERENDS                                  A4EA0040
C  PLASTIC HINGE FORMATION (OR FRACTURE) OF ADHERENDS INCLUDED                  A4EA0050
C  POTENTIAL BOND SHEAR STRENGTH ACCOUNTED FOR FOR SHORT OVERLAPS               A4EA0060
C  SHEAR STRENGTH USUALLY EXCEEDS PEEL STRENGTH FOR LONG OVERLAPS               A4EA0070
C  PEEL STRESS (OR INTERLAMINAR TENSION) FAILURES INCLUDED                      A4EA0080
      DIMENSION THICKN(17), OLOVTH(11), STRGTH(17,11), STRBND(17,11),           A4EA0090
     1   STRGPL(17,11), EFFNCY(11), EFFBND(17,11), EFFPL(17,11),               A4EA0100
     2   STORE(11), LOVTH(11), BNDSTR(17,11), BNDEFF(17,11), EKBNDG(11)        A4EA0110
      DOUBLE PRECISION XIL2, V28                                                A4EA0120
C READ IN DATA                                                                  A4EA0130
C READ IN ADHEREND AND ADHESIVE PROPERTIES                                      A4EA0140
      READ (5,10) NICNT                                                         A4EA0150
   10 FORMAT (I2)                                                               A4EA0160
C NICNT .EQ. NUMBER OF INPUT DATA SETS TO BE READ IN                            A4EA0170
      DO 660 N2CNT = 1, NICNT                                                   A4EA0180
      READ (5,20) AKB, EYOUNG, SIGMAX, POISSN, ETRNSV                           A4EA0190
   20 FORMAT (5F10.1)                                                           A4EA0200
      READ (5,30) G, GAMMAR, ETA, TAUMAX, PEELSG, EPEEL                         A4EA0210
   30 FORMAT (6F12.4)                                                           A4EA0220
      IF (N2CNT .GT. 1) GO TO 70                                                A4EA0230
C READ IN ADHEREND THICKNESS ARRAY                                              A4EA0240
      READ (5,40) (THICKN(I), I = 1, 17)                                        A4EA0250
   40 FORMAT (12F6.3)                                                           A4EA0260
C READ IN OVERLAP TO THICKNESS RATIO ARRAY                                      A4EA0270
      READ (5,50) (OLOVTH(J), J = 1, 11)                                        A4EA0280
   50 FORMAT (11F6.1)                                                           A4EA0290
C PRESET BOND SHEAR STRENGTH AND EFFICIENCY ARRAYS                              A4EA0300
      DO 60 I = 1, 17                                                           A4EA0310
      DO 60 J = 1, 11                                                           A4EA0320
      BNDSTR(I,J) = 10000000.                                                   A4EA0330
      BNDEFF(I,J) = 100.                                                        A4EA0340
   60 CONTINUE                                                                  A4EA0350
C                                                                               A4EA0360
C START COMPUTATIONS OF JOINT STRENGTHS                                         A4EA0370
C SET CONSTANTS                                                                 A4EA0380
   70 V2 = 1. - POISSN**2                                                       A4EA0390
      NFLAG = 0                                                                 A4EA0400
      N3CNT = 0                                                                 A4EA0410
      V23 = 2. * GAMMAR                                                         A4EA0420
      PROPNL = 3. * SIGMAX * V2 / (EYOUNG * AKB)                                A4EA0430
C ADHEREND BENDING EFFICIENCY DEPENDS UPON L/T ONLY AND NOT T SEPARATELY        A4EA0440
C SET INITIAL ESTIMATE (LOWER BOUND) ON JOINT EFFICIENCY                        A4EA0450
      V3 = 0.25                                                                 A4EA0460
      DO 100 J = 1, 11                                                          A4EA0470
      LOVTH(J) = OLOVTH(J)                                                      A4EA0480
      OLOVT2 = OLOVTH(J)**2                                                     A4EA0490
      DO 80 N = 1, 500                                                          A4EA0500
      XIL2 = V3 * OLOVT2 * PROPNL                                               A4EA0510
C EVALUATE ECCENTRICITY PARAMETER                                               A4EA0520
      EK = 1. / (1. + DSQRT(XIL2) + XIL2/6.)                                    A4EA0530
      V4 = 1. / (1. + 3. * EK )                                                 A4EA0540
      R = V3 / V4                                                               A4EA0550
      IF ( (1.0001 .GT. R) .AND. (0.9999 .LT. R) ) GO TO 90                     A4EA0560
      V3 = V4                                                                   A4EA0570
   80 CONTINUE                                                                  A4EA0580
C STOP IF NLOOP FAILS TO CONVERGE                                               A4EA0590
      GO TO 690                                                                 A4EA0600
C STORE JOINT EFFICIENCY IN BENDING PLUS TENSION OF ADHEREND                    A4EA0610
   90 EFFNCY(J) = V3                                                            A4EA0620
      EKBNDG(J) = EK                                                            A4EA0630
  100 CONTINUE                                                                  A4EA0640
C SELECT JOINT GEOMETRY BY NESTED DO LOOPS                                      A4EA0650
      DO 320 I = 1, 17                                                          A4EA0660
      T = THICKN(I)                                                             A4EA0670
      STR = SIGMAX * T                                                          A4EA0680
C ESTABLISH OVERLAP NON-DIMENSIONALIZING PARAMETER FOR ADHESIVE SHEAR           A4EA0690
      ALAMDA = SQRT (2. * G / (EYOUNG * T * ETA) )                              A4EA0700
C COMPUTE EFFECTIVE TRANSVERSE TENSION MODULUS OF ADHESIVE IN JOINT             A4EA0710
C THE CONSTANT 6 IN THE FOLLOWING INSTRUCTION CORRESPONDS WITH THE PEEL         A4EA0720
C     1   STRESSES AFFECTING THE ADHERENDS TO A DEPTH OF THREE TIMES           A4EA0730
C     2   THE BONDLINE THICKNESS.   OR ONE TIME, USE 2, ETC.                   A4EA0740
      ECPRM = 1. / ( (1. / EPEEL) + (6. / ETRNSV) )                             A4EA0750
      V1 = SQRT(3. * ECPRM * V2 * T / (2. * AKB * EYOUNG * ETA) )               A4EA0760
      DO 320 J = 1, 11                                                          A4EA0770
      OLOVT2 = OLOVTH(J)**2                                                     A4EA0780
      OLAP = T * OLOVTH(J)                                                      A4EA0790
C COMPUTE ADHEREND TENSION PLUS BENDING STRENGTH                                A4EA0800
      V5 = EFFNCY(J) * STR                                                      A4EA0810
      STRGTH(I,J) = V5                                                          A4EA0820
      EK = EKBNDG(J)                                                            A4EA0830
C COMPUTE ADHESIVE SHEAR STRESS CUT-OFF FOR SHORT OVERLAPS                      A4EA0840
      OLAPND = SQRT (8. * GAMMAR / (1. + 3. * EK * V2 / AKB) )                  A4EA0850
      OLREF = OLAPND / ALAMDA                                                   A4EA0860
      V11 = OLREF                                                               A4EA0870
      IF (OLREF .GE. OLAP) OLREF = OLAP                                         A4EA0880
```

```
      STRBND(I,J) = TAUMAX * OLREF                                          A4EA0890
      EFFBND(I,J) = STRBND(I,J) / STR                                       A4EA0900
C COMPUTE PEEL STRESS CUT-OFF                                               A4EA0910
      V7 = T * PEELSG / V1                                                  A4EA0920
      V8 = V7 / EK                                                          A4EA0930
      IF (V8 .GT. V5) GO TO 120                                             A4EA0940
C REDUCE LOAD DUE TO LIMITING PEEL STRENGTH                                 A4EA0950
      V9 = PROPNL / V5                                                      A4EA0960
      V3 = V8 / STR                                                         A4EA0970
      DO 110 N = 1, 500                                                     A4EA0980
      V10 = V8 * V9                                                         A4EA0990
      XIL2 = V3 * OLOVT2 * V10                                              A4EA1000
      EK = 1. / (1. + DSQRT(XIL2) + XIL2/6.)                                A4EA1010
      V4 = 1. / (1. + 3.*EK)                                                A4EA1020
      R = V3 / V4                                                           A4EA1030
      IF ( (1.0001 .GT. R) .AND. (0.9999 .LT. R) ) GO TO 120                A4EA1040
      V3 = V4                                                               A4EA1050
      V8 = V7 / EK                                                          A4EA1060
  110 CONTINUE                                                              A4EA1070
C STOP IF NLOOP FAILS TO CONVERGE                                           A4EA1080
      GO TO 690                                                             A4EA1090
C STORE COMPUTED PEEL STRENGTH AND EFFICIENCY LIMITED BY PEEL               A4EA1100
  120 STRGPL(I,J) = V8                                                      A4EA1110
      EFFPL(I,J) = V9 / STR                                                 A4EA1120
      C1 = STRBND(I,J)                                                      A4EA1130
      C2 = 1.5 * STRGTH(I,J)                                                A4EA1140
      C3 = 1.5 * STRGPL(I,J)                                                A4EA1150
      IF (C1 .GT. C2) GO TO 320                                             A4EA1160
      IF (C1 .GT. C3) GO TO 320                                             A4EA1170
C IF NOT, BOND STRENGTH MAY LIMIT LOAD CAPACITY                             A4EA1180
      STI = STRBND(I,J)                                                     A4EA1190
      IF (V11 .GE. OLAP) GO TO 320                                          A4EA1200
C IF SO, BOND STRENGTH LIMITED BY SHORT OVERLAP                             A4EA1210
C CONVERGENCE PROBLEMS IN ITERATION LOOPS BELOW                             A4EA1220
C     IF V11 ONLY JUST .LT. OLAP                                            A4EA1230
      C4 = 0.99 * OLAP                                                      A4EA1240
      IF (V11 .GE. C4) GO TO 320                                            A4EA1250
      IF (GAMMAR)710,130,170                                                A4EA1260
C IDENTIFY THAT PRECISE COMPUTATIONS OF SHEAR STRENGTH ARE TO BE DONE       A4EA1270
  130 NFLAG = 1                                                             A4EA1280
C SPECIAL PROCEDURE FOR PURELY ELASTIC ADHESIVE                             A4EA1290
C SET INITIAL ESTIMATE ON ECCENTRICITY FACTOR                               A4EA1300
C EK MAY HAVE TO BE INCREASED AS LOAD IS REDUCED                            A4EA1310
      V12 = EK                                                              A4EA1320
C NON-DIMENSIONALIZE JOINT PARAMETERS                                       A4EA1330
      OLSC = ALAMDA * OLAP                                                  A4EA1340
      V21 = (OLSC / TANH(OLSC) - 1.) / (1. + 3.*V2/AKB)                     A4EA1350
      ECCNTY = TAUMAX / ((AKB*EYOUNG*(T**3)/(12.*V2))*4.*(ALAMDA**3))       A4EA1360
      V22 = OLSC * OLSC * ECCNTY                                            A4EA1370
C START ITERATING, USING N AS COUNTER                                       A4EA1380
      DO 150 N = 1, 500                                                     A4EA1390
C COMPUTE NON-DIMENSIONALIZED STRENGTH                                      A4EA1400
      STF = OLSC / (1. + (1. + 3.*V12/AKB)*V21)                             A4EA1410
C BYPASS CONVERGENCE CHECK FOR FIRST TEN ITERATIONS                         A4EA1420
      IF (N .LT. 10) GO TO 140                                              A4EA1430
C CHECK FOR CONVERGENCE                                                     A4EA1440
      R = STF / STI                                                         A4EA1450
      IF ( (1.0001 .GT. R) .AND. (0.9999 .LT. R) ) GO TO 160                A4EA1460
  140 XIL2 = STF * V22                                                      A4EA1470
      V12 = 1. / (1. + DSQRT(XIL2) + XIL2/6.)                               A4EA1480
      STI = STF                                                             A4EA1490
  150 CONTINUE                                                              A4EA1500
C STOP IF NLOOP FAILS TO CONVERGE                                           A4EA1510
      GO TO 690                                                             A4EA1520
C RE-DIMENSIONALIZE COMPUTATIONS                                            A4EA1530
  160 V14 = STF * TAUMAX / ALAMDA                                           A4EA1540
      BNDSTR(I,J) = V14                                                     A4EA1550
      BNDEFF(I,J) = V14 / STR                                               A4EA1560
C END OF COMPUTATIONS FOR THIS VARIABLE SET                                 A4EA1570
      GO TO 320                                                             A4EA1580
C IDENTIFY THAT PRECISE COMPUTATIONS OF SHEAR STRENGTH ARE TO BE DONE       A4EA1590
  170 NFLAG = 1                                                             A4EA1600
C GENERAL PROCEDURE FOR ELASTIC-PLASTIC ADHESIVE                            A4EA1610
C NOTE THAT AKB IS SET EQUAL TO UNITY HERE, SINCE PROBLEM IS CONFINED       A4EA1620
C     TO THICKER LAMINATES OF MANY PLIES UNIFORMLY INTERSPERSED             A4EA1630
C SET INITIAL ESTIMATE ON ECCENTRICITY FACTOR                               A4EA1640
C EK MAY HAVE TO BE INCREASED AS LOAD IS REDUCED                            A4EA1650
      V12 = EK                                                              A4EA1660
C NON-DIMENSIONALIZE JOINT PARAMETERS                                       A4EA1670
      OLSC = ALAMDA * OLAP                                                  A4EA1680
      ECCNTY = TAUMAX / ( (EYOUNG*(T**3)/(3.*V2))*(ALAMDA**3) )             A4EA1690
      V22 = OLSC *OLSC * ECCNTY                                             A4EA1700
      DO 300 N1 = 1, 500                                                    A4EA1710
      N3CNT = 1                                                             A4EA1720
      V26 = (1. + 3. * V2 * V12)                                            A4EA1730
      VKL = V26 / 4.                                                        A4EA1740
C     VKU = 1.                                                              A4EA1750
C SET INITIAL ESTIMATES ON EXTENT OF ELASTIC TROUGH                         A4EA1760
```

```
      ODSC = OLSC + 1 - SQRT(1. + V23)                                  A4EA1770
      N3CNT = 2                                                         A4EA1780
      DO 190 N2 = 1, 500                                                A4EA1790
      V24 = TANH(ODSC)                                                  A4EA1800
      V28 = V24 * V24 + V23                                             A4EA1810
      V25 = OLSC + V24 - DSQRT(V28)                                     A4EA1820
C BYPASS CONVERGENCE CHECK FOR FIRST TEN ITERATIONS                     A4EA1830
      IF (N2 .LT. 10) GO TO 180                                         A4EA1840
C CHECK ON CONVERGENCE                                                  A4EA1850
      R = V25 / ODSC                                                    A4EA1860
      IF ( (1.0001 .GT. R) .AND. (0.9999 .LT. R) ) GO TO 200            A4EA1870
  180 ODSC = V25                                                        A4EA1880
  190 CONTINUE                                                          A4EA1890
C STOP IF N2LOOP FAILS TO CONVERGE                                      A4EA1900
      GO TO 690                                                         A4EA1910
C EVALUATE ODSC AND VK THROUGH ITERATION OF TWO SIMULTANEOUS EQUATIONS  A4EA1920
  200 N3CNT = 3                                                         A4EA1930
C UPPER LIMIT ESTABLISHED FOR EXTENT OF ELASTIC TROUGH                  A4EA1940
      ODSCU = ODSC                                                      A4EA1950
      ODSC = OLSC + 1 - SQRT(1. + V23 / VKL)                            A4EA1960
      DO 220 N3 = 1, 500                                                A4EA1970
      V24 = TANH(ODSC)                                                  A4EA1980
      V28 = V24 * V24 + V23 / VKL                                       A4EA1990
      V25 = OLSC + V24 - DSQRT(V28)                                     A4EA2000
C BYPASS CONVERGENCE CHECK FOR FIRST TEN ITERATIONS                     A4EA2010
      IF (N3 .LT. 10) GO TO 210                                         A4EA2020
C CHECK ON CONVERGENCE                                                  A4EA2030
      R = V25 / ODSC                                                    A4EA2040
      IF ( (1.0001 .GT. R) .AND. (0.9999 .LT. R) ) GO TO 230            A4EA2050
  210 ODSC = V25                                                        A4EA2060
  220 CONTINUE                                                          A4EA2070
C STOP IF N3LOOP FAILS TO CONVERGE                                      A4EA2080
      GO TO 690                                                         A4EA2090
  230 N3CNT = 4                                                         A4EA2100
C LOWER LIMIT ESTABLISHED FOR EXTENT OF ELASTIC TROUGH                  A4EA2110
      ODSCL = ODSC                                                      A4EA2120
      DO 270 N4 = 1, 5000                                               A4EA2130
C NOTE THAT 5000 ITERATIONS MAY BE NECESSARY IN THIS LOOP TO OBTAIN     A4EA2140
C     1  FOUR-FIGURE ACCURACY                                           A4EA2150
      ODSCI = ODSCU - (ODSCU - ODSCL) / 10.                             A4EA2160
      V24 = TANH(ODSCI)                                                 A4EA2170
      VK = V23 / ( ((OLSC - ODSCI + V24)**2) - (V24 * V24) )            A4EA2180
      ODSCE = V24 + SQRT(V24 * V24 + V23 / VK) *                        A4EA2190
     1  ((4. * VK / V26) - 1.) / (1. - VK)                             A4EA2200
C BYPASS CONVERGENCE CHECK FOR FIRST TEN ITERATIONS                     A4EA2210
      IF (N4 .LT. 10) GO TO 240                                         A4EA2220
C CHECK ON CONVERGENCE                                                  A4EA2230
      R = ODSCE /ODSCI                                                  A4EA2240
      IF ( (1.001 .GT. R) .AND. (0.999 .LT. R) ) GO TO 280              A4EA2250
C NOTE THAT WITH NESTED ITERATION LOOPS, FIVE-FIGURE ACCURACY IS NOT    A4EA2260
C     1  OBTAINABLE WITHIN A REALISTIC NUMBER OF ITERATIONS             A4EA2270
C RE-ESTIMATE ODSCU AND ODSCL                                           A4EA2280
  240 V27 = ODSCE - ODSCI                                               A4EA2290
      IF (V27)250,280,260                                               A4EA2300
  250 ODSCL = ODSCI                                                     A4EA2310
      GO TO 270                                                         A4EA2320
  260 ODSCU = ODSCI                                                     A4EA2330
  270 CONTINUE                                                          A4EA2340
C STOP IF N4LOOP FAILS TO CONVERGE                                      A4EA2350
      GO TO 690                                                         A4EA2360
C CONVERGENCE ESTABLISHED FOR ODSC AND VK                               A4EA2370
C COMPUTE ASSOCIATED JOINT STRENGTH                                     A4EA2380
  280 V28 = V24 * V24 + V23 / VK                                        A4EA2390
      STE = (4. * VK / V26) * DSQRT(V28)                                A4EA2400
C BYPASS CONVERGENCE CHECK FOR FIRST TEN ITERATIONS                     A4EA2410
      IF (N1 .LT. 10) GO TO 290                                         A4EA2420
C CHECK FOR CONVERGENCE OF JOINT STRENGTHS                              A4EA2430
      R = STE / STI                                                     A4EA2440
      IF ( (1.001 .GT. R) .AND. (0.999 .LT. R) ) GO TO 310              A4EA2450
C IF NOT, RECOMPUTE EK AND ITERATE                                      A4EA2460
  290 XIL2 = STE * V22                                                  A4EA2470
      V12 = 1. / (1. + DSQRT(XIL2) + XIL2/6.)                           A4EA2480
      STI = (STI + STE) / 2.                                            A4EA2490
  300 CONTINUE                                                          A4EA2500
C STOP IF N1LOOP FAILS TO CONVERGE                                      A4EA2510
      GO TO 690                                                         A4EA2520
C STORE COMPUTED STRENGTH AND EFFICIENCY AFTER CONVERGENCE ESTABLISHED  A4EA2530
  310 V33 = STE * TAUMAX / ALAMDA                                       A4EA2540
      BNDSTR(I,J) = V33                                                 A4EA2550
      BNDEFF(I,J) = V33 / STR                                           A4EA2560
  320 CONTINUE                                                          A4EA2570
C                                                                       A4EA2580
C PRINT OUT TABULATIONS OF COMPUTATIONS IN SETS OF SIX OR EIGHT PAGES   A4EA2590
      WRITE (6,330) (LOVTH(J), J = 1, 11)                               A4EA2600
  330 FORMAT (1HI, 10(/), 39X, 33HSINGLE-LAP ADHESIVE-BONDED JOINTS//   A4EA2610
     1 46X, 18HBALANCED ADHEREND S//                                    A4EA2620
     2 32X, 47HADHEREND STRENGTH IN BENDING AT EDGE OF OVERLAP///       A4EA2630
     3 41X, 38HJOINT STRENGTH (POUNDS PER INCH WIDTH)//                 A4EA2640
```

```
     4 1X, 9HTHICKNESS/, 1X, 8H(INCHES),                                    A4EA2650
     5 37X, 26HOVERLAP TO THICKNESS RATIO//, 9X, 11(I7, 2X)///)             A4EA2660
      DO 360 I = 1, 17                                                      A4EA2670
      DO 340 J = 1, 11                                                      A4EA2680
  340 STORE(J) = STRGTH(I,J)                                                A4EA2690
      WRITE (6,350) THICKN(I), (STORE(J), J = 1, 11)                        A4EA2700
  350 FORMAT (1H , F5.3, 4X, 11(F8.1, 1X) )                                 A4EA2710
  360 CONTINUE                                                              A4EA2720
      WRITE (6,370) (LOVTH(J), J = 1, 11)                                   A4EA2730
  370 FORMAT (1H1, 10(/), 39X, 33HSINGLE-LAP ADHESIVE-BONDED JOINTS//       A4EA2740
     1 46X, 18HBALANCED ADHEREND S//                                        A4EA2750
     2 39X, 33HPOTENTIAL ADHESIVE SHEAR STRENGTH///                         A4EA2760
     3 41X, 38HJOINT STRENGTH (POUNDS PER INCH WIDTH)//                     A4EA2770
     4 1X, 9HTHICKNESS/, 1X, 8H(INCHES),                                    A4EA2780
     5 37X, 26HOVERLAP TO THICKNESS RATIO//, 9X, 11(I7, 2X)///)             A4EA2790
      DO 400 I = 1, 17                                                      A4EA2800
      DO 380 J = 1, 11                                                      A4EA2810
  380 STORE(J) = STRBND(I,J)                                                A4EA2820
      WRITE (6,390) THICKN(I), (STORE(J), J = 1, 11)                        A4EA2830
  390 FORMAT (1H , F5.3, 4X, 11(F8.1, 1X) )                                 A4EA2840
  400 CONTINUE                                                              A4EA2850
      IF (NFLAG .EQ. 0) GO TO 450                                           A4EA2860
      WRITE (6,410) (LOVTH(J), J = 1, 11)                                   A4EA2870
  410 FORMAT (1H1, 10(/), 39X, 33HSINGLE-LAP ADHESIVE-BONDED JOINTS//       A4EA2880
     1 46X, 18HBALANCED ADHEREND S//                                        A4EA2890
     2 39X, 33HPOTENTIAL ADHESIVE SHEAR STRENGTH///                         A4EA2900
     3 41X, 38HJOINT STRENGTH (POUNDS PER INCH WIDTH)//                     A4EA2910
     4 1X, 9HTHICKNESS/, 1X, 8H(INCHES),                                    A4EA2920
     5 37X, 26HOVERLAP TO THICKNESS RATIO//, 9X, 11(I7, 2X)///)             A4EA2930
      DO 440 I = 1, 17                                                      A4EA2940
      DO 420 J = 1, 11                                                      A4EA2950
  420 STORE(J) = BNDSTR(I,J)                                                A4EA2960
      WRITE (6,430) THICKN(I), (STORE(J), J = 1, 11)                        A4EA2970
  430 FORMAT (1H , F5.3, 4X, 11(F8.1, 1X) )                                 A4EA2980
  440 CONTINUE                                                              A4EA2990
  450 WRITE (6,460) (LOVTH(J), J = 1, 11)                                   A4EA3000
  460 FORMAT (1H1, 10(/), 39X, 33HSINGLE-LAP ADHESIVE-BONDED JOINTS//       A4EA3010
     1 46X, 18HBALANCED ADHEREND S//                                        A4EA3020
     2 44X, 22HLIMITING PEEL STRENGTH///                                    A4EA3030
     3 41X, 38HJOINT STRENGTH (POUNDS PER INCH WIDTH)//                     A4EA3040
     4 1X, 9HTHICKNESS/, 1X, 8H(INCHES),                                    A4EA3050
     5 37X, 26HOVERLAP TO THICKNESS RATIO//, 9X, 11(I7, 2X)///)             A4EA3060
      DO 490 I = 1, 17                                                      A4EA3070
      DO 470 J = 1, 11                                                      A4EA3080
  470 STORE(J) = STRGPL(I,J)                                                A4EA3090
      WRITE (6,480) THICKN(I), (STORE(J), J = 1, 11)                        A4EA3100
  480 FORMAT (1H , F5.3, 4X, 11(F8.1, 1X) )                                 A4EA3110
  490 CONTINUE                                                              A4EA3120
      WRITE (6,500) (LOVTH(J), J = 1, 11)                                   A4EA3130
  500 FORMAT (1H1, 10(/), 39X, 33HSINGLE-LAP ADHESIVE-BONDED JOINTS//       A4EA3140
     1 46X, 18HBALANCED ADHEREND S//                                        A4EA3150
     2 32X, 47HADHEREND STRENGTH IN BENDING AT EDGE OF OVERLAP///           A4EA3160
     3 52X, 16HJOINT EFFICIENCY/                                            A4EA3170
     4 1X, 9HTHICKNESS/, 1X, 8H(INCHES),                                    A4EA3180
     5 37X, 26HOVERLAP TO THICKNESS RATIO//, 9X, 11(I7, 2X)///)             A4EA3190
      DO 520 I = 1, 17                                                      A4EA3200
      WRITE (6,510) THICKN(I), (EFFNCY(J), J = 1, 11)                       A4EA3210
  510 FORMAT (1H , F5.3, 4X, 11(F8.5, 1X) )                                 A4EA3220
  520 CONTINUE                                                              A4EA3230
      WRITE (6,530) (LOVTH(J), J = 1, 11)                                   A4EA3240
  530 FORMAT (1H1, 10(/), 39X, 33HSINGLE-LAP ADHESIVE-BONDED JOINTS//       A4EA3250
     1 46X, 18HBALANCED ADHEREND S//                                        A4EA3260
     2 39X, 33HPOTENTIAL ADHESIVE SHEAR STRENGTH///                         A4EA3270
     3 52X, 16HJOINT EFFICIENCY/                                            A4EA3280
     4 1X, 9HTHICKNESS/, 1X, 8H(INCHES),                                    A4EA3290
     5 37X, 26HOVERLAP TO THICKNESS RATIO//, 9X, 11(I7, 2X)///)             A4EA3300
      DO 560 I = 1, 17                                                      A4EA3310
      DO 540 J = 1, 11                                                      A4EA3320
  540 STORE(J) = EFFBND(I,J)                                                A4EA3330
      WRITE (6,550) THICKN(I), (STORE(J), J = 1, 11)                        A4EA3340
  550 FORMAT (1H , F5.3, 4X, 11(F8.5, 1X) )                                 A4EA3350
  560 CONTINUE                                                              A4EA3360
      IF (NFLAG .EQ. 0) GO TO 610                                           A4EA3370
      WRITE (6,570) (LOVTH(J), J = 1, 11)                                   A4EA3380
  570 FORMAT (1H1, 10(/), 39X, 33HSINGLE-LAP ADHESIVE-BONDED JOINTS//       A4EA3390
     1 46X, 18HBALANCED ADHEREND S//                                        A4EA3400
     2 39X, 33HPOTENTIAL ADHESIVE SHEAR STRENGTH///                         A4EA3410
     3 52X, 16HJOINT EFFICIENCY/                                            A4EA3420
     4 1X, 9HTHICKNESS/, 1X, 8H(INCHES),                                    A4EA3430
     5 37X, 26HOVERLAP TO THICKNESS RATIO//, 9X, 11(I7, 2X)///)             A4EA3440
      DO 600 I = 1, 17                                                      A4EA3450
      DO 580 J = 1, 11                                                      A4EA3460
  580 STORE(J) = BNDEFF(I,J)                                                A4EA3470
      WRITE (6,590) THICKN(I), (STORE(J), J = 1, 11)                        A4EA3480
  590 FORMAT (1H , F5.3, 4X, 11(F8.5, 1X) )                                 A4EA3490
  600 CONTINUE                                                              A4EA3500
  610 WRITE (6,620) (LOVTH(J), J = 1, 11)                                   A4EA3510
  620 FORMAT (1H1, 10(/), 39X, 33HSINGLE-LAP ADHESIVE-BONDED JOINTS//       A4EA3520
```

```
     1 46X, 18HBALANCED ADHERENDS//                                          A4EA3530
     2 44X, 22HLIMITING PEEL STRENGTH///                                     A4EA3540
     3 52X, 16HJOINT EFFICIENCY//                                            A4EA3550
     4 1X, 9HTHICKNESS/, 1X, 8H(INCHES),                                     A4EA3560
     5 37X, 26HOVERLAP TO THICKNESS RATIO//, 9X, 11(17, 2X)///)              A4EA3570
       DO 650 I = 1, 17                                                      A4EA3580
       DO 630 J = 1, 11                                                      A4EA3590
  630  STORE(J) = EEPL(I,J)                                                  A4EA3600
       WRITE (6,640) THICKN(I), (STORE(J), J = 1, 11)                        A4EA3610
  640  FORMAT (1H , F5.3, 4X, 11(F8.5, 1X) )                                 A4EA3620
  650  CONTINUE                                                              A4EA3630
C                                                                           A4EA3640
C READ IN NEW MATERIAL ALLOWABLES AND REPEAT COMPUTATIONS                   A4EA3650
  660  CONTINUE                                                              A4EA3660
  670  WRITE (6,680)                                                         A4EA3670
  680  FORMAT (1H1, 17HPROGRAM COMPLETED/)                                   A4EA3680
       STOP                                                                  A4EA3690
C PRINT OUT DIAGNOSTICS                                                     A4EA3700
  690  WRITE (6,700) N3CNT, I, J                                             A4EA3710
  700  FORMAT (1H1, 19HDIVERGENT ITERATION, 3I10//)                          A4EA3720
       STOP                                                                  A4EA3730
  710  WRITE (6,720)                                                         A4EA3740
  720  FORMAT (1H1, 58HNEGATIVE GAMMAR VALUE IN INPUT DATA - PHYSICALLY IA4EA3750
     1MPOSSIBLE//)                                                          A4EA3760
       STOP                                                                  A4EA3770
       END                                                                   A4EA3780
```

SINGLE-LAP ADHESIVE-BONDED JOINTS

BALANCED ADHERENDS

ADHEREND STRENGTH IN BENDING AT EDGE OF OVERLAP

THICKNESS (INCHES)	JOINT STRENGTH (POUNDS PER INCH WIDTH) OVERLAP TO THICKNESS RATIO										
	5	10	15	20	25	30	35	40	45	50	100
0.010	137.7	165.6	195.0	223.9	251.0	275.3	296.6	315.0	330.8	344.2	409.3
0.015	206.5	248.5	292.5	335.9	376.4	413.0	444.9	472.5	496.2	516.3	614.0
0.020	275.3	331.3	390.0	447.8	501.9	550.6	593.2	630.0	661.5	688.4	818.6
0.030	413.0	496.9	585.0	671.7	752.9	825.9	889.8	945.1	992.3	1032.6	1227.9
0.040	550.6	662.6	780.0	895.6	1003.9	1101.2	1186.5	1260.1	1323.1	1376.9	1637.2
0.060	825.9	993.9	1169.9	1343.4	1505.8	1651.9	1779.7	1890.1	1984.6	2065.3	2455.8
0.080	1101.2	1325.2	1559.9	1791.2	2007.7	2202.5	2372.9	2520.2	2646.2	2753.7	3274.4
0.100	1376.6	1656.5	1949.9	2239.1	2509.6	2753.1	2966.2	3150.2	3307.7	3442.1	4093.0
0.130	1789.5	2153.4	2534.9	2910.8	3262.5	3579.0	3856.0	4095.3	4300.0	4474.8	5321.0
0.160	2202.5	2650.3	3119.8	3582.4	4015.4	4404.9	4745.9	5040.4	5292.4	5507.4	6548.9
0.200	2753.1	3312.9	3899.7	4478.0	5019.2	5506.2	5932.3	6300.4	6615.5	6884.3	8186.1
0.250	3441.4	4141.1	4874.7	5597.4	6273.9	6882.6	7415.4	7875.6	8269.3	8605.3	10232.6
0.300	4129.7	4969.3	5849.6	6716.9	7528.6	8259.0	8899.1	9450.7	9923.2	10326.4	12279.1
0.350	4817.9	5798.1	6824.5	7836.3	8783.3	9635.4	10382.2	11025.8	11577.0	12047.5	14325.7
0.400	5506.2	6626.4	7799.4	8955.7	10037.9	11011.8	11865.2	12600.3	13230.9	13768.5	16372.2
0.450	6194.5	7454.7	8774.3	10075.2	11292.6	12388.1	13348.3	14176.5	14884.8	15489.6	18418.7
0.500	6882.8	8283.0	9749.2	11194.6	12547.3	13764.5	14831.3	15751.6	16538.2	17210.7	20465.2

SINGLE-LAP ADHESIVE-BONDED JOINTS

BALANCED ADHERENDS

POTENTIAL ADHESIVE SHEAR STRENGTH

THICKNESS (INCHES)	JOINT STRENGTH (POUNDS PER INCH WIDTH) OVERLAP TO THICKNESS RATIO										
	5	10	15	20	25	30	35	40	45	50	100
0.010	********	********	********	1297.8	1459.7	1592.0	1702.8	1794.8	1871.9	1937.0	2265.9
0.015	********	********	********	1868.9	1863.5	2042.6	2167.2	2278.6	2370.7	2448.6	2829.8
0.020	********	********	********	1976.4	2208.3	2398.4	2554.1	2681.3	2787.4	2875.7	3303.4
0.030	********	********	********	2476.5	2762.2	2996.5	3188.2	3345.0	3474.4	3581.5	4093.7
0.040	********	********	********	2982.7	3213.7	3436.1	3709.1	3890.7	4040.8	4166.6	4755.4
0.060	********	********	********	3533.9	3939.2	4275.7	4553.1	4780.1	4967.8	5124.4	5855.5
0.080	********	********	********	4057.1	4524.2	4914.8	5238.5	5505.3	5725.9	5910.1	6773.5
0.100	********	********	********	4503.7	5020.2	5454.8	5823.8	6125.5	6377.3	6588.0	7574.9
0.130	********	********	********	5069.9	5656.1	6156.4	6576.3	6927.5	7220.7	7466.6	8628.8
0.160	********	********	4837.0	5553.0	6201.4	6755.9	7225.3	7619.3	7950.5	8229.8	9557.6
0.200	********	4510.2	5340.3	6125.9	6834.1	7451.1	7978.8	8425.3	8802.8	9122.0	10657.9
0.250	4110.4	4995.2	5847.4	6746.2	7517.3	8202.3	8793.6	9289.1	9728.6	10094.1	11874.2
0.300	4495.4	5427.9	6371.1	7280.6	8116.6	8860.9	9509.2	10066.4	10543.6	10951.1	12961.5
0.350	4947.1	5920.3	6907.6	7765.7	8653.7	9451.1	10150.4	10755.5	11275.7	11723.1	13951.7
0.400	5172.3	6141.4	7208.3	8209.3	9144.0	9988.9	10733.8	11383.6	11943.9	12429.1	14865.2
0.450	5476.4	6517.6	7579.6	8619.8	9596.9	10484.5	11271.9	11962.2	12561.0	13079.7	15715.9
0.500	5762.4	6832.8	7927.0	9003.0	10014.1	10945.4	11773.1	12500.7	13135.2	13686.5	16514.5

SINGLE-LAP ADHESIVE-BONDED JOINTS

BALANCED ADHERENDS

LIMITING PEEL STRENGTH

THICKNESS (INCHES)	JOINT STRENGTH (POUNDS PER INCH WIDTH) OVERLAP TO THICKNESS RATIO										
	5	10	15	20	25	30	35	40	45	50	100
0.010	427.2	554.7	741.2	960.0	1222.1	1527.7	1874.9	2262.6	2689.5	3154.2	9755.8
0.015	523.3	691.7	907.8	1175.7	1497.0	1871.0	2296.3	2771.2	3293.9	3863.1	11948.4
0.020	604.1	798.7	1048.2	1357.6	1728.6	2160.5	2651.5	3199.8	3803.5	4460.8	13796.8
0.030	739.9	978.1	1283.8	1662.8	2117.1	2646.1	3247.4	3919.0	4658.3	5463.3	16897.5
0.040	854.4	1129.5	1482.4	1920.0	2444.6	3055.4	3749.9	4525.3	5379.9	6309.5	19511.6
0.060	1046.4	1383.3	1815.6	2351.5	2994.1	3742.1	4592.6	5542.5	6588.8	7726.3	23896.7
0.080	1209.3	1597.3	2096.5	2715.3	3457.2	4321.0	5303.0	6393.7	7607.0	8921.5	27593.6
0.100	1346.7	1785.8	2343.9	3035.8	3865.2	4831.0	5929.3	7155.1	8504.8	9974.6	30850.5
0.130	1504.7	1994.0	2672.5	3461.3	4407.1	5509.2	6760.1	8158.1	9697.0	11372.8	35175.0
0.160	1644.7	2133.6	2869.6	3841.0	4449.2	6110.8	7499.6	9055.5	10757.9	12617.0	39023.2
0.200	1811.8	2332.6	3003.0	4121.9	5466.1	6832.1	8384.8	10118.8	12027.7	14106.2	43629.2
0.250	1997.8	2492.5	3167.2	4179.1	5901.6	7634.5	9374.5	11313.2	13447.3	15771.5	48779.0
0.300	2163.4	2664.8	3324.0	4268.5	5776.3	9367.6	10269.3	12393.0	14730.8	17276.5	53434.7
0.350	2319.2	2823.4	3472.1	4376.9	5741.0	9119.7	11092.1	13385.9	15911.1	18660.7	57716.0
0.400	2461.9	2971.1	3612.7	4479.3	5751.4	7653.6	11890.4	14310.2	17009.1	19949.2	61701.0
0.450	2595.7	3103.7	3746.4	4507.7	5733.1	7695.7	11136.5	15178.2	18041.5	21159.3	65463.8
0.500	2722.0	3240.8	3874.1	4695.7	5842.3	7603.9	10647.7	15993.3	19017.4	22303.9	68983.9

SINGLE-LAP ADHESIVE-BONDED JOINTS
BALANCED ADHERENDS
ADHEREND STRENGTH IN BENDING AT EDGE OF OVERLAP

JOINT EFFICIENCY

OVERLAP TO THICKNESS RATIO

THICKNESS (INCHES)	5	10	15	20	25	30	35	40	45	50	100
0.010	0.30590	0.36811	0.43331	0.49757	0.55770	0.61180	0.65915	0.70005	0.73505	0.76492	0.90957
0.015	0.30590	0.36811	0.43331	0.49757	0.55770	0.61180	0.65915	0.70005	0.73505	0.76492	0.90957
0.020	0.30590	0.36811	0.43331	0.49757	0.55770	0.61180	0.65915	0.70005	0.73505	0.76492	0.90957
0.030	0.30590	0.36811	0.43331	0.49757	0.55770	0.61180	0.65915	0.70005	0.73505	0.76492	0.90957
0.040	0.30590	0.36811	0.43331	0.49757	0.55770	0.61180	0.65915	0.70005	0.73505	0.76492	0.90957
0.060	0.30590	0.36811	0.43331	0.49757	0.55770	0.61180	0.65915	0.70005	0.73505	0.76492	0.90957
0.080	0.30590	0.36811	0.43331	0.49757	0.55770	0.61180	0.65915	0.70005	0.73505	0.76492	0.90957
0.100	0.30590	0.36810	0.43331	0.49757	0.55770	0.61180	0.65915	0.70005	0.73505	0.76492	0.90957
0.130	0.30590	0.36810	0.43331	0.49757	0.55770	0.61180	0.65915	0.70005	0.73505	0.76492	0.90957
0.160	0.30590	0.36810	0.43331	0.49756	0.55770	0.61180	0.65915	0.70005	0.73505	0.76492	0.90957
0.200	0.30590	0.36810	0.43331	0.49756	0.55769	0.61180	0.65915	0.70005	0.73505	0.76492	0.90957
0.250	0.30590	0.36810	0.43330	0.49755	0.55768	0.61179	0.65915	0.70005	0.73505	0.76492	0.90957
0.300	0.30590	0.36810	0.43330	0.49755	0.55767	0.61178	0.65919	0.70005	0.73505	0.76492	0.90957
0.350	0.30590	0.36813	0.43330	0.49754	0.55767	0.61177	0.65919	0.70005	0.73505	0.76492	0.90957
0.400	0.30590	0.36813	0.43330	0.49754	0.55766	0.61176	0.65918	0.70002	0.73505	0.76492	0.90957
0.450	0.30590	0.36813	0.43330	0.49754	0.55766	0.61176	0.65917	0.70007	0.73505	0.76492	0.90957
0.500	0.30590	0.36813	0.43330	0.49754	0.55766	0.61176	0.65917	0.70007	0.73503	0.76492	0.90957

SINGLE-LAP ADHESIVE-BONDED JOINTS
BALANCED ADHERENDS
POTENTIAL ADHESIVE SHEAR STRENGTH

JOINT EFFICIENCY

OVERLAP TO THICKNESS RATIO

THICKNESS (INCHES)	5	10	15	20	25	30	35	40	45	50	100
0.010	********	********	********	2.88398	3.24155	3.53779	3.78390	3.98853	4.15977	4.30455	5.03533
0.015	********	********	********	2.47239	2.76314	3.01121	3.21064	3.37570	3.51216	3.62759	4.19231
0.020	********	********	********	2.19598	2.45364	2.66495	2.83793	2.97920	3.09708	3.19523	3.67050
0.030	********	********	********	1.83441	2.04629	2.21962	2.36165	2.47778	2.57364	2.65295	3.03240
0.040	********	********	********	1.60151	1.78541	1.93673	2.06059	2.16152	2.24498	2.31478	2.64188
0.060	********	********	********	1.39384	1.45377	1.58359	1.68633	1.77042	1.83992	1.89791	2.16869
0.080	********	********	********	1.12698	1.25573	1.36521	1.45513	1.52926	1.59054	1.64169	1.88152
0.100	********	********	********	1.00015	1.11560	1.21307	1.29418	1.36123	1.41718	1.46401	1.68331
0.130	********	********	********	0.86656	0.96686	1.05238	1.12415	1.19419	1.23431	1.27635	1.47501
0.160	********	********	0.67180	0.77208	0.85136	0.93832	1.00352	1.05824	1.10424	1.14303	1.32745
0.200	********	0.50114	0.59336	0.68055	0.75934	0.82790	0.88653	0.93614	0.97809	1.01355	1.18421
0.250	0.36537	0.44411	0.52332	0.59911	0.66420	0.72910	0.78166	0.82658	0.86477	0.89725	1.05549
0.300	0.33239	0.40207	0.47193	0.53927	0.60123	0.65537	0.70438	0.74556	0.78101	0.81120	0.96011
0.350	0.30775	0.36954	0.43224	0.49306	0.54344	0.60007	0.64447	0.68289	0.71592	0.74432	0.88582
0.400	0.28735	0.34341	0.40046	0.45627	0.50400	0.55494	0.59632	0.63241	0.66355	0.69045	0.82585
0.450	0.27044	0.32135	0.37430	0.42567	0.47392	0.51775	0.55664	0.59072	0.62029	0.64591	0.77609
0.500	0.25611	0.30368	0.35231	0.40013	0.44525	0.48646	0.52325	0.55559	0.58379	0.60329	0.73398

SINGLE-LAP ADHESIVE-BONDED JOINTS
BALANCED ADHERENDS
LIMITING PEEL STRENGTH

JOINT EFFICIENCY

OVERLAP TO THICKNESS RATIO

THICKNESS (INCHES)	5	10	15	20	25	30	35	40	45	50	100
0.010	0.94933	1.25446	1.64713	2.13332	2.71622	3.39430	4.16645	5.02808	5.97659	7.00943	21.67953
0.015	0.77512	1.02467	1.34497	1.74185	2.21778	2.77192	3.40189	4.10541	4.87986	5.72317	17.70126
0.020	0.67127	0.89733	1.15465	1.50949	1.92066	2.40055	2.94612	3.55539	4.22609	4.95641	15.32574
0.030	0.54809	0.72455	0.95037	1.23167	1.56821	1.96034	2.40550	2.90296	3.45059	4.04649	12.51660
0.040	0.47466	0.62744	0.82356	1.06566	1.35411	1.69745	2.08323	2.51424	2.98829	3.50471	10.39977
0.060	0.38756	0.51234	0.67244	[illegible]	1.13483	1.38596	1.70095	2.05275	2.43993	2.86158	8.85063
0.080	0.33564	0.44372	0.58235	0.75624	0.95033	1.20023	1.47306	1.77763	2.11304	2.47821	7.66498
0.100	0.29927	0.39645	0.52297	0.67462	0.85874	1.07336	1.31755	1.59002	1.88976	2.21658	6.85568
0.130	0.25722	0.34045	0.45643	0.59159	0.75314	0.94158	1.15557	1.39454	1.65761	1.94407	6.01243
0.160	0.22844	0.29630	0.39355	0.53333	0.67906	0.84472	1.04161	1.25702	1.49415	1.75236	5.41989
0.200	0.20131	0.25584	0.33367	0.45797	0.60737	0.75412	0.93165	1.12431	1.33641	1.56736	4.84770
0.250	0.17759	0.22155	[illegible]	0.37147	0.52659	0.67498	0.83329	1.00562	1.19532	1.40199	4.33591
0.300	0.16041	0.19734	0.24522	0.31619	0.42741	0.61942	0.76069	0.91900	1.09117	1.27974	3.95912
0.350	0.14725	0.17327	0.22245	0.27752	0.36451	0.51554	0.70426	0.84990	1.01023	1.18481	3.66451
0.400	0.13677	0.16526	0.20071	0.24174	0.31952	0.43631	0.65936	0.79501	0.94493	1.10829	3.42734
0.450	0.12818	0.15357	0.18501	0.22655	0.24594	0.38304	0.54995	0.74954	0.89094	1.04490	3.23179
0.500	0.12094	0.14403	0.17218	0.20870	0.25966	0.33795	0.47323	0.71108	0.84522	0.99129	3.06595

END

DATE

FILMED

FEB 7 1974